Development of a skin-on-a-chip platform for the study of wound healing

being a thesis submitted for the degree of

DOCTOR OF PHILOSOPHY

by

Kamil Talar, BSc (HONS), MSc (Res)

University of Hull

Department of Chemistry

June 2022

Contents

5   Conclusions

List of Figures

List of Tables

Nomenclature

AMPs   Antimicrobial peptides

APTES   (3-Aminopropyl)triethoxysilane

APTMS   (3-Aminopropyl)trimethoxysilane

bFGF   Basic fibroblast growth factor

ECM   Extracellular matrix

IFN-α   Interferon alpha

PDGF   Platelet derived growth factor

TGF-β   Transforming growth factor beta

VEGF   Vascular endothelial growth factor

VLUs   Venous leg ulcers

DFU   Diabetic foot ulcer

DMEM   Dulbecco's Modified Eagle Medium

EGFR   Epidermal Growth Factor Receptor

FBS   Foetal Bovine Serum

FDM   Fused Deposition Modelling

FDM	fusion deposition modelling
GFP	Green fluorescent protein
HSE	Human Skin Equivalent
HUVECs	Human Umbilical Vein Endothelial Cells\{}\{}
IL-1β	Interleukin-1β
LDH	Lactate dehydrogenase
M.O.M.	Mouse-on-Mouse
MDCK	Madin-Darby Canine Kidney
NHDFs	Normal Human Dermal Fibroblasts
NHEKs	Normal Human Epidermal Keratinocytes\{}\{}
PADs	Paper Microfluidic Devices
PC	Polycarbonate
PDMS	Polydimethylsiloxane
PET	Polyethylene terephthalate
PETG	polyethylene terephthalate glycol
PMMA	Poly(methyl methacrylate)
PS	Polystyrene
TNFα	Tumour Necrosis Factor α
vHSE	Vascularised human skin equivalent
µTAS; microTAS	Micro total analysis systems

Acknowledgements

I would like to express my gratitude to Nicole Pamme for her constant and unfailing support through the ups and downs of the project. Many thanks to Matt Hardman for guidance with anything related to skin biology. Alex Iles deserves a special mention for his support with fabrication of the devices and all the advice he provided me with. My gratitude is also extended to Holly Wilkinson, for her help with the explants. I would also like to thank Laden Fenercioglu and Stefano Caserta their help with the immunology experiments. This section would not be complete without thanking my friends and collogues - Sam, Pablo, Por, Martin, and Danny. This journey would not have been the same without you. Finally, I would like to thank the University of Hull for funding this project.

Abstract

Wound healing abnormalities and non-healing chronic wounds are a major clinical problem, primarily affecting diabetic and elderly patients. Wound management associated costs resulted in a £5.3 billion financial burden to the NHS between 2012 and 2013. These serious medical states are being recognised as mortal disease, with the fatality rates often higher than those of common cancers. Half of all patients undergoing chronic-wound associated amputation related to diabetes are expected to die within 5 years. The current chronic wound treatments are inadequate, and more sophisticated models are needed to advance this field, leading to better therapies. The aim of this work was to design, manufacture, and test a microfluidic device that would address the need for a physiologically accurate model of wound healing with improved assay lifespan, when compared to the classical static models. Here we present a new microfluidic device optimised for maintaining human skin samples for prolonged period of time, and wound healing analysis. Briefly, full thickness human skin explant samples were cultured on custom-made microfluidic devices, and in static culture. The skin samples were collected at the end of the culture period, fixed, sectioned and either stained using fluorescent TUNEL assay to analyse the tissue apoptosis, or using IHC, for K6 and K14 to study tissue architecture. Wound healing outcome was measured using wound samples wholemount-stained for K1 and K14. FACS analysis was performed on digested samples to study the immunological profile in the cultured samples. The final version of the skin-on-a-chip device (V4.0) was found to be successful at prolonging tissue survival. After the seven day culture period, four-fold decrease in the epidermal apoptotic cell death (1.4% apoptosis for the on-chip sample vs. 6.1% for the static control), and two-fold decrease in the dermal apoptosis (4.1% cell death in the flow-chip samples vs. 8.3% in the static controls) were observed. Day 7 samples maintained on the V4.0 device significantly outperformed the static control samples (p = 0.007). Furthermore, the average

dermal cell death for the control samples collected on day 14 was 38.1% whilst the on-chip samples exhibited dermal cell death averaging 8.3%. V4.0 samples contain significantly less apoptotic cells in the dermal section when compared to the static controls on day 14 (p = 0.0433675). The improved tissue viability makes the model more suitable for prolonged culture experiments.

Next, it was observed that the wound area is reducing in size over the period of seven days, in both cases of the V4.0 samples and the control samples. The on-chip samples yield reduced wound perimeter when compared to the static controls from the same day. the culture method has a very significant influence on the wound size ($f(1) = 75.684$, $p=5.61 \times 10^{-6}$). Interestingly, the same analysis showed that the culture method does have a greater impact on the wound closure that the assay day ($f(2) = 24.615$, $p = 0.012$). The on-chip samples produced a significantly different smaller wounds on day seven of the assay than the control static culture samples ($p = 0.012$). In addition, the overall theme seen from the FACS data demonstrated that the wounded skin samples cultured on the V4.0 microfluidic devices yielded higher levels of immune cells than the static control samples collected on the corresponding days.

Overall, The V4.0 device allowed for an increased number of cells to be collected on day seven in every single marker group, apart from in the $CD56^+ CD3^+$ group, where the levels dropped more in the V4.0 samples than in the control samples. The same relationship was noted on day three. This indicates that maintaining samples on the V4.0 device helps to improve the immune cell retention, making the microfluidic model's immune microenvironment more comparable to the real human skin microenvironment.

Chapter 1

Introduction

1.1 Skin

Skin is not only the largest organ in human body, accounting for as much as 15% of the total body weight in the adult individuals. Due to its external localisation, encapsulating almost every single other organ and tissue, it acts as a biological armour, protecting the organism from the dangers of the external world. This includes a wide range of potential hazards, including biological agents such as bacteria, mechanical hazards such as physical force which could damage delicate tissues and vital organs hidden underneath, and chemical dangers. The skin also contributes to thermoregulation Kanitakis (2002).

1.1.1 Skin anatomy and structure

Skin is a multi-layered organ, composed of three main layers - epidermis, dermis and the hypodermis (also known as the subcutaneous tissue). Fig. 1.1.1 depicts the architecture of the epidermis with its strata, which are discussed in more details below.

Epidermis is a stratified squamous epithelium acting as the topmost layer of the skin. It is considered to be a stratified epithelium because it is composed of four
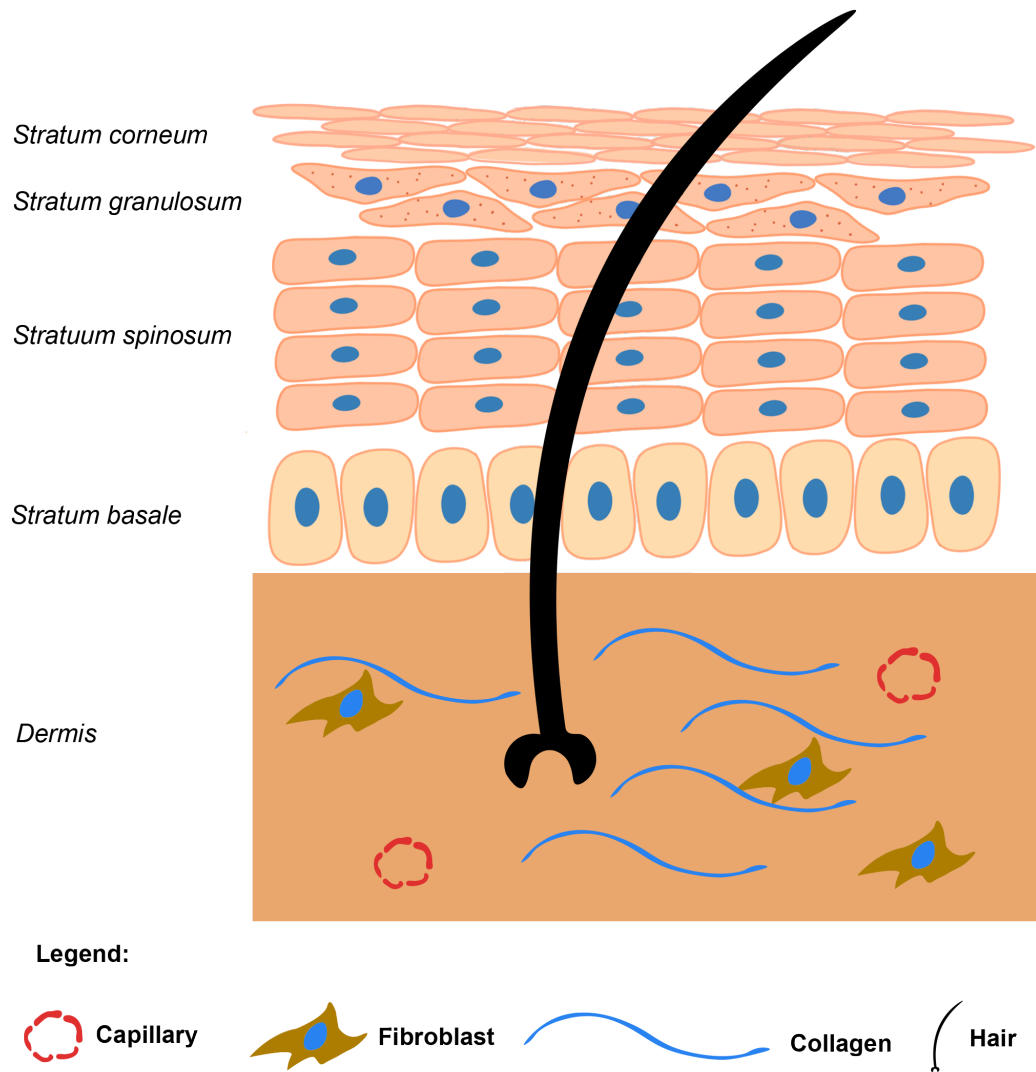
Figure 1.1.1: *Skin structure.* A schematic representation of the layers in the epidermis, with the underlaying dermis.

sub-layers, commonly referred to as strata. The names of the strata, starting from the top, are Cornified (horny) Layer - *Stratum corneum*, Granular Layer - *Stratum granulosum*, Squamous Layer - *Stratum spinosum*, Basal Layer - *Stratum germinativum* . The main cellular components of the epidermis are the keratinocytes and the dendritic cells, however one can also find melanocytes, Langerhans cells, and Merkel cells residing in this layer of the skin (James et al., 2011). Starting from the bottom of the epidermis, the first layer is *Stratum germinativum*, also known as *Stratum basale* or the basal layer, composed of a single layer of column-shaped keratinocytes attached to the basement membrane . The cells are also joined to each other and the higher layer of cells via desmosomes (Murphy, 1997). The basal layer is crucial to maintenance of a healthy skin as this is a major hotspot of mitotic activity in the epidermis, however it should be pointed out that not all cells within this layer are stem cells capable of division. (Lavker and Sun, 1982; Jones, 1996). It takes about 14 days for the basal cells to move from the basal layer to the cornified layer, and then similar amount of time for these cells to reach the surface of the epidermis (Wolff and in general medicine Fitzpatrick, 2008; Chu, 2008).

The next layer of the epidermis is *Stratum spinosum* often referred to as the squamous layer. "*Spinosum*" is Latin for spiny, and it refers to spine-resemblance of the desmosomes along cell edges. These desmosomes regulate cell-cell connection, cross-talk, and they play a major role in mechanical force distribution across the epidermis (Murphy, 1997; Chu, 2008). The thickness of this stratum is much greater than that of the unicellular basal layer, and it takes five to ten cell layers (Murphy, 1997). Another difference between *Stratum germitivum* and *Stratum basal* is the shape of the cells, which in this case are of different shapes and sizes depending on their position within the stratum (Chu, 2008).

Stratum granulosum, or the granular layer, is the next stratum in order, and also the last stratum containing live cells. This layer owes its name to the granular ap-

pearance caused by the presence of the keratohyaline granules. Keratinocytes of the granular layer are of great importance to the normal physiology of skin as they are needed for the normal keratinisation (Chu, 2008). Presence or absence of these baso-philic granules is what determines the fate of the keratinocytes. The cornified layer of the epidermis is the result of formation of soft keratin with cells, thanks to the presence of keratohyaline granules which enzymatically cleave the keratin fibres. On the other hand, hard keratin formation in the absence of keratohyaline leads to formation hair and nails (Matoltsy, 1976).

Finally, *Stratum corneum*, or the cornified layer is the most superficial stratum of the epidermis and it greatly contributes to the mechanical strength of the skin due to its keratin content. It also is this keratin content which helps the skin fulfil its function as a barrier preventing entrance of biological and chemical hazards into the body, and regulation of water loss (Jackson et al., 1993). The keratinocytes in this layer lost their nucleus in the process of irreversible differentiation and are dead (Chu, 2008; Murphy, 1997).

Crucial to skin's tensile strength and barrier function are keratins. Keratins, being one of the most abundant proteins in the integument, are of great importance to both proper functioning and also many pathologies of skin and cutaneous wound healing. There are 54 genes associated with keratin expression in humans, and as much as half of all of them are found in different parts of hair follicles. The rest are primarily skin keratins, however some are expressed in tissues throughout the body. Keratins, being intermediate filaments of the cell cytoskeleton, are essential in providing mechanical stability to the epithelial cells and tissues throughout the body (Moll et al., 2008). Keratins are often classified under two types - type I - acidic, and type II - basic or neutral. Keratins need to form obligatory pairs between these type I and type II filaments. The role of keratins is however not limited to providing tensile strength to healthy tissues. Different types of keratins are expressed in different strata of human skin, and play

different roles in wound healing. Keratin expression can be used to study keratino-cyte maturation. Certain keratins are constitutively expressed in healthy skin, for instance, the expression of K6 and K16 is associated with hyper-proliferating cells, K1 and K10 are know to be expressed in suprabasal cells undergoing differentiation, and K5 and K14 expressing keratinocytes are found in the basal stratum (Coulombe, 1997; Patel et al., 2006). During the acute wound healing, it is know that the kerat-inocytes involved in the wound healing process but positioned distal from the wound edge express K1, K10, K6, and K16. Another group of keratinocytes adjacent to the wound edge was found to express K1, K10, K6, K16, and K17. Finally, the keratino-cytes found right at the wound edge were show to express only K5 and K14 (Patel et al., 2006). Staining for K1 keratin can be used to identify the distal wound edge. The K14 staining can be used as means of visualising the leading wound edge, and K6 can be used as a marker of keratinocyte hyperproliferation.

1.1.2 Skin physiology and functions

Having discussed the anatomy and architecture of skin, let us now consider the main functions of this organ. Fig. 1.1.2 summarises some of the key physiological functions of skin.

Skin is a physical barrier, separating the external world from the vulnerable in-terior of our bodies. Control of water homeostasis is one of the most basic and yet most important tasks of the integumentary system. High death rates caused by ser-ious burns of large body areas which in turn result in dehydration, renal failure and shock from large amounts of transepidermal water loss are witness to the importance of well maintained water homeostasis by the integument (Shpichka et al., 2019).

The water-tightness and its physical barrier function of the epidermis can be de-scribed using the "Brick and Mortar" hypothesis coined by Nemes and Steinert where the architecture of *Stratum corneum* is compared to that of a brick wall, where the
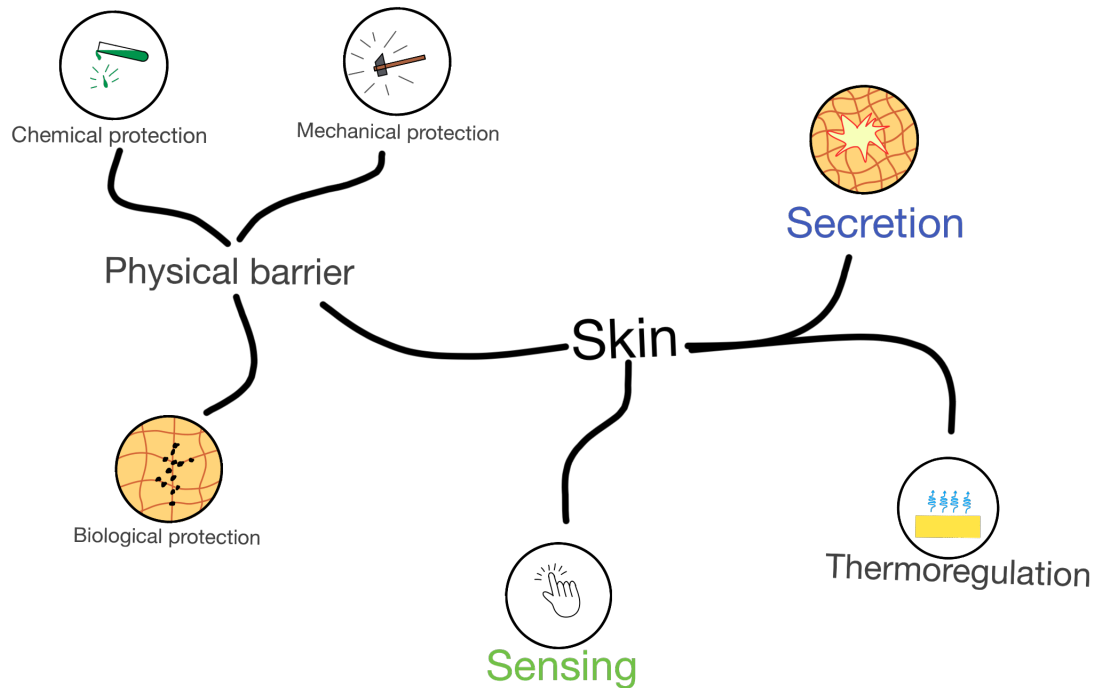
Figure 1.1.2: *The key functions of the skin.* A schematic represenatioin of some of the main physiological roles of the skin, including its roles as a physical barrier, and involvelvement in secretion, sensing, and thermoregulation.

bricks are individual corneocytes, which are linked to one another by corneodesmosomes which act like rivets. This brick assembly is then glued with mortar, which in the case of the cornified layer is a matrix composed of lipid lamellar bilayers. It is this lipid matrix which helps to trap water, which can go as far as *Stratum corneum* (Pappas, 2009).

One of the physiological roles of the skin organ crucial to wound healing is its involvement in the [response. There are two types of immune protection skin can provide - innate and adaptive. Skin fulfils its innate immunity function by acting as a physical barrier to biological hazards. *Stratum corneum* produces a range of substances with antimicrobial properties which build up in the intercellular spaces. The antimicrobial agents include glycosphingolipids, free fatty acids, polar lipids, and antimicrobial peptides (AMPs)(Ericksen et al., 2005). We are aware of sixteen AMPs produced by the skin, and they can be categorised as either defensins or thelicidins.

(Braff et al., 2005; Abdo et al., 2020).

Another protective function of skin is to shield us from the harmful ultraviolet radiation coming from the sun. This is achieved by production of melanin in melanosomes of melanocyte cells based in *Stratum basale* and just above it. Melanosomes form melanin caps that act as protective shields, reducing the negative impact of the UV radiation (Costin and Hearing, 2007). Vitamin D production is another sun-related function of skin. Vitamin D is a lipid-soluble prohormone typically found in the cell membranes of keratinocytes in *Stratum basale*. Dermal fibroblasts also express it. Vitamin D is produced from its precursor 7-dehydroxycholestrol which is then modified into previtamin D3. This is then hydroxylated in liver or kidney to 1,25-dihydroxyvitamin D. (Piotrowska et al., 2016; Pillai et al., 1988) (Pillai et al., 1988)

When discussing skin's role in body's response to the radiation of the sun, it is worth stopping to consider temperature control. The integument system is crucial to how our body perceives the outside world, and the temperature of the surroundings is of great concern as it is constantly affecting human physiology. First of all, skin has a passive body temperature control ability via the adipose tissue that accumulates under the skin which acts as an insulation layer reducing heat loss. On the other hand, skin has the ability to increase heat loss by encouraging sweat production and increasing blood flow through highly vascularised dermis. For active temperature control, the integument utilises its thermosensory function as it can sense the temperature of the surroundings and then feed it back to the thermoregulatory system in order to produce a range of reactions such as vasoconstriction, vasodilation, erection of the hair pilli and so on (Nagasaka et al., 1987; Romanovsky, 2014).

Finally, we have already touched on skin's sensory function in terms of its ability to assess the temperature of the surroundings. Skin's sensory abilities are much greater than just sensing temperature. Mitsuhiro Denda went as far as suggesting that skin can be considered "the third brain" (after the gut being second). This suggestion is

based on the fact that skin possesses a wealth of environmental sensors, it is capable of processing sensory information and it is capable of affecting the emotional state of the person through by releasing neurotransmitting agents and signalling molecules like hormones (Denda, 2015).

1.2 Wound healing

Since skin is the outermost organ of human body, constantly exposed to the outside world and mediating our experience of everything around, it will be no surprise to find out that it often gets injured. A lot of time the injury to the integument is accidental, but there are occasions when it's inflicted deliberately - during medical interventions (Sen et al., 2009).

Injury to the skin creates several problems to the human body. First of all, lack of skin's integrity allows bacteria and other pathogens to enter the system. Secondly, the injury to the vascular system may lead to uncontrolled blood loss which could be fatal. As a result, the wound healing process needs to not only repair the injury to the skin but also stop the haemorrhage. Because of this, the first stage of wound healing actually involves initiation of coagulation cascades to limit the blood loss which could prove fatal, if not controlled (Reinke and Sorg, 2012; Eming et al., 2014).

Wound healing process is typically very successful, and most of smaller wounds heal well without any complications. The problems begin to appear when the wound size is greater or when the patient has comorbidities that can affect wound healing. Unfortunately we know relatively little about wound healing abnormalities such as pathological scaring (Reish and Eriksson, 2008).

Here we will discuss the standard wound healing process in healthy humans, and then we will consider the wound healing abnormalities. Fig. 1.2.1 summarises the key stages, cells, and molecules involved in the wound healing process.
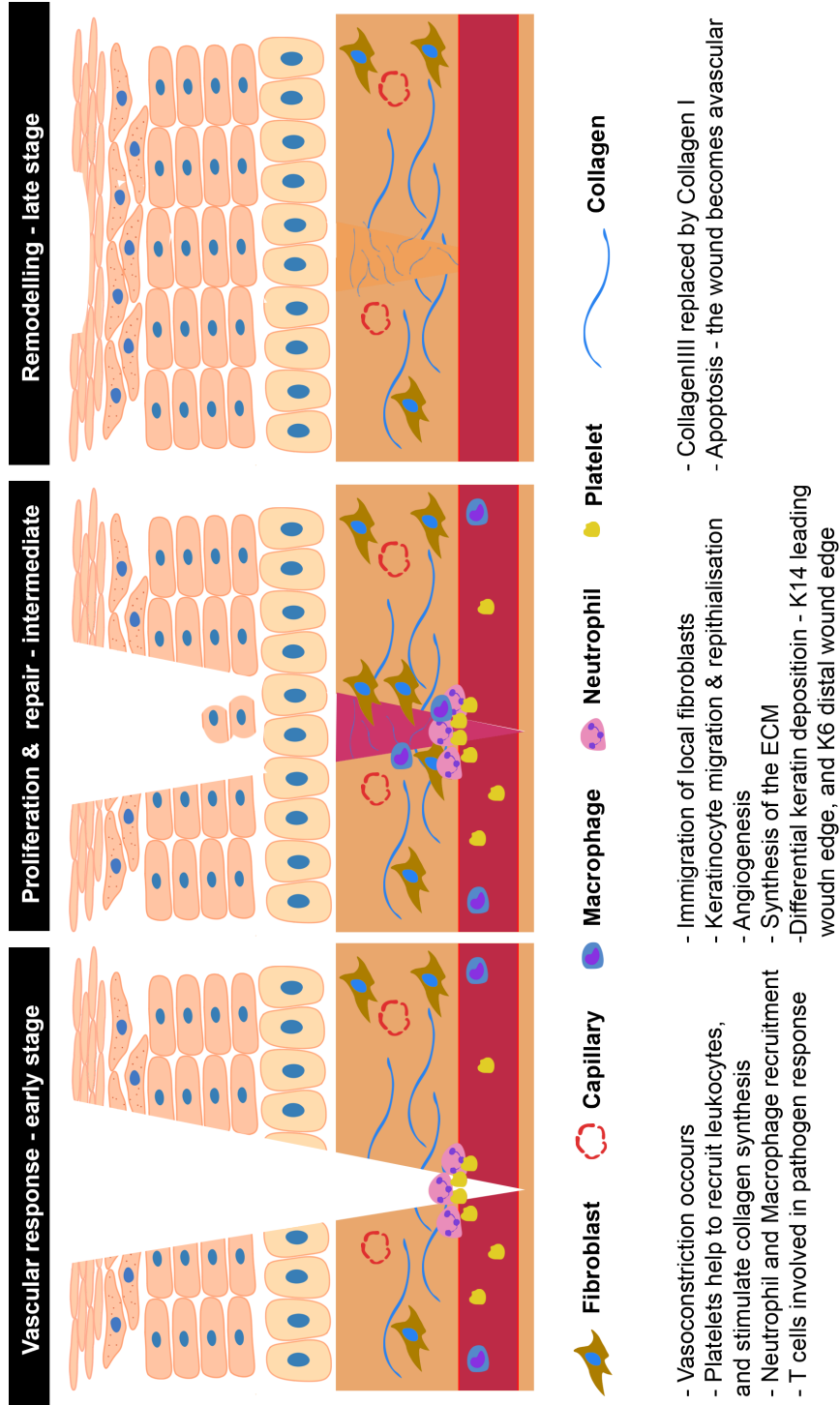
Figure 1.2.1: *Wound healing process overview*. A graphical summary of the key three stages of the wound healing process: the vascular response, proliferation & repair, and the remodelling stages.

1.2.0.1   The vascular response

The thrombosis (clotting process) is brought about by two clotting pathways. The intrinsic pathway is mediated by the clotting factors released from the site of the injury, whereas the extrinsic pathway involves the thrombocytes being activated by the exposed collagen fibres in the wound area.

The result of those two pathways is formation of a thrombus (clot) which not only stops haemorrhage, but also creates a physical barrier stopping entrance of pathogens into the body. The thrombus additionally plays a role of a matrix or a scaffold allowing the immune system cells, keratinocytes, fibroblasts and the endothelial cells to migrate on during regeneration of the injured tissue. The clot also acts as a reservoir for numerous growth factors. The main molecules contributing to the composition of the clot include fibrin, thrombospondins, fibronectin and fibronectin (Reinke and Sorg, 2012).

Apart from initiation of clot formation, the injury also induces the process of local vasoconstriction (constriction of the vessel) via activated platelets, which typically lasts 5-10 minutes. This is crucial in assisting reduction of blood loss and allowing the clot to develop. The combination of vasoconstriction and thrombosis consequently reduce oxygen access to the wound area, and what comes with it, higher rates of glycolysis and alterations in the pH. Healthy wound healing requires vasodilation to occur after vasoconstriction. This will allow perfusion of the injured area, bringing thrombocytes to the newly created clot. Platelets, the key cellular part of clot formation, play important role in wound healing. One of those roles involves release of the chemoattractants such as cytokines and growth factors (Reinke and Sorg, 2012).

1.2.0.2   The cellular response

The second phase of the wound healing process takes place shortly after vasoconstriction and initiation of thrombosis. There are two parts to the inflammatory phase.

22

The early phase involves neutrophil recruitment, which is then followed by the late phase involving monocytes being recruited to the site of injury, and their transformation. The establishment of inflammation during wound healing is crucial not only for debridement, removal of the decaying tissue or pathogenic agents, but also it produces a plethora of signalling molecules which will orchestrate cellular movements which are fundamental to the upcoming repair processes that will follow, leading to successful wound closure (Leibovich and Ross, 1975).

Interestingly, it has been suggested that the amount of inflammation is directly proportional to the amount of scarring present at the site of wound repair (Bullard et al., 2003; Redd et al., 2004). This is an interesting concept that could benefit the field of regenerative medicine, if explored properly, leading to scarless wound healing. The neutrophils are typically present at the site of injury for 2-5 days. Their contribution to the process of wound healing is invaluable. Neutrophils can phagocytose the encountered bacteria, but also, they are capable of using secreted proteases to kill the invading bacterial pathogens. It is also important to point out that the neutrophils do not act on their own. In fact, one of their jobs is to release chemoattractants which would bring other immune cells to the site of injury (Eming et al., 2007). Apart from recruitment of immune system cells, neutrophils also help to clean up the necrotic tissue by releasing a cocktail of several proteases and antimicrobial agents (Eming et al., 2007).

1.2.0.3 Proliferation and repair

Reepithialisation

This stage is key to wound healing as this is when the injured surface of the skin is replaced with a new one and the vascular system is reestablished. This complex process is orchestrated by the stem cells which typically reside in the sweat glands and the hair follicles, and the keratinocytes from the edges of the wound (Martin,

1997; Miller et al., 1998; Roh and Lyle, 2006; Lau et al., 2009).

As most of the other wound-healing processes, the reepithelization phase is also controlled by cytokines. Since one of the aims of reepithialisation is to close the gaps in the injured tissue, and to regain mechanical strength in the wounded area of the skin; remodelling of the extracellular matrix (ECM) in the wound area is of great importance, as it is the ECM which will greatly contribute to both restoration of the strength of the skin, and it will allow for migration of keratinocytes to resurface the skin gap. Synthesis of new matrix is regulated by molecules such as Interferon alpha (IFN-α) or Transforming growth factor beta (TGF-β) and they control production of collagen fibronectin, and other ECM components.

Wounding of skin results in mechanically-induced signalling which contributes to the initiation of wound healing. Namely, the injury leads to loss of contact inhibition and physical tension at cellular junction such as desmosomes and hemidesmosomes, leads to activation of SRC kinases, the effect of which includes up-regulated membrane permeability to calcium ions. In the process of keratinocyte shuffling, collagenase and elastase enzymes loosen the desmosome junctions between the cells, allowing keratinocytes to begin migration along a chemotactic gradient, over fibronectin-based clot, towards the epicentre of the wounded area (Clark et al., 1982; Clark, 1983; Jacinto et al., 2001).

The keratinocytes, now free to migrate, move to the centre via the process of lamellipodial crawling which is regulated by RhoGTPases such as Rho, Rac and Cdc42. The movement process depends on polymerisation of cytoskeletal actin fibres and formation of new integrin-mediated focal adhesions, and it ends when the cells touch each other. At that point, when the opposing epithelial sheets come close together, the filopodial actin fibres are degraded and replaced by intercellular adhesion complexes which reinforce the closed epithelium (Nobes and Hall, 1995, 1999; Jacinto et al., 2001).

Neovascularisation and Angiogenesis Closure of the injured tissue is not the only part of wound healing. Another equally important process is that of vasculature repair and restoration. This can be classified as either neovascularisation, which is *de-novo* vasculature production, and angiogenesis, which is formation of blood vessels from the existing vasculature. Repair and restoration of the injured vasculature is a complex process, orchestrated by growth factors such as vascular endothelial growth factor(VEGF), platelet derived growth factor (PDGF), basic fibroblast growth factor (bFGF), and thrombin (Reinke and Sorg, 2012).

New vessel formation relies on vessel sprouting – a process where the endothelial cells of the existing vasculature begin migration towards the wound, forming tubular structures which will grow to become the restored vasculature. This begins with the growth factors to different receptors located on the endothelial cells of the existing vasculature, which leads to initiation of singling cascades. For the sprouting to occur, the endothelial cells need to be able to move through the dense mesh of fibres of the extracellular matrix, and to leave the confinement of the basal lamina. This is brought about by release of proteolytic enzymes by those endothelial cells, which cleave the fibrous proteins of the basal lamina, allowing the cells to migrate (Reinke and Sorg, 2012; Eming et al., 2014).

Granulation Tissue Formation

The proliferation phase of wound healing ends with formation of the granulation tissue, which is a transitional tissue which acts as a replacement for the fibrin-based matrix and then may turn into a scar tissue once matured. The components of the granulation tissue are mainly cellular and apart from collagen and capillaries, also include immune system cells such as macrophage and granulocytes, but also fibroblasts. This high cellular content gives the tissue a granular appearance, hence the name. Also, at this stage, restoration of the vascular system has not finished yet, therefore the area is highly vascularised (Eming et al., 2014).

1.2.0.4 Remodelling

The last process of wound healing is remodelling, mainly considered with remodelling of the ECM. This process begins around day 21 after the injury and can last for up to one year. One of the main events taking place during this phase involve replacement of Collagen III by Collagen I which is stronger and will provide the wound with the much-needed tensile strength. Additionally, myofibroblasts utilise their attachments to collagen to contract the wound and reduce the surface area of the developing scar. Mature wound tissue after formation of the granulation tissue should now be acellular and avascular. Angiogenesis should stop all together, restriction blood flow to the wound, leading to decrease and eventually complete termination of metabolic activity in the area (Reinke and Sorg, 2012).

1.2.1 The immune system and wound healing

As already mentioned, the immune role plays a crucial role in orchestrating many events essential to the successful healing of a wound.

The first cell type to arrive at wound site is platelets. Platelet activity initiates coagulation cascade which helps to reduce blood loss and it provides ECM as a platform for the cells coming to the site to work on.

Platelets also secrete growth factors such as PDGFs and TGF-1. These have chemotaxic activity by attracting fibroblasts and mesenchymal cells. Growth factors released by platelets also activate fibroblasts, mesenchymal cells, and neutrophils and macrophages in the wound vicinity (Diegelmann and Evans, 2004; Martin and Leibovich, 2005).

Neutrophils are typically the first immune cells to enter the wound site. They release a range of cytokines and antimicrobial agents such as reactive oxygen species (ROS), and antimicrobial peptides and proteases. Neutrophils secrete cytokines and growth factors such as IL-17 and VEGF which have a dual action – by attracting im-

mune cells, and inducing proliferation of fibroblasts, keratinocytes and endothelial cells (Kolaczkowska and Kubes, 2013; Wilgus et al., 2013).

Neutrophils enter apoptosis around 24 hours after coming into the wound site, which is associated with release of chemoattractants which recruit monocytes into the wound site, which then differentiate into macrophages. Monocyte-derived macrophages are considered to be the most important immune cell type involved in the process of wound healing. They can remain at the wound site for up to several weeks (Temenoff and Mikos, 2008; Willenborg and Eming, 2014; Murray and Wynn, 2011).

Macrophages undergo phenotype changes from M1 state, which is also called classically activated state, into M2 state which is called alternatively activated state. This switch in states changes the wound environment from pro-inflammatory to anti-inflammatory (Delavary et al., 2011).

The M1 macrophages help to remove microbes, fragments of the damaged matrix, cell debris, but also neutrophils. On the other hand, they secrete cytokines and growth factors such as IL-1, FGF-2, PDGF, VEGF or IFN-γ. These in turn upregulate proliferation of fibroblasts, keratinocytes and epidermal cells and help the macrophages to transition to M2 state (Farrar and Schreiber, 1993). The additional role of IFN-$\gamma$is attraction of the T cells to the wound site and stimulation of CD4+ type 1 T-helper (TH1) polarisation (Sallusto and Baggiolini, 2008; Baggiolini, 1998; Farrar and Schreiber, 1993).

Once the macrophages enter the M2 phase, they start releasing anti-inflammatory cytokines such as TGF-1 which in turn upregulate ECM synthesis and stimulate wound contraction (Smigiel and Parks, 2018). M2 macrophages also need to phagocytose the remaining debris from the wound area and reorganise the ECM in the final stage of the wound closure (Temenoff and Mikos, 2008).

This highlights how essential the immune system is in orchestrating the different events and stages of the wound healing process so that everything occurs at the right

time and in the right order.

The earlier mentioned T lymphocytes require more attention since they are skin resident, and therefore are of particular in *ex-vivo* models.

Each T cell carries a T cell receptor (TCR) of which epitope is CD3. TCR plays a role in antigen identification. The T cells also express either a CD4 or CD8 receptor, which are involved in binding to the Major histocompatibility Complex (MHC) in the process of antigen presentation with an antigen presenting cell (APC)(Gao et al., 2002).

CD4 and CD8 receptors can be used to categorise the T cells as either helper T cells, if expressing CD4, and cytotoxic T cells if expressing CD8.

The roles of those T cell subtypes are fairly self-explanatory. The helper CD4 T cells help to recruit other immune cells to the site. This can be done via chemoattraction of immune cells, or cytokine-mediated activation of nearby cells to involve them in the immune response.

Helper CD4 T cell support the immune response by the robust generation of cytokines and chemokines that either activate neighbouring cells to perform specific functions (cytokines) or recruit (chemokines) new immune cell subsets to sites of pathogen encounter.

The role of CD8 expressing cytotoxic T cells is more acute, as they directly engage with the pathogen or a tumour cell and kill them by lysis, which is mediated by the delivery of cytotoxic granules.

The regulatory T cells are another subset of T lymphocytes. These CD25 expressing cells help to regulate and control the immune response to ensure that it is not excessive, the consequence of which could be immunological pathology (Kuniyasu et al., 2000; Marabelle et al., 2013).

Another T cell subtype that is important to the cellular response of the wound healing is the CD56 expressing Natural Killer (NK) T cell. Similarly to the regulat-

ory T cells, NK T cells also regulate the immune response in the wound healing process (Godfrey et al., 2000). These cells are not skin resident, however they enter the wound site early during the healing process, similarly to neutrophils (Harding et al., 1992).

1.2.2 Wound healing problems

Should the would healing process not go according to plan, the end result can be either a chronic wound (ulcerative skin defect) or a hypertrophic scar, also known as a keloid (Eming et al., 2014).

1.2.2.1 Chronic wounds

If the wound healing process does not finish within the expected time period, we can normally classify such wound as chronic. Those wounds are further categorised based on their aetiology. The main types of chronic wounds include venous leg ulcers (VLUs), arterial ulcers, diabetic foot ulcers (DFUs) and pressure ulcers.

The basis of VLUs are largely unknown, but some of the recent finding led to theories suggesting that alterations in the molecular singling, changes in expression of specific microRNAs, affected or impaired migration of keratinocytes and chronic or persistent inflammation contribute to the wound pathology (Eming et al., 2007; Stojadinovic et al., 2008; Charles et al., 2008; Pastar et al., 2012). This type of chronic wound is the most frequently found variety of leg wound in and it is one one of the consequences of the chronic venous disease(Bergan et al., 2006). The other two types of chronic wounds also frequently found on legs or feet include arterial ulcers and diabetic foot ulcers.

Arterial ulcers result from reduced blood flow and so necrotic tissue damage and hypoxia. These wounds are the second most common type of chronic wounds. Diabetic foot ulcers are associated with the occurrence of diabetes mellitus - the most fre-

quent comorbidity linked to non-healing wounds. Interestingly, it is unclear whether the diabetic wounds are caused by insulin deficiency or by its consequences (Nolan et al., 2011).

Pressure ulcers occur mainly in bed-bound or wheelchair-bound patients who are often elderly and suffering from several co-morbidities. Extensive sitting or laying down might lead to tissue necrosis caused by the mechanical forces associated with constant pressure created by the weight of the body trapping soft tissue between a bony area such as the pelvis, and an external object such as a bed or a wheelchair.

The common characteristics of the chronic wounds include the localisation - they typically occur on the lower body extremities, and the age group - they are typically found on elderly patients. These serious medical states are being slowly recognised as mortal disease, with the fatality rates often higher than those of common cancers such as breast or prostate cancer. The magnitude of the problem is well pictured when one realises that half of all patients undergoing amputation related to a diabetic state will die within 5 years (Armstrong et al., 2007; Aulivola et al., 2004; Sargen et al., 2013).

1.2.2.2 Pathological scarring

The other type of wound healing abnormality is scarring. Scaring is the result of imperfect regeneration of injured tissue. Human skin has the capacity to regenerate perfectly only in the foetus (Lorenz et al., 1992). Pathological scaring can be classified as either hypertrophic or keloid. Everyone is familiar with hypetrohpic scarring - the classical scar tissue formed in response to skin injury. Keloids on the other hand are scars that extend beyond the wound area, and might have underlying genetic causes.

Pathology of wound healing

We will now have a closer look at the mechanisms governing the wound healing abnormalities mentioned so far. These mechanisms can be either of immunological nature,

they might be associated with a microbial infection, activity of proteases, there might be a stem cell involvement, or the problem could be of senescence nature.

It is well know that the immune system is crucial to the normal wound healing, however deregulation of the immune response can have the opposite effects, delaying or stopping complete wound closure. Chronic wounds have been show to be locked in state of inflammation which doesn't resolve (Eming et al., 2009). The delayed healing due to prolonged inflammatory response is believed to be caused by increased and prolonged presence of macrophages and neutrophils in the would site (Sindrilaru et al., 2011; Loots et al., 1998). This in turn leads to abnormal levels of IL-1β (Interleukin-1β) and TNFα (Tumour Necrosis Factor α), which are important proinflammatory cytokines with the capacity to delay wound closure if deregulated, by upregulating the presence of proteases such as MMPs in the wound area. This in turn causes increased cleavage of the ECM, negatively impacting cell migration (Beidler et al., 2009; Barrientos et al., 2008; Tarnuzzer and Schultz, 1996). Gelatinases A and B are MMPs that are know to be overexpressed in the chronic wounds (Eming et al., 2010; Yager et al., 1996).

Presence of infection is inevitable, and it affects all wounds to lesser or greater extent. Microbial presence in the wound is not a problem unless it can no longer be managed by the body's immune system. One of the greatest problems bacteria can pose to wound healing is formation of a biofilm (Pastar et al., 2013). Furthermore, the success of wound healing is improved by the activity of stem cells such as adipocyte progenitor or melanocyte progenitor cells (Chou et al., 2013). We are aware that recruitment of those cells to the wound site is affected in medical conditions that have negative effect on the process of wound healing, such as advanced age and diabetes (Pastar et al., 2010; Barrientos et al., 2008). Another mechanism leading to non-healing wounds involves abnormalities in vasculature formation within the injury area. Healthy vasculature is key to delivery of sufficient levels of oxygen and

nutrients to the respiring cells. This is as important to a healthy tissue as it is to a regenerating skin after damage. It will not come as a surprise to find out that compromised angiogenesis (vasculature formation from pre-existing vasculature) will be contributing to the healing impediment of chronic wounds such as diabetic foot ulcers (Brem and Tomic-Canic, 2007). Angiogenesis deregulation in the non-healing wounds is associated with imballance of pro- and anto-angiogenic molecules. For instance, it has been observed that the chronic wounds such as DFUs are characterised by upregulated expression of myeloperoxidase, an anti-angiogenic factor. On the other hand, the levels of the pro-angiogenic factors such as extracellular superoxide dismutase are lowered that those in the acute wounds (Krisp et al., 2013). Other pro-angiogenic factors such as VEGF and its family members are also degraded in chronic wounds, which is a major contributor to the pathology (Hoffmann et al., 2013; Lauer et al., 2000). Finally, senescence, or the biological ageing, has also been recognised to be a factor in the pathology of non-healing wounds. It is not entirely clear how the senescence contributes to the delayed healing however several hypothesis have bee put forward (Rodier and Campisi, 2011). It has been proposed that senescent fibroblasts might be proliferating uncontrollably, leading to fibrosis seen in keloids (Blazić and Brajac, 2006). Senescent fibroblasts have also been reported to be inefficient at migration (Brem et al., 2008). On the other hand, keratinocytes affected by senescence are know to secrete maspin, a protein negatively regulating angiogenesis (Nickoloff et al., 2004). There are many such examples of different mechanisms driving the pathology of non-healing wounds interacting and affecting one another. This is also why it is such a great challenge to design effective therapies against this mortal disease.

1.3　Micro total analysis systems

1.3.1　Introduction to microfluidics and micro total analysis systems

The advent of micro total analysis systems in the second half of 1970s is what gave birth to microfluidics - a multidisciplinary field bringing together expertises such as chemistry, physics, engineering, and biology in order to design, create and utilise miniaturised analytical devices with the capacity to efficiently and quickly carry out reactions and procedures which would otherwise require greater reagent costs, larger time investment or they would be compromised in a different way. The scientific community and the general public have been referring to the field of microfluidics and the microfluidic devices using a range of terms which can be used interchangeably most of the time. These include microfluidic chip, microfluidic device, chip, lab-on-a-chip and microTAS device. The frequent use of "chip" in the nomenclature is a witness to microfluidics' heritage in precision manufacturing such as photolitography, which was, and still is used to create silicone electronic chips. The first microfluidic devices were actually also manufactured in silicone, and their fluidics channels also bore a level of resemblance of the circuitry of the electronic chips.

The first modern microfluidic device to be published in a peer reviewed journal was a gas chromatograph device presented by Stephen Terry et al.(Terry et al., 1979). Unfortunately, the scientific community was slow to adapt the invention (Reyes et al., 2002). The world of microfluidics entered its "Renaissance" period in the early 1990s, starting with Andreas Manz' presentation of a miniaturised liquid chromatograph, and a revolutionary publication on "Miniaturised Total Chemical Analysis Systems" which coined now frequently used term of microTAS or μTAS (micro total analysis systems) (Manz et al., 1990b,a).

The rationale behind miniaturisation of scientific apparatus and chemical reac-

tions was actually not reduction in size, but improvement in the performance of the devices, which weren't capable of particularly good sensitivity. It then appeared that the reduced size of the analytical device had additional advantages such as reduced reagent consumption and so lower operation cost. In addition, the new µTAS chips could integrate sample handling, analysis and detection in a single device (Reyes et al., 2002).

Exactly 30 years on from the year µTAS term was coined, microfluidics grew into a large research field and its applications include industrialised processes, medicine, environmental monitoring, and basic research in life sciences. New methods designed specifically for microfluidic devices, and the old and established methods that were modified for use on microfluidic platforms benefit from the aforementioned advantaged of the µTAS technology(Kovarik et al., 2013).

Microfluidics takes its advantages over the classical methods from the difference in fluid behaviour at the micro scale. In the next section we will consider the most important differences in fluid dynamics at a small scale, and their implications for µTAS devices.

1.3.2   The physics of microfluidics

In order to fully understand the benefits of the microfluidics technology, it is essential to consider the physics governing it. Fluids at small scale behave fundamentally differently than they do at a macro scale. There are four key flow characteristics which we will briefly discuss here to explain how and where microfluidics surpasses conventional scale assay systems. The first characteristics is linked to the relationship between the velocity of the fluid, its density, viscosity and the channel dimensions. This is describe by the Reynolds equation (see Eq. 1.1). Reynolds number is a dimensionless value that considers the ratio of inertial and viscous forces involved in the fluid flow.

$$Re = \frac{\rho v d}{\mu} \qquad (1.1)$$

Here ρ indicates fluid density (kg m^{-3}), v - velocity of flowing fluid (m s^{-1}), d - diameter of the channel (m) and μ - viscosity of fluid (N s m^{-2}). For the channels with a non-circular area, d can be replaced by $\frac{4A}{P}$, where A indicates cross sectional area of the channel (m^2) and P - wetted perimeter of channel (m).

It is clear from the equation that the Reynolds number decreases when so do the channel dimensions (Reynolds, 1883). When Re is smaller than 2000, the flow within the channels is laminar. This is of great advantage over the turbulent flow, which has corresponding Re number of 4000 or more. Laminar flow is one of the fundamental advantages of microfluidics. Because of lack of eddy currents and stochastic mixing, the flow is highly predictable and it is much easier to carry out flow dynamics calculations on laminar flow. Furthermore, lack of turbulence means that the only way liquids can mix is via diffusion, which is also highly predictable and it makes it much easier to design and create more accurate models. Mixing only via diffusion can however pose problems whenever mixing is required. In such cases, additional microfluidic mixing features have to be implemented in order to improve mixing.

The second set of physical phenomena contributing to microfluidics performance are surface tension and interfacial tension. The effects of the surface tension and the interfacial tensions are more significant than the effect of gravity at microfluidic scale. The benefits of this is what makes droplets microfluidic devices a possibility (Becker and Gärtner, 2012).

The dominance of the capillary forces over the gravity is the third physical difference between microfluidics and the macro-scale systems. The capillary action allows fluid to travel through capillary channels and through materials with appropriately sized pores such as paper. This is the basis of the flow mechanism in many simple analytical devices such as pregnancy tests or paper analytical devices (PADs) which

are also considered to be a type of microfluidic devices (Martinez et al., 2007).

Because of the small sizes of the microfluidic features such as channels, the diffusion times are much reduced. This is another key difference between "normal scale" and microfluidics assays. The diffusion time can be assessed using Eq. 1.2, where t is the diffusion time (s), x is the diffusion distance (m) and D is the diffusion coefficient (m^2 s^{-1}).

$$t = \frac{x^2}{2D} \tag{1.2}$$

1.3.3 Fabrication approaches in microfluidics

A wide range of manufacturing techniques are suitable for microfabrication of the µTAS devices. Historically, the the devices were made out of silicone or glass. This has changed substantially over the years.

Different fabrication techniques are available for different types of materials. The researcher needs to be able to select the right material based on the purpose of the microfluidic device. Next, the suitable fabrication technique has to be selected to achieve the desired feature. Sometimes the material and technique is chosen simply because it is easier to carry out, cheaper or perhaps it might be the only easily available fabrication method available to the researcher. For example, one of the many reasons why PDMS (Polydimethylsiloxane) moulding appealed to so many scientists over the years is because once the mould of the device has been obtained, the moulding and preparation of the devices can be achieved without the need for expensive machines such as a CNC milling machine, or without use of very dangerous substances such as HF acid. Here we will briefly discuss some of the key fabrication approaches, together with the suitable materials that can be used with them.

As already mentioned, moulding is one of the most common techniques used to fabricate entire devices or their parts. This is typically done by filing a negative mould with a pre polymer, such as PDMS, which would then cure to form a more rigid polymer. PDMS moulding is in fact the most frequently adopted fabrication technology in the microfluidics world. PDMS moulding is suitable for devices of almost any size. Both large and small features can be faithfully recreated in this material. The benefits of this method include ease of fabrication. Once a suitable mould is obtained, it can be reused almost indefinitely to produce identical copies of the device. The cost of PDMS is also considered to be inexpensive. The material itself has interesting properties valued in biosciences, such as oxygen permeability and biocompatibility, making it an appealing candidate for fabrication of chips that would be used for tissue or cell culture. In case of PDMS moulding, a bottom or top plate made out of a different material (such as glass, a thermoplastic etc) is used to seal off the channels. It is important to highlight that PDMS is not without disadvantages. Even though oxygen permeability might be very appealing to many, it can be a serious disadvantage to those who work with systems where oxygen concentration has to be modified. An example of that could be hypoxia studies - having an oxygen permeable membrane would make it challenging to control the oxygen conditions inside of the culture chamber. Furthermore, PDMS pores are large enough to allow for certain small molecules to be absorbed inside, leading to potential alterations in the concentrations of molecules crucial to the experimental success. Furthermore, the oligomers of the uncured PDMS can leach out and affect the experiments, especially if it relies on cell culture (Toepke and Beebe, 2006).

Another form of moulding applicable to making of microfluidic devices is injection moulding.

Next, hot embossing is another technique suitable for fabrication of microfluidic devices. A negative of the device is made, typically in metal, to form a "stamp". This

stamp is heated up to around 50°C above the glass transition temperature of the thermoplastic used, and then it is pressed against the face of the polymer to create an impression of the microfluidic channels and other features. Poly(methyl methacrylate) (PMMA) is a material frequently used with this technique, but other thermoplastics such as PC are also gaining popularity. One of the advantages of embossing is no need to wait for the material to cure. The rigidity of the material may also be of interest as the top of the channels embossed in a rigid plastic like PMMA is not likely to cave in like it could with PDMS. The choice of a thermoplastic such as PMMA or PC is also important when the downstream fabrication or modification techniques might require rigid construction, for example when the device has to be threaded to accept screws, or if a gasket has to be firmly held in between two hard surfaces.

CNC milling is another approach suitable for rigid thermoplastics like the ones already mentioned. Furthermore, it is not limited to only plastics, but can be successfully used with glass and even metals. This technique requires a trained operator to use a computer controlled milling machine to mill out the channels and other features in the material of choice. One of the main limitation of the technique is the tool size. The finest milling tools have a cutting diameter of around 300 µm, essentially limiting the minimum channel width to that value. For milling in glass, the finest milling bits available are around 1 mm. The technique is considered much slower than the previously mentioned ones, but it also allows the user to manufacture features with greater aspect ratio than those made by embossing. The moulds and stamps mentioned in the previous techniques would be produced by CNC milling. Another disadvantage of milling is wall roughness, which is eliminated in the other techniques.

When working with glass, the method of choice for many scientists will be photolithography. This was originally the method used in the first microfluidic devices as it was inspired by the MEMS industry. It was however adapted to be used with glass, and not silicone wafers. Briefly, the method requires a design of the channels

and features to be transferred onto a photoresist mask. Hydrofluoric acid etching is used with the method to remove glass. Recently, a novel method for fabricating channels in glass has been described, where a picosecond pulsed laser is utilised to etch the channels in glass without the need for chemicals such as hydrofluoric acid (Wlodarczyk et al., 2019).

Finally, fabrication of PADs can be performed using various methods, with one of the most commonly used being wax printing. PAD devices can be made on a wax printer, where wax is melted through a paper of suitable porosity to create liquid impermeable barriers, to keep the reagents in defined areas. Such PADs can be used in various lateral flow or spot assays. In addition, SU-8 can be applied onto paper, and photolithography can be used to create the desired patterns (Yu and Shi, 2015; Martinez et al., 2008).

It is very important to mention that modern microfluidics rarely relies on one material or one fabrication method, as this used to be the case in the early days. Many devices, like the ones presented by Uwe Marx' group are composed of layers of different materials chosen in such way to maximise the device's performance thanks to material's advantageous properties (Ataç et al., 2013a; Wagner et al., 2013a). Different fabrication and post fabrication methods are used to produce individual layers, to bond them and to treat the surfaces of the microfluidic features if needed.

1.4 Applications of Lab-on-a-chip

1.4.1 Organ-on-a-chip

One of the major and fastest-growing applications of the lab-on-a-chip technology is organ-on-a-chip. Organ-on-a-chip is a concept of reproducing the application-dependent biological aspects of the complexity of the human body on a microfluidic device. These aspects might include the cell types, tissue architecture, perfusion rate,

shear forces, molecular environment including cytokines, or other desired characteristics. It sometimes is referred to as human-on-a-chip in order to emphasise the attempt at modelling not only one organ, but actually some aspect of interactions between several organs or tissue types. Most of the applied and fundamental research into human physiology and pathology is carried out on simplified models, where cells are isolated from tissues, and very often a biological experiment would utilise a 2D monolayer of such cells grown on a typically plastic surface, coated in such way to allow the cells to adhere. This approach has many advantages as we possess a wide array of tools that we can use to both control and modify the behaviour and physiology of cells in 2D culture. On the other hand, the 2D models differ vastly from the actual biological systems that they are to represent. For instance, a monolayer of keratinocytes cannot represent the complexity of skin as an organ. This becomes very obvious when one considers wound healing as a case scenario, where several cell types are involved in a long and complex process making use of plethora of molecular events (Ravi et al., 2014). A step forward from the simple 2D cell culture system is a 3D culture system. There are several types of 3D cell culture including the spheroid culture, where the cells are cultured in round-bottomed wells on a low-adhesion substrate, forcing the cells to assemble together and form spherical aggregates. The advantages of the spheroid model are the added complexity of cell-cell interactions in 3D. The trade-off is the fact that due to the considerable size of the spheroid (hundreds of micrometers), the centre becomes hypoxic due to insufficient oxygen diffusion. This can be a very attractive model, however, to those wishing to study the aspects of hypoxia. It is important to point out that spheroids can be grown in several ways, yet that is beyond the scope of this thesis. The other type of 3D culture is an acinum culture. Acini are hollow spheres of cells, naturally found in glandular tissues, where they are responsible for secretion of products of the glands they belong to. A classical way of growing these 3D structures is by seeding cells capable of forming acini (e.g.

prostate epithelial cells) on well surface coated with a hydrogel that can stimulate the acini formation providing the structural support and a source of mechanosensory signalling.

The cells can be alternatively mixed with the hydrogel, allowing them to adhere to each other rather than to a hard substrate. Such set-up might be utilised for studying anchorage-independent survival (Zeeberg et al., 2016).

A classical hydrogel of choice is Matrigel, as it is a well-studied model of the ECM. This system is a great platform for studying many biological scenarios (Ravi et al., 2014). It benefits from physiologically accurate cell-cell interactions and also cell-ECM interactions. Also, the lumen of the acini is intact which can be used to study the secretion processes that would occur in the acini of the glandular organs. Organoid culture is pretty similar to the acini culture in a way that they form morphological representatives of the organs that they are supposed to model, whilst retaining some physiological activity of those organs. A selection of singling molecules such as growth factors must be used in order to produce these structures. Despite this wide array of cell and tissue methods, there is still need for improvement.

As we have seen, there are numerous types of simple biological models that can be used to recreate and study human physiology and pathology. The main problem with the simple models is that they are not always good representations of the physiological mechanisms occurring in the human body, however, increasing the complexity and sophistication of the models does have its trade-offs. More advanced models tend to be more expensive to set up, and the experiments are often more time and resource consuming (Esch et al., 2011; Shuler, 2012; Sung and Shuler, 2012; van der Meer and van den Berg, 2012). Even when one decides to upgrade a simple 2D cell culture model to a 3D model, it still is a great simplification of the biological scenario or system to be studied. No tissue-tissue interactions can be reproduced in such model. Other physiological aspects of human physiology that cannot be included in

the standard models include complex interactions between various cell types (e.g. the immune cells), the effect of cytokines released by other organs or tissues (for instance hormones), and their changing gradients that vary with time and activity of other cells, tissues and organs (Huh et al., 2011; Ghaemmaghami et al., 2012; Sung and Shuler, 2012; van der Meer and van den Berg, 2012).

In summary, the models used in experimental biology can be broadly classified as either top down (engineered), or bottom up (typically tissue explants). The engineered models are constructed from primary or immortalised cells, and can occur in forms of 2D, 3D or organotypic co-cultures. They benefit from a high degree of control, and reproducibility, as the researcher can decide on the cellular. And molecular make-up of the model. Furthermore, performing cellular, molecular, or genetic control protocols on cellular models is typically simpler than it is the case with explant models. The bottom up models can easily be scaled up or down. It is not difficult to grow more or less cells to meet the requirements for additional western blots, ELISAs, microscopy experiments and so on. Conversely, the bottom up models might lack the physiological accuracy and relevance to the in vivo tissue. The top down models such as tissue explants, on the other hand, are more physiologically relevant, and their cellular tissue architecture is the exact representation of the architecture within the native organism. That means they can be used to create better models of complex physiological and pathological processes, that would be difficult to represent in bottom up models. The disadvantages of the top down models include the fact that they can be difficult to control in the same way bottom up models are. The sample availability can also be problematic. Whilst cell lines can be easily purchased almost any time, explants might be limited to patient availability, which can be very difficult to control. Human skin explants are a good choice of material for wound-on-a-chip research as they allow to create a physiologically accurate environment for the healing assays. Furthermore, selecting patients with comorbidities that could affect the

healing process, such as diabetes, could help to establish a model that can then be compared to healing assays with patients with no known comorbidities. That way, a more complex model might be crated, which would be difficult to set up with bottom up approach. Choosing a cell based model might be a necessity when the access to explants is difficult, as it was the case during COVID-19 lock down when human skin samples were generally not available.

For those reasons, animal models remain in use whenever it is crucial to understand the complex interactions occurring within organs, and/or when the effect of other organs or systems on the studied aspects of biology need to be put into the equation (Shuler et al., 1996; Esch et al., 2011; Huh et al., 2012). However, animal models are not the perfect solution to the problem. Their relevance to research into human physiology has been widely questioned, as it is often difficult to assess how well the data can be related to human biology (Shuler et al., 1996; Esch et al., 2011; Huh et al., 2011; Ghaemmaghami et al., 2012; Huh et al., 2012). Humans and other animals often chosen as the models vary significantly in their genetics and physiology. It has been shown that many studies animal studies on the same subject produced conflicting results. The case of Tirilazad is a good example. A total of 18 research studies in animal models demonstrated Tirilazad's ability to improved the clinical outcome in ischemic stroke models. On the other hand, research in human subjects has shown that Tirilazad led to higher death amongst the subjects. As an example of a situation where both the animal and human subjects responded similarly to the drug tested, tissue plasminogen activator was tested as a pharmaceutical intervention for the same condition as above. Both human and animal subjects responded with improved clinical outcome (Perel et al., 2007; Hall et al., 1988).

Furthermore, it has been shown that the animal research results rarely reach clinical trail phase. Only about a third of animal model studies were translated to human trials Hackam and Redelmeier (2006). In some cases, the animal models are clearly

unsuccessful in producing results that can be used in human medicine. That is the case with the HIV animal models used to test vaccines - which worked with over 100 formulations, of which none was found successful in humans (Gamble and Matthews, 2010). That is not to say that animal models are without value. Animal models benefited transplantation research for a long time, where the complex immune environment of the in vivo studies allowed for better understanding of organ rejection scenarios and pharmaceutical interventions that could counteract it (Calne et al., 1962). There has been a steady movement towards replacement of the animal models with better alternatives since the late 1950s when the three Rs of animal research have been introduced (Burden et al., 2015). These stand for Replacement, Reduction, and Refinement. NC3Rs - the National Centre for the Replacement, Refinement, and Reduction of Animals in Research has been working to implement the principles of the 3 Rs - trying to replace the animals models where they would have otherwise been used; ensuring that the minimum number of animals is used, if they are essential; and minimising the pain and discomfort in any animal test subjects (Gamble and Matthews, 2010; Kilkenny et al., 2010).

An advance in this respect may come from the world of microfluidics. Organ-on-a-chip is a concept of using microfluidic devices to maintain an/or analyse either samples of tissues or organs, or simple 3D cellular models such as spheroids. When used with tissue samples, this technology can combine the physiological complexity and relevance of the tissue or organ studied, with the high-throughput and simplicity aspects that one could expect from simpler biological models (Elder and Lever, 1997; van der Meer and van den Berg, 2012).

A review by Shabestani Monfared et al. (2021) identified that novel full thickness skin models that are specific to wound healing pathologies could be used as better platforms for identifying new treatments. Making such platforms patient specific by including patient-derived cells was identified as a step towards personalised medi-

cine for patients with wound healing pathologies. All identified "wound-on-a-chip" devices relied on either cellular or skin equivalent models(Shabestani Monfared et al., 2021).

One of the additional benefits that come from the use of microfluidics in explant culture is the ability to control the fluid flow, which helps to deliver needed nutrients, but also to remove the by-products of metabolism (Meyvantsson and Beebe, 2008).

1.4.2   Skin-on-a-chip and wound-on-a-chip

Before discussing different types of skin-on-a-chip papers that appeared in scientific articles, it is worth comparing skin equivalent models, and skin explants, as these are the sample types that could allow assembly of the most complex skin-on-a-chip models. A selection of commercial engineered skin models are currently in existence. Engineered skin equivalent models can be set up in the lab, or purchased from a specialist supplier. The availability of those models, especially the commercial ones, has particular benefits. The commercially available models are typically well documented, with already a range of scientific publications in existence (Zhang and Michniak-Kohn., 2012). The production of the model is typically standardised, and the produced models will be reproducible. This is a great benefit as the model itself will benefit from little variation in-between the tested model samples. Conversely, the explants frequently suffer from variability. There can be significant biological variability in skin thickness, composition, tensile strength, and stiffness both between different donors, but also between different collection sites within the same donor. This variability is removed with the use of a skin equivalent. Even though such simplification sounds like a significant advantage, it is a simplification nevertheless, and the investigator cannot set up a study with variables such as age group, sex of the skin donor, sample collection site, or co-morbidities. Furthermore, when purchasing a skin equivalent model, the researchers can benefit from a product that is ready

to use when it comes, without the requirement for lengthy preparation, requiring a lot of specialist knowledge. As a result, a commercial skin equivalent model can be easily prepared by a technician. The engineered nature of a skin equivalent model also means that a good deal of control is available for such model, which means that genetic engineering is much easier than in the case of the explants.

Even the best skin equivalent models are not without disadvantages though. The commercially available models can be expensive, with Labskin retailing for £2000 per a plate of 12 cultures of the model (Holland et al., 2008). Even though the product comes ready to use, there is a wait time of four weeks between the order is placed and delivered to the lab. Furthermore, even though skin equivalents can be relatively complex; containing both the dermal and epidermal components such as keratinocytes, collagen, fibrin, and fibroblasts; they also lack many components a real human skin wound have. The immune system, the vasculature, and the hair follicles are some of the key missing elements that are not represented in skin equivalent models such as the Labskin, but they are very important for the normal wound healing process. Even though that a type of ECM is present in skin equivalent models, they are always simplifications of the human matrix, with several proteins missing. Furthermore, the natural biological diversity in the explant samples, and the potential for collection of samples from donors of different age groups, sexes, ethnicities, and suffering from different co-morbidities such a diabetes, gives the researcher the ability to set up complex studies with multiple variables, helping to elucidate the impact of one or more of the aforementioned factors on wound healing. The outcome of the study is likely to be more relevant to human health, especially if the sample number studied is high enough to overcome the natural variability. Finally, a great benefit of commercial skin equivalent models, is their availability. Not every lab has access to sufficient, or in many cases any human skin samples. In such instance, easily available commercial human skin equivalents can be purchased whenever required. Conversely, gaps

in supply might become a real problem even for those labs that established contacts with hospital departments willing to supply samples.

Numerous papers have been published on a range of organ-on-a-chip devices with tissue samples or biopsies from a wide range of organs. Here we will consider the main publications dealing with the aspects of organ-on-a-chip devices used specifically for the task of maintaining and analysing skin samples. Table 1.1 Summarises the reviewed literature on skin-on-chip devices, and Fig. 1.4.1 demonstrates the key device designs.

As we have seen in the previous section, understanding of the physiology and pathology of human skin is of great importance to management of skin diseases, including scaring and wound healing issues. A common methodology in skin research is maintaining skin biopsies as explants in a static culture. This approach does have disadvantages and it could benefit from the advantages of microfluidic systems.

Several papers have been published to this date on skin-on-a-chip. It is important to note that the "skin-on-a-chip" term, when used in publications, also refers to skin-equivalent and cell-based models, and not only real skin samples.

The first paper that could be considered skin-on-a-chip, was published in 2012 by Zhao et al. where the authors presented a PDMS device which consisted of two parallel channels which were used to introduce cells onto a petri dish which acted as the bottom of the channels. Once the cells adhered, the device was pealed off, leaving two rows of cells separated by a 500 μm gap. This was an alternative version of a scratch assay. The researchers applied electrospun wound dressings onto such assay to test their efficacy in improving the healing outcome. The cells used in the assay were mouse fibroblasts (NIH-3T3) and MDCK (Madin-Darby Canine Kidney) cells that were presumably used to model keratinocytes. The authors did not attempt justifying the selection of the cell lines. The outcomes were then compared to the results from a rat model.
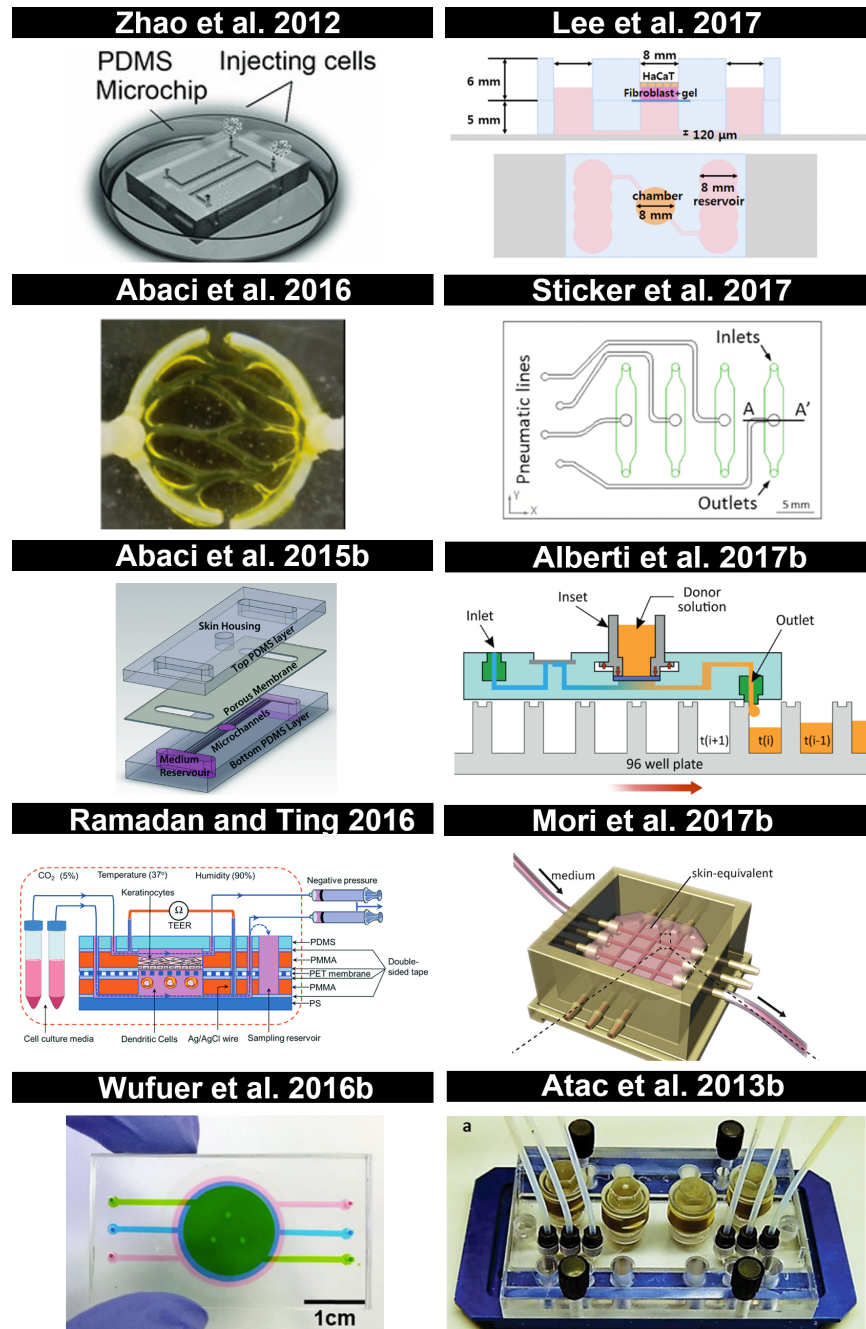
Figure 1.4.1: *Published skin-on-a-chip devices*. A panel of photos and designs of microfluidic devices for skin and wound healing biology applications. Table 1.1 presents a summary of the key informations for these models. (Zhao et al., 2012; Lee et al., 2017; Abaci et al., 2016; Sticker et al., 2017; Abaci et al., 2015b; Alberti et al., 2017b; Ramadan and Ting, 2016; Mori et al., 2017b; Wufuer et al., 2016b; Ataç et al., 2013b)

Table 1.1: *Skin-on-a-chip publications.* The "Model" collumn refers to whether the biological model was created using cell culture (monolayer or 3D structure), HSE - human skin equicalent model, vHSE - vascularised huuman skiin equicalent model, organotypic model, or HS - human skin. The "Wound" column specifies whether the model attempted at investigating an aspect of a skin wound. The "Materials" column gives the details of the key materials used to make the microfluidic device. The "Usage" column indicates the intended purpose of the model. MOC - Multi organ Chip.

Model	Wound	Materials	Usage	Reference
Cell	Yes	PDMS	Dermal healing assay	Biglari et al. (2019)
Cell	Yes	PMMA	Migration assay	Lin et al. (2019)
HSE	No	as in Wagner	Pharmaceutical testing	Hübner et al. (2018)
Organo-typic	No	PMMA, PC, PTFE	Skin permeation assay	Alberti et al. (2017b)
HSE / vHSE	No	PDMS	3D co-culture	Lee et al. (2017)
vHSE	No	No external device	vHSE	Mori et al. (2017b)
Cell	Yes	OTOMER and PDMS	Pneumatic scratch assay	Sticker et al. (2017)
Cell	No	PDMS, PET	Co-culture model	Wufuer et al. (2016b)
vHSE	No	No external device	vHSE	Abaci et al. (2016)
Cell	No	PMMA, PS, PDMS, PET	Immune assay	Ramadan and Ting (2016)
HSE	No	PDMS, PC, Glass	Drug testing	Abaci et al. (2015b)
HS	No	PDMS, PC, Glass	MOC	Maschmeyer et al. (2015d)
HS	No	PDMS, PC, Glass	MOC	Maschmeyer et al. (2015b)
HSE	No	PDMS, PC, Glass	MOC	Ataç et al. (2013b)
HS	No	PDMS, PC, Glass	MOC	Wagner et al. (2013b)
Cell	Yes	PDMS	Dressing test	Zhao et al. (2012)

The team concluded that to the best of their knowledge this was the first study to present an *in vitro* model of wound healing that could produce results comparable to an *in vivo* model (Zhao et al., 2012).

A year later, Atac et al. published results that attempted to address the lack of more sophisticated models of skin biology that could combine not only epidermis (which was already part of many skin-equivalent models) but also dermis, and other components such as the immune system or the skin appendices (Ataç et al., 2013a). The study presents an attempt to extend the culture period of human skin using a PDMS-based organ-on-a-chip device developed earlier by the same team (Sonntag et al., 2010; Marx et al., 2012). The presented device was roughly the size of a typical microscope slide. The fluidics system was propelled using on-chip micropumps producing 30 μL min⁻¹ flow with pulsatile frequency of 0.3 Hz. The channel dimensions in the device were 100 μm x 500 μm. The skin biopsies were placed in Transwell inserts which were then pushed into the device(Ataç et al., 2013a). This design was also used for multi organ co culture studies (Wagner et al., 2013a). The device presented in the aforementioned study was then used in other projects for co-culture studies of skin with liver, kidney and intestine (Maschmeyer et al., 2015c,a). Interestingly, most of skin-on-a chip projects decided to go down the skin-equivalent route. The proposed application for these models was toxicology studies and drug testing (Abaci et al., 2015a; Wufuer et al., 2016a; Alberti et al., 2017a; Mori et al., 2017a; Schimek et al., 2018).

A pumpless design of a skin-on-a-chip device was proposed by Ataci et al. where a full thickness (containing both the epidermis and dermis) Human Skin Equivalent (HSE) model was used. The device proved to be successful at maintaining HSE in a proliferative state for three weeks. The platform was also successfully used for toxicity testing (Abaci et al., 2015a).

Because of its potential in toxicological studies, a MOC device with a culture com-

partment for skin samples was presented as a platform for substance exposure evaluation. The device was fabricated using the design proposed by Wagner et al. 2013a and it was set up to house a barrier organ such as skin, intestine or lung, and a metabolically active organ such as liver. The study used full thickness human prepuce biopsies Maschmeyer et al. 2015a. The same device was then adopted to a four-organ culture; where skin, liver, intestine and kidney samples were maintained for a period of 28 days. The source of skin was also human prepuce biopsies (Maschmeyer et al., 2015c). The same device was used as a targeted cancer therapy testing platform, where lung cancer micro-tissues were co-cultured with HSE model, and cetuximab was used as an anti-EGFR (Epidermal Growth Factor Receptor) antibody therapy. This allowed to study the effect of the treatment not only on the tumour tissue, but also on skin cell (Hübner et al., 2018).

Apart from drug testing, skin-on-a-chip was also proposed as a new solution to disease modelling. Wufuer et al. suggested a different device design, comprised of PDMS layers used for culture of different cell lines, corresponding to epidermal, dermal and endothelial components of skin. These were separated by polyethylene phenolphthalein (PET) membranes that allowed communication in-between the cultured cellular layers. The team was able to stimulate inflammatory state by introduction of TNFα, and Dexamethasone was used as a pharmaceutical intervention to rescue the initial phenotype before inflammation induction (Wufuer et al., 2016a). Additional benefit of the microfluidic culture is the possibility of creating perfusable vasculature within the model. This could in theory provide a very unique opportunity to model not only atopic but also systemic drug delivery Such system would form the basis of highly advanced models of diseases affecting wound healing where the vasculature state plays an important role. The first vascularised human skin equivalent (vHSE) models was proposed by Abaci et al. in 2016. Even though it didn't make use of a lab-on-a-chip device, the study utilised micro-patterned channels, and we

believe that it should be mentioned here. The authors utilised sacrificial channels made of alginate casted in 3D-printed moulds. A dermal layer composed of collagen and fibroblasts was formed around the channels, and an epidermal portion was then formed by keratinocyte seeding. The sacrificial channels were dissolved and the open channels were seeded with endothelial cells. The model was grafted into a mouse and it was found that it was perfused with the host blood within 14 days. This involved formation of host vasculature in the grafted implant (Abaci et al., 2016).

The tissue microenvironment is often neglected in human skin equivalent models. Ramadan and Ting presented a new immunocompetent HSE model on a microfluidic chip, that was used for co-culture of HaCaT keratinocytes and U937 cell line as a model of human dendritic cells. The device itself was complex and multilayer, comprising of layers of PDMS, PMMA, PET and Polystyrene (PS). The novel system was proposed as a platform for testing chemical, biological, and physical impacts on the skin barrier (Ramadan and Ting, 2016).

Another skin-on-chip model with a vasculature system was reported by Lee et al. in 2017, however this study claimed to be the first proposing a model of vascular structure for mass transport. The published device was relatively simple, being made out of PDMS, and not requiring external pumps to operate. The tissue culture medium flow was created by varying volumes of liquid in two different reservoirs connected by the proposed vasculature channel. The tissue culture chamber was located in the centre. The dermal layer was modelled using human dermal primary fibroblasts mixed with collagen I. The epidermis was modelled using HaCaT cells seeded on top of the dermis (Lee et al., 2017). Another very interesting vHSE model that can be perfused was published by Mori et al. in 2017. The study didn't utilise any external microfluidic devices. Instead, a network of vascular channels was created within a skin equivalent model. This was achieved by 3D printing a mould with microfluidics tubing connectors on each side of the mould. Nylon wires (0.52 mm diameter) were

passed through the connectors, and a collagen solution containing Normal Human Dermal Fibroblasts (NHDFs) was poured around it to allow formation of the dermal portion of the model. The nylon wires were removed, allowing the model to hang on the fluidic connectors, and Human Umbilical Vein Endothelial Cells (HUVECs) were introduced into the open vasculature channels to coat them. Lastly, Normal Human Epidermal Keratinocytes (NHEKs) were seeded on top of the model to create an epidermal layer that became cornified when air-liquid interface was established. Histological analysis showed that this model formed vasculature of typical architecture, with the endothelial cells forming tight junctions (Mori et al., 2017b).

It is clear that creating vascularised skin equivalent models is a possibility, and it can be successfully achieved. Creating a vascularised model using a skin explant would be much more difficult to do as the existing vasculature would have to be connected to - a procedure that would be very difficult or impossible to achieve, even with specialist equipment, and surgical expertise. For that reason, whenever a vascularised model is desired, the skin equivalent route appears to the best choice. Having that in mind, finding a way to establish medium flow through a vasculature (be it native, or some form of implanted channels) in skin explants would potentially be very beneficial as it could help to improve nutrient and oxygen delivery in the typically thick tissue. Additional reasons for creating a vascularised model include modelling systemic drug delivery - where the vasculature plays a crucial role, improving sample survival - by enhancing oxygen and nutrient delivery to more distant cells, improving engraftment - when that is desired in a model that is grown as as an engraftment tool, and modelling a realistic route of immune cell delivery to the sample - where the immune cells can be introduced into the wound area.

Another device that could be considered as wound-on-a-chip has been published in 2018 by Sticker et al. This was a simple chip made of PDMS sandwiched between two layers of dual-cure thermoset called OSTEMER. The unique feature of the presen-

ted devices was the pneumatic system in the top layer of the chip, which allowed for either cell depletion or cell exclusion within the cell culture area in order to create a highly replicable version of the standard scratch assay that works in a microfluidic system. The study used GFP (Green fluorescent protein) transformed HUVEC cell line for the culture experiments (Sticker et al., 2017). To the best of our knowledge the first publication to brand their device as wound-on-a-chip was presented in 2019 by Biglari et al and it was created in attempt to address the lack of advanced assays of dermal healing(Biglari et al., 2019). The device utilised a previously published design (Farahat et al., 2012), and it was fabricated out of PDMS, and it consisted of three interconnected parallel channels, with the middle channel being filled with Matrigel mixed with HUVECs and the lateral channels containing separately fibroblasts and macrophages. The macrophages were used to recreate wound inflammation conditions, which was also possible by addition of TNFα. Increased levels of IL-1β, IL-6 and IL-8 in the effluent confirmed that the device successfully recreated wound inflammatory state (Biglari et al., 2019). Another wound-on-a-chip device, although not branded as such by the authors, was published by Lin et al. in 2019 and it was a microfluidic device designed for culture of fibroblasts which would then be subjected to flow of trypsin mixed with tissue culture medium as means of cell removal from regions of the culture chamber. This resulted in microfluidics scratch assay that benefited the model with additional shear forces (Lin et al., 2019).

When discussing lab-on-a-chip approaches to wound healing assays, it is important to consider the conventional wound healing assays, and their limitations. Most of conventional wound healing assays rely on physical depletion or exclusion of cells grown in monolayer. The cells then migrate to close the gap. The most common type of a physical depletion assay is a scratch assay where the cells are removed by scratching the cell monolayer with a pipette tip. This method is very common due to its ease of execution, however it suffers from poor reproducibility. It also damages cell mat-

rix, which in itself will affect the assay outcome. An alternative method is a physical cell exclusion assay, where an insert is placed in the culture dish, preventing the cells from growing in an area. This method is more reproducible, but it lacks the benefit of breaking up cells that the scratch assay offers. Such cell destruction is more realistic representation of the wounding damage. This method is also typically more difficult to automate (Shabestani Monfared et al., 2021). Microfluidics also offers the physical exclusion and depletion methods for wound creating in a cell monolayer (Sticker et al., 2017; Zhao et al., 2012). There however also exists a potential to use a flow of enzyme such as trypsin to dislodge the cells (Lin et al., 2019). In either case, the microfluidic solutions are only suitable for monolayers of cells. If a skin equivalent model or an explant is desired, the wound will have to be produced off the device. Having said that, the benefits of the microfluidic enzymatic depletion or mechanical exclusion and depletion assays are clear. It is relatively easy to multiplex them to achieve higher repeat numbers, and there is relatively little variability in the wounds produced (Shabestani Monfared et al., 2021).

Traditionally, ex vivo skin explants have been cultured either short term (for up to 48 h) entirely submerged in tissue culture medium (Bonifati et al., 1998), or long term, at air-liquid interface. The air access is important for correct differentiation of the epidermis(Kivinen et al., 2003; Lebonvallet et al., 2010). Trowell et al established a method for maintaining skin samples with the epidermis at the air-liquid interface (Trowell, 1959). In that method, a stainless steel grid was used to elevate the skin sample above the medium, and a piece of lens paper was placed on top of the grid to wick up the medium towards the skins sample. Alternative methods used Transwell-style inserts, or stacks of filter papers to elevate the skin samples at the medium level(Lebonvallet et al., 2010).

The literature search identified no publications on skin-based microfluidic devices concerned with wound biology studies.

Skin-on-a-chip applications

Skin models find their applications in several areas of research. Skin-on-a-chip models created with skin explants are particularly well-suited for certain applications where high physiological accuracy is particularly required. Studies into skin physiology of different sorts, for example the involvement of the immune system, hair follicles, and even skin microflora which can be separately added, will be able to benefit from the complexity of the explant used with the microfluidic system. A skin equivalent model would be too simplistic for these applications. An explant skin-on-a-chip would also be a good choice for any studies into skin disease, such as chronic wounds, where samples can be collected from patients that suffer from diseases such as diabetes, which are highly relevant to healing problems. Here the physiological accuracy and the disease-transformed state of the skin samples will be crucial to the success of the model. Another application of skin-on-a-chip is topical testing of agents for efficacy and toxicity studies. This might be applicable to pharmaceutical and cosmetic industries. The skin-on-a-chip once again carries the advantages of physiological accuracy. In addition, the presence of microfluidic channels could be used for measuring the levels of the compounds that are applied topically. Aliquots can be collected in timed intervals, allowing for the study of transdermal permeability over a period of time.

1.5   Oxygen in tissue culture

Cell culture is not a perfect model system, and it suffers from numerous limitations which weigh on its usefulness and translatability. These limitations can be detrimental to research projects relying on the cell culture model's ability to accurately represent the physiology of the studied condition or biological system (Place et al., 2017). One of the major caveats in tissue culture is the oxygen accessibility to the

cells, which is primarily limited by diffusion, as the gas exchange in the vast majority of tissue culture experiments depends on oxygen and carbon dioxide exchange at the surface of the tissue culture medium(Place et al., 2017). Once the oxygen molecules enter the tissue culture medium, they need to diffuse all the distance from the liquid surface to the cells which are typically adhered to the bottom of the tissue culture flask. That distance is is typically of several millimetres. On the other hand, the distance the oxygen molecules have to travel in organisms with a cardiovascular system aiding oxygen transport around the body is typically within the range of 10-30 μm and very rarely reaches 100 - 200 μm (Krogh, 1919b; Kety, 1951). This limitation of cell and tissue culture has been know to the scientific community for over a century, and yet there has been very little or no change in the way this benchmark model system has been carried out. The realisation of the problem began with Dr. Krogh's work into diffusion of gases in cell culture media, and it was then complemented by the results from McLimans' team which demonstrated that oxygen diffusion into the cultured media rarely meets the metabolic demands of the respiring cells at the bottom of the culture flasks (Krogh, 1919a; McLimans et al., 1968).

These cell culture oxygen levels should be matched as best as possible to the oxygen level values experienced by the target cell or tissue. The epidermis doesn't have vasculature, therefore its oxygen need is met by diffusion from the dermis. Silver et al reported oxygen tension of 20 mm Hg at the basal layer, and only 7 mm Hg at the level of stratum corneum (Winter, 1978). Generally, the epidermal oxygen levels can vary between as little as 5 mm Hg and as much as 50 mm Hg. Dermis has direct contact with the vasculature, and the oxygen levels are much higher - in the range of 40 -80 mmHg. The values vary as the measurements can be affected by factors such as the patient's ventilation, skin thickness, metabolic activity, or co-morbidities (Evans and Naylor, 1967, 1966). The average transcutaneous oxygen tension is cited as 60 mm Hg (Rich, 2001). In comparison, oxygen tension range in other organs ranges from

28 mmHg for muscle fibres, to 87 mmHg for ovaries (Palacio-Castañeda et al., 2022). This means that the epidermis naturally receives a relatively small oxygen load, when compared to the underlaying dermis. A wound-on-a-chip device would benefit from measurements of the oxygen levels in the dermis and epidermis to asses how well the oxygen delivery occurs in the model.

In this section we will discuss the main factors affecting oxygen availability to the metabolising cells. These are atmospheric oxygen levels, the kinetics of oxygen solubility in the aqueous medium, kinetics of oxygen diffusion through the aqueous medium and the metabolic demand of the respiring cells. At the end we will also consider the advantages that come from the microfluidic culture.

1.5.1   Atmospheric gaseous oxygen

The first limiting factor is the atmospheric oxygen concentration. Even though it is often cited as 21% v/v, this does not translate well into tissue culture setting, which is typically carried out in a humidified incubator with additional CO_2 supply, where the extra carbon dioxide and water vapour decrease the available space oxygen can take up.

The partial pressure of water under incubation conditions of 37°C and 100% humidity is equal to 47 mmHg (Pittman, 2011) and so it will occupy 6.2% (v/v) of the air gasses under sea level pressure. The presence of 5% CO_2 typically present in the cell culture incubator's further reduces the available space oxygen molecules can occupy.

The equation 1.3 can be used to calculate the final oxygen concentration in the incubator.

$$\%O_{2(final)} = (\%O_{2(initial)} \times (1 - \%gas_{(1)} - \%gas_{(n)...})) \times 100 \qquad (1.3)$$

After taking into account the initial oxygen concentration (21%), water partial

pressure (6.2% v/v) and 5% of CO_2 which is used in tissue culture incubators, the final oxygen concentration appears to be 18.6%.

Expressing oxygen concentration in terms of percentage is not very meaningful since the actual number of gas molecules will differ depending on the environmental pressure and temperature. For this reason, partial oxygen pressure (PO_2) is a better way of referring to the oxygen concentration since the ideal gas law (Eq. 1.4) can be used to calculate the molar concentration of the gas.

$$PV = nRT \tag{1.4}$$

In the ideal gas law equation P = pressure (mmHg), V = volume (L), n = number of gas molecules (mol), R = ideal gas constant (62.364 L mmHg K^{-1} mol^{-1}), and T = temperature (K).

The expected oxygen concentration in a humidified tissue culture incubator at the sea level pressure of 760 mmHg will read 7.23 mM, however this is nowhere near the level of oxygen that will be available to the respiring cells, as this atmospheric oxygen has to dissolve in the tissue culture medium before it becomes available to the cells.

1.5.2   Dissolved oxygen

When considering cellular oxygen availability, it is important to remember that the atmospheric oxygen found in the tissue culture incubator, already occurring at a lower level due to CO_2 and water vapour partial pressures, will have to dissolve in the tissue culture medium in order to access the cells, and so oxygen solubility is another factor affecting this process.

Henry's law describes the solubility of a gas in a liquid and therefore it can be used to assess the oxygen environment in tissue culture. Equation 1.5 summarises this law.

$$C_{(d)} = P_{(g)}/H \tag{1.5}$$

Here $C_{(d)}$ refers to the concentration of the dissolved gas in mM, $P_{(g)}$ to partial pressure of the gas in the surrounding environment in mmHg, and H is the Henry's constant expressed in mmHg mM^{-1}.

The Henry's constant can be affected by the temperature, and the concentrations of proteins and electrolytes in the solution, however for the sake of this discussion we can assume Henry's constant for typical tissue culture experiments to be 771.65 mmHg mM^{-1}. Using this value for the constant, Henry's law equation can then be applied to calculate oxygen concentration in cell culture system to be 0.181 mM (assuming PO$_2$ of 141.4 mmHg), which is 40 times lower that the O$_2$ levels in the surrounding incubator air. The concentration of 0.181 mM is actually higher than the physiological partial pressure of unbound oxygen which is 0.13 mM, however it is important to remember that the haemoglobin in an essential part of oxygen delivery in the bloodstream, and without it cells would quickly become deprived of oxygen. Haemoglobin increases the oxygen levels 60-fold without contributing to the unbound partial pressure. Furthermore, the time required to reach the oxygen concentration of 0.13 mM in the tissue culture medium can be lengthy. This aspect will be discussed later on in this section, but for know it is also important to appreciate that haemoglobin's great affinity for oxygen means that the oxygen diffusion into the bloodstream occurs much faster than it is the case in the tissue culture medium.

Temperature is another very important factor in the dynamics of oxygen coming into solution. The oxygen solubility increases by a factor of 1.92 as the solution's temperature drops from 37°C to 5°C .

1.5.3   Oxygen diffusion

As already mentioned, oxygen diffusion is another important factor to consider when trying to understand the oxygen environment of the cell culture.

As the metabolic activity of a tissue increases, the blood flow through the capillaries goes up to meet that extra demand (Poole et al., 2011). The oxygen availability can be further increased in the body by employing oxygen carriers such a myoglobin, and haemoglobin which is an intrinsic part of the oxygen transport in the blood, yet one of many missing parts in the tissue culture (Wittenberg and Wittenberg, 1989). Unfortunately, the situation is further complicated because of the requirements for a particular volume of the medium, which if kept too low might evaporate, or might not satisfy the metabolic demands of the metabolising cells. On the other hand, if the medium volume is too large then it will have negative impact on the diffusion time.

The typical distance an oxygen molecule has to travel in human body between a capillary and a cell is around 30 μm, and it rarely exceeds 100 μm (Kety, 1951; Krogh, 1919b). This is can be 100 times less than the distance oxygen has to travel in a tissue culture flask, and this depth is one of the known limitations of classical cell culture . Fick's first law (eq. 1.6), commonly used to assess the diffusibility of oxygen across the alveolar membrane, can be successfully used to assess oxygen diffusion from the air and into the cell monolayer at the bottom of a tissue culture flask (Kety, 1951).

$$F = D \times \frac{\Delta C}{\Delta X} \tag{1.6}$$

F = rate of diffusion, or Flux D = diffusion constant, taking into account the solubility of the gas in the medium

The diffusion constant in cell culture medium at 37°C can be estimated as 2.69 x 10^{-5} cm² s^{-1}. In this case the depth of the tissue culture medium corresponds to the thickness of the alveolar membrane. Fig. 1.5.1 demonstrates the principles of Fick's

first law. We can see that the rate of diffusion of a molecule is directly proportional to the quotient of concentration and distance. The grater the distance the slower the diffusion. Conversely, the greater the concentration difference the faster the diffusion, so in order to optimise oxygen influx to the cells, we would like to minimise the diffusion distance (depth of the tissue culture medium), and/or maximise the oxygen concentration in the incubator air.
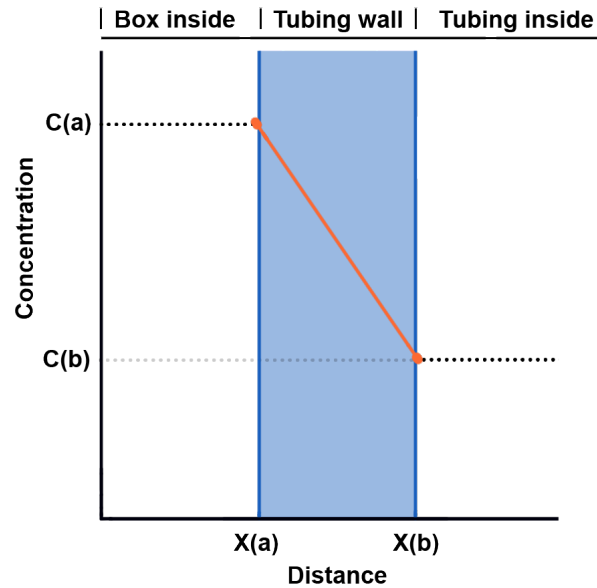

Figure 1.5.1: Fick's first law

The easier of the two is obviously reducing the volume of the medium, however the minimum volume is often dictated by the high metabolic demand of the cultured cells, or by possibility of the medium evaporating off if the level is too low. Specialised gas mixes can be utilised in cell culture to achieve a higher oxygen level in the culture. Alternative approaches to solving the oxygenation problem will be discussed in section 1.5.6 on the following page.

1.5.4 Time

Equilibration of the gaseous levels in the tissue culture medium is not a fast process. According to the results by Allen *et al.* and Newby *et al.*, it might take as long as three

hours for the media to equilibrate tot the atmospheric gas levels, and no noticeable changes might occur for the first 40 minutes (Allen et al., 2001; Newby et al., 2005). This suggests that once a respiring layer of cells depletes the oxygen available in the medium, it might take as long as three hours to replenish the levels. Depending on the metabolic demand of the culture, the rate of oxygen depletion might be faster than the rate of oxygen replenishment via oxygen dissolving into the medium and then diffusing to the proximity of the cells. Both of those processes require some time to pass before they take place and hence they are the rate limiting steps.

1.5.5 Metabolic demand

We have already seen that the time needed for oxygen to dissolve in the medium and diffuse to the cells means that if the cell density is too high, their cumulative oxygen demand will exceed the oxygen availability. The density required for it to happen will differ greatly amongst the cell lines and cell types though.

1.5.6 Microfluidics as a solution to oxygen problem

Oxygen supply to the respiring cells is a well documented limitation of the classic cell culture models. Microfluidics has been suggested as a potential solution to the problem (Rigual-González et al., 2016). The depth of the microfluidic channels is often within the typical distance the cells are positioned away from the capillaries in the body, already making the model more physiological. Additionally, the continuous flow of the medium within the microfluidic chip means that the cells are constantly exposed to fresh medium full of nutrients. The oxygen level in the medium can be further modified to fine-tune the model conditions by exposing the medium to high oxygen levels before it enters the device.

Although the microfluidic tissue culture is a potential solution to the oxygen problem, it is not a perfect solution, and definitely not a solution to every tissue culture

case scenario. A simple 2D tissue culture example is likely to benefit the most from the solution, as the cells are cultured in single layer, allowing direct access of oxygen. On the other hand, 3D culture systems, or thick tissue samples are still likely to suffer from oxygen depletion.

1.6 State of the art and the research gap

Millions of patients are affected by wound healing complications. They are typically elderly, and suffering from co-morbidities such as diabetes (Eming et al., 2014). The economic burden to the National Health Service (NHS) in the UK resulting from wound care procedures amounted £5.3 billion in 2012/2013. This involved treatment of 2.2 million wounds (Guest et al., 2015). In the US, the median cost for hospitalisation of patients suffering from non healing wounds was estimated to be between $12 851 and $16 267, and it was associated with the frequent need of amputation (Olsson et al., 2019).

These serious conditions are in fact not only lowering the quality of life of the patients, but are in fact lethal. The five year survival for amputation patients suffering from diabetes mellitus was found to be as low as 30.9% (Aulivola et al., 2004).

In order to study the wound healing process, and its complications, a model system has to be chosen. Traditionally, skin would be cultured in a static Petri dish system, placed on a support material elevating it so that the epidermis is interfaced with the air above the tissue culture medium that is added to the Petri dish. The support material could be a metal grid, or a stack of filter paper to keep the sample above the liquid layer. The air-liquid interface allows the skin sample to undergo normal keratinisation process (Zhou et al., 2018).

The static nature of the method has drawbacks such as poor difusibility of the metabolites and nutrients in the tissue culture medium (Mehling and Tay, 2014).

It is evident from analysis of the literature that despite several papers on skin-on-a-chip, there appears no work on lab on a chip devices used to culture and analyse wounded skin, with the primary focus being research into wound healing biology. Out of the 16 publications on the topics of skin-on-a-chip, and wound-on-a-chip, only three used full-thickness human skin samples. Vast majority of the work relied on skin-equivalent, or cellular models. Cell-based models of wound healing are important, however they fail to reproduce the complexity of skin architecture and interactions, and so they are not always the right choice. The outcome of the 2012 Wound Healing Society annual meeting suggested that the process of generating data critical for hypothesis formulating should rely on the use of human wound healing assays. Furthermore, only four publications attempted at reproducing some form of a wound in their models. All these "wound-on-a-chip" devices were based on cellular assays, and none of them full-thickness skin, or even just the epidermal layer harvested from a human or animal model. Subsequently, all the wounds were types of a scratch assay. There is a clear lack of human full-thickness organ-on-a-chip studies using such OoC model for cutaneous wound healing. This would combine the benefits of the microfluidic culture, and the benefits of full-thickness human skin explants.

These new, more physiological models of wound healing are needed to improve our understanding of wound healing disorders, hopefully leading to better therapies, and improved treatment outcome.

1.7 Aims and Objectives

The aim of this project was to address the research gap, and create a novel tissue-on-a-chip device for maintenance of wounded human skin samples, which will serve as a more physiologically-accurate model of wound healing, when compared to the currently used static culture models.

At the same time, it was desired to improve the life-span of the tissue in culture. An optimal culture duration of four weeks was desired, however with that being four times as long as the currently used static culture length it might be challenging to achieve. A more realistic target length of two weeks will be used as a target. Being able to maintain the tissue for a period of 14 days would be beneficial, and when used for wound healing assays, it would allow the researcher to monitor the tissue during the vascular, inflammatory, and proliferative stages of the wound healing process. The proliferation stage is the last one that could be captured with a skin sample that has a viability of up to 14 days, as the proliferation stage occurs between days three and 21 from the injury. The next stage - remodelling, begins around 21 days post wounding.

This was achieved and assessed by designing and fabricating microfluidic devices suitable for skin maintenance, testing skin's behaviour in microfluidic culture and comparing it to the static culture system.

Skin behaviour was assessed by studying skin viability and the spatial distribution of apoptosis using TUNEL assay; testing epidermal hyperproliferation and epidermal thickening by studying the expression of K6 and K14 via immunohistochemistry; testing the skin's ability to close a wound created with a 2 mm biopsy punch, using confocal microscopy with a wholemount-stained skin samples against K1 and K14; and by assessing the immunological profile of the samples using flow cytometry with a range of lymphocyte-specific biomarkers, and comparing the outcomes to the static model results.

This is the first study to combine the benefits of microfluidic tissue culture and a full-thickness human skin culture for the purposes of wound healing studies. Furthermore, this is the first model to investigate the influence of the microfluidic culture on the immune cell retention maintained human skin samples and the closure of cultures wounded human skin samples.

We hypothesised that the microfluidic flow will improve sample survival, immune cell retention, and wound contraction by maximising the nutrient availability to the skin cells, maximising their viability.

Chapter 2

Materials and Methods

2.1 Materials

2.1.1 Buffers and media

Holding media

Dulbecco's Modified Eagle Medium (DMEM), 10% Foetal Bovine Serum (FBS), 1% Pen Strep (Gibco; 15140-122), 1% Amphotericin B (Gibco; 15290-026).

Tissue culture media

DMEM (4.5 g/L D-Glucose, Gibco; 11960-044) supplemented with 2 mM L-Glutamine (Gibco; A2916801), 10% FBS (Gibco; 10500-064), 1% Pen Strep (Gibco; 15140-122), 1% Amphotericin B (Gibco; 15290-026)

PBST

PBS with 0.5% Triton X-100

Citrate buffer

1:10 solution of 10x Citrate buffer crystals prepared in dH2O

FACS staining buffer

2% FBS, 0.2% NaNO3 prepared in PBS

Table 2.1: List of key materials used in the project

Item	Supplier
PTFE tubing (0.3mm ID)	Sigma Aldrich
Tygon tubing	Cole-Parmer
Fused silica capillary 0.1 mm ID	CM Scientific
Flangeless fitting	Kinesis
Luer adapter	Kinesis
Transwell inserts	Sigma Aldrich
PMMA	Kingston Plastics
PC	Kingston Plastics
PETG	eSUN

Table 2.2: List of equipment used in the project

Equipment	Supplier
Ender 3 3D printer	Creality
Dartron M7 CNC machine	Datron Dynamics
CO_2 incubator	Milipore sigma
ddH_2O apparatus	Milipore sigma
Degassing set up	Fisherbrand
Embedder	Leica
Furnace	Cole Parmer
Collin P200 PM hot press	Collin solutions
Airstream Gen 3 Class II laminar flow hood	Esco
Microtome	Leica
Microwave	Panasonic
Oven	Akribis Scientific
Henniker HPT300 plasma oven	Henniker
Harvard PHD 2000 Syringe pumps	Harvard
Water bath	Leica
O_2 Flow-Through Cell FTC-PSt7	PreSens
Needle-Type Oxygen Microsensor NTH-PSt7	PreSens
OXY-4 ST (G2) Oxygen meter	PreSens

Table 2.3: Reagents used in the project

Reagent	Supplier
ABC-HRP kit	VECTOR labs
Acetone	VWR Chemicals
Amphothericin B	ThermoFisher
APTES	Sigma Aldrich
APTMS	Sigma Aldrich
Brilliant blue	Sigma Aldrich
Citrate Buffer, pH 6.0	Sigma Aldrich
Chloroform	VWR Chemicals
DMEM	ThermoFisher
DPBS	ThermoFisher
Embedding wax	Fisherbrand
Eosin	Sigma Aldrich
Erythrosin B	Sigma Aldrich
Ethanol	VWR Chemicals
FBS	Thermofisher
FACS Lysing Solution 10X Concentrate	BD Biosciences
Goat serum	Thermofisher
Haematoxylin	Fisherbrand
HEPES	Thermofisher
Heptane	Sigma Aldrich
K1 rabbit-human mAb	Abcam
K14 rabbit-human mAb	Abcam
K6 rabbit-human mAb	Abcam
Ki67 rabbit-human mAb	Abcam
goat-mouse Alexa Fluor 594 20 Ab	ThermoFisher
goat-rabbit Alexa Fluor 488 20 Ab	ThermoFisher
L -Glutamine	ThermoFisher
LDH kit	Thermo Scientific
MOM kit	VECTOR labs
Mowiol mounting medium	Sigma Aldrich
NaNO3	Sigma Aldrich
NovaRED	VECTOR labs
PDMS Sylgard 184 kit	Dow Chemical Company
Penicillin-Streptomycin	Thermofisher
Pertex	CellPath
Poly-D-Lysine	Sigma Aldrich
Proteinase K solution	Sigma Aldrich
Sodium azide	Sigma Aldrich
Triton X100	Sigma Aldrich
TUNEL kit	Sigma Aldrich
Vectabond	VECTOR labs
Vectashield mounting medium	VECTOR labs
Whole Skin Dissociation Kit	Miltenyi Biotec
Xylene	Fisherbrand

2.2 Methods

2.2.1 Fabrication of microfluidic devices

The key fabrication process that is the same for all the devices presented in this work is the CAD design and CNC milling. The fabrication process begins with the CAD design of the microfluidic device. Once the geometry of the device has been designed, a tool path needs to be generated, which will instruct the CNC machine to carry out individual milling operations. The CAD designs of the microfluidic flow-cells, the CAM tool paths, and the corresponding G-codes were produced in Fusion360 (Autodesk). Once CAM paths have been produced, they are used to generate a gcode which can be imported to the CNC machine, and the milling can commence. All the machining of the device parts was carried out on Datron M7 CNC machine (Datron Dynamics, Inc). After the machining, the parts have to be post-processed. For V1.0 device, the post processing involved thermal bonding of the glass parts. For V2.0, V3.0, and V4.0 devices, the post processing involved threading the bolt openings, and hot press bonding of the polycarbonate parts. These devices also contained nylon membranes which were chloroform bonded onto them. The PDMS membranes used in these devices were casted in a petri dish, and cut to size with a scalpel. V4.C1 device utilised the CNC milled parts connected to coverslip that had a casted PDMS layer. The parts wee connected with the aid of a 3D printed clamp. C4.C2 did not require the 3D printed clamp. Instead the CNC milled part was combined with the PDMS layer casted on a glass, slide using plasma bonding.

The devices presented in this work have been designed to be reusable. V1.0 device's glass fluidics part meant that it could be cleaned with either Piranha solution, or by treatment in furnace. The PMMA part could be cleaned with ethanol. For the devices V2.0, V3.0, and V4.0, the bolts used to hold the lids and connectors in place mean that the devices could be easily taken apart. That involved removing the lids, con-

nectors, the sample, and the sample holder. The bonded fluidics part would not be disassembled. All the parts could be then ethanol cleaned, and autoclaved. For V4.1 and V4.2 the PC components of these devices could be removed from the PDMS layer with a scalpel, after which they could be reused. The PDMS layer would be the only part to be thrown away.

2.2.2 Thermal bonding of glass

Firstly, the glass parts were placed in heptane and sonicated for 5 min. Next, the pieces were rinsed with ethanol and sonicated for another 5 min in a 50% washing detergent solution (v/v, H_2O), and then rinsed in ddH_2O and sonicated for further 3 min in acetone. The last sonication was carried out for 10 min in a 50 % liposol solution (v/v, H_2O). Once sonicated, the pieces of glass to be bonded were scrubbed with a brush. These were then rinsed with ddH_2O, and placed in a lidded container with ddH_2O for 5 min. After that, the pieces were moved into acetone for further 5 min to dehydrate the surfaces. After this final wash, the pieces of glass were removed from the acetone container in a laminar flow hood, and a nitrogen gun was used to blow-dry the glass parts. Finally, whilst still in the hood, the glass parts were aligned, and strips of sticky tape were used to secure pieces in position. The glass parts were then placed in a furnace on top of a steel weight, and another steel weight was placed on top of the assembled glass parts. The aligned glass parts were then left in the furnace set to $585^{\circ}C$ for three hours, with a temperature gradient of $120^{\circ}C$ h^{-1}. The bonded glass assembly was then retrieved from the furnace once it cooled down.

2.2.3 Hot press bonding

The parts milled in PC or PMMA were cleaned with isopropanol to remove any debris, dried using compressed air, aligned, and bonded inside of the hot press until the two

plastic parts were sealed.

2.2.4   3D Printing and casting of the channels

The layout of the channels was printed on 3D fusion deposition modelling (FDM) printer (Creality Ender 3) using polyethylene terephthalate glycol(PETG) filament. The slicing was carried out using Cura software (v4.2.1). The features printed were 150 µm deep, and their dimensions in x and y axes did not exceed 35 mm. The printer resolution was 100 µm. The feature design was the same as that of the channel outline presented in 3.1.23. Once the channel layouts were printed on a glass wafer, a cotton swab was used to wipe the surface encompassed by the printed channel mould perimeter. PDMS was prepared as outlined in method 2.2.5, and poured onto the wafer with the printed moulds. Clean glass microscopy slides were then gently placed on top of the mould with PDMS whilst paying attention to avoid trapping air bubbles. Gentle pressure was applied by hand to press out any excess PDMS, and the wafer was then moved into a 60°C oven for 1 h. The excess PDMS was discarded, and the PDMS cats of the channel outlines were kept for cell on a chip experiments.

2.2.5   PDMS casting

Sylgard 184 kit was used to prepare PDMS elastomer, by combining the silicone elastomer and the curing agent in a 10:1 ratio. Degassing under negative pressure for 30 min was used to remove air bubbles from the solution. Next, the solution was poured into a suitable mould. This was either a 9 cm petri dish to achieve a thickness of about 1 mm, or the 3D printed channel mould to create the PDMS channel layer. The PDMS in the mould was then moved into a 60°C over for 1 h to allow the elastomer to cure.

2.2.6 Chloroform bonding

Firstly, a syringe was prepared for chloroform handling. A fragment of 5 mm of the pipette tip, which would normally interact with a pipette, was cut off with scissors, and the rest of the tip was pushed onto a 1 mL syringe. A 1 cm long piece of TYGON was interfaced with the pipette tip, which was then interfaced with a equally sized piece of PTFE tubing. Finally, a piece of silica capillary of the same length was pushed into the PTFE tubing. A nylon mesh membrane was then placed on a glass Petri dish, and a piece of polycarbonate to be bonded to the mesh was then placed on top of the membrane. Next, the syringe was used to withdraw ~500 μL of chloroform.

Small droplets of chloroform were dispensed onto the membrane in close proximity to the piece of polycarbonate. The piece of polycarbonate was then firmly pressed to the membrane for 30 s to allow for bonding to occur between the surfaces. All the chloroform handling was performed in a chemical fume hood.

2.2.7 Slide coating with Poly-D-Lysine

All of the following steps were carried out in a BSL2 laminar flow hood. 50 mL of sterile tissue culture ddH_2O was added to 5 mg of poly-D-lysine, producing a final concentration of 1 mg / mL. Sterile slides or coverslips to be coated were then covered with the solution, ensuring that the cell culture area is evenly coated with the liquid. The solution was aspirated off the treated surfaces after 5 min, and ddH_2O was used to rinse the surfaces thoroughly. The surfaces were allowed to dry for 2 h prior to commencing with tissue culture experiments.

2.2.8 Plasma bonding

In all cases, the parts of the devices to be bonded were cleaned using isopropanol, and dried using compressed air. All plasma treatments were performed at 50% power.

Firstly, the polycarbonate components were plasma treated for 1 or 1:30 min. This was then followed by the key stage -silanisation. 5% (v/v) (3-Aminopropyl)trimethoxysilane (APTMS) or 1% (v/v) 3-Aminopropyl)triethoxysilane (APTES) was applied onto the Plasma treated PC and incubated under protocol specific conditions. An optional protocol specific wash off procedure was used to remove the excess of the silanisation agent from the PC parts. The PDMS plasma functionalisation was then followed for a period of 1 or 1:30 min. An optional second wash-off was used, and the parts were interfaced together, under protocol-specific conditions.

The initial use of APTMS was due to its ease of access for the initial boding attempts. The switch to APTES was made due to the difficulty in achieving optimal bonding result with APTMS, and the typical preference in the literature to use APTES for PDMS bonding protocols. Protocols A, B, and C were inspired by (Vlachopoulou et al., 2008) and (Tang and Lee, 2010). Protocol D was inspired by (Sunkara et al., 2011).

2.2.9   Preparation of human skin biopsies

Human skin samples were collected from patients undergoing plastic surgeries at Castle Hill Hospital (Cottingham, UK). The patients were fully informed, and they gave their written consent under ethical approval (LREC: 17/SC/0220). The collected skin was then placed in holding media Dulbecco's Modified Eagle Medium (DMEM), 10% Foetal Bovine Serum (FBS), 1% Pen Strep, and 1% Amphotericin B,) and transported promptly into the lab. All the steps involving tissue handling were carried out in a BSL2 laminar flow hood. Any excess fat was removed with scissors. The samples were then washed in DPBS with 1% Pen Strep and 1% Amphotericin B, and then two more times in DPBS, after which the samples in the medium were shaken vigorously to remove any remaining fat. Once the fat was removed, the skin was washed again in DPBS. An 8 mm biopsy punch was used to cut the skin samples to the right size for

| 1. Removal of excess fat | 2. Samples punched out | 3. Culture experiment |

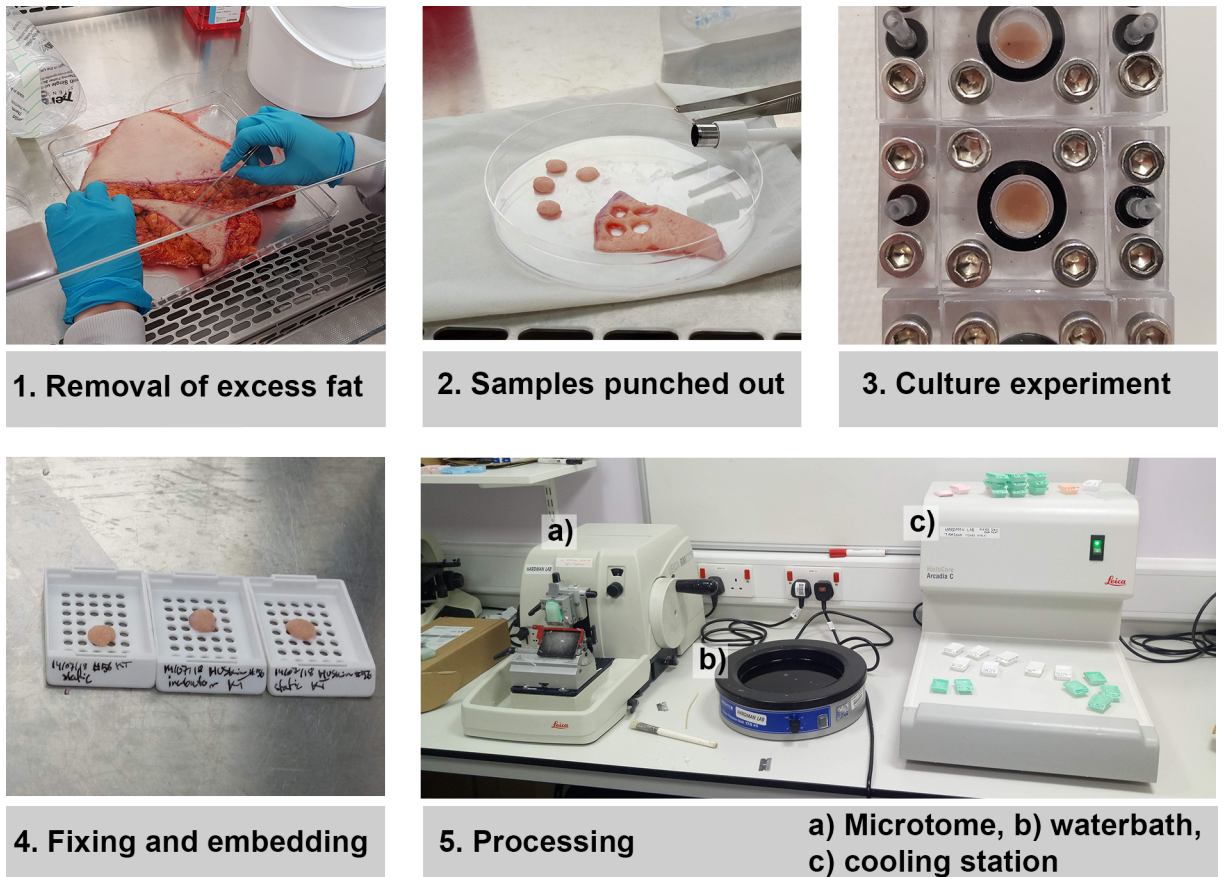| 4. Fixing and embedding | 5. Processing | a) Microtome, b) waterbath, c) cooling station |

Figure 2.2.1: *Processing of the skin samples.* 1. Excess fat is removed from the skin samples, which are then washed as per protocol 2.2.9. 2. Circular samples are then punched out using an 8 mm biopsy punch. A wound would be produced in the samples if desired. 3. These are then used for culture experiments, for either on-chip or static use. 4. Once the experiment is over, the samples are fixed and embedded in wax. 5. c) The wax blocks are set on a cooling station, and a) microtome is used to section the tissue blocks, which are then transferred onto slides using b) a heated water bath.

further experiments. Fig. 2.2.1 summarises the steps of skin sample preparation and processing.

2.2.10 Wounding of the skin explants

Where a wound was needed to be created, protocol 2.2.9 was followed, with the following exception. Prior to using an 8 mm biopsy punch to create 8 mm explants, a 2 mm biopsy punch was gently applied to the selected skin sample area which was to be cut out for further culture, and a rotary monition was used to create a partial thickness wound, with special care paid not to punch all the way through the skin. The tissue cut with the 2 mm would have still been attached to the dermis, therefore it was then gently pulled onto with tweezers, and scissors were then used to cut it off from the dermis. Next, an 8 mm biopsy punch was used to excise the explant, as detailed in 2.2.9.

2.2.11 Static explant culture

For static explant culture, the skin biopsy samples were placed in a 3 cm petri dish on a stack of two absorbent pads, and one filter membrane, ensuring that the epidermis is above the liquid level. The culture medium was a high glucose DMEM (4.5 g/L D-Glucose, Gibco; 11960-044) supplemented with 2 mM L-Glutamine (Gibco; A2916801), 10% FBS (Gibco; 10500-064), 1% Pen Strep (Gibco; 15140-122), 1% Amphotericin B (Gibco; 15290-026), 25 mM HEPES (Sigma; H0887-100mL). 2 mL of the culture medium were added to the dish, and the skin explant was left in an incubator at 37°C. The medium was changed every two days. Fig. 2.2.2 demonstrates the skin culture incubation set-up used.
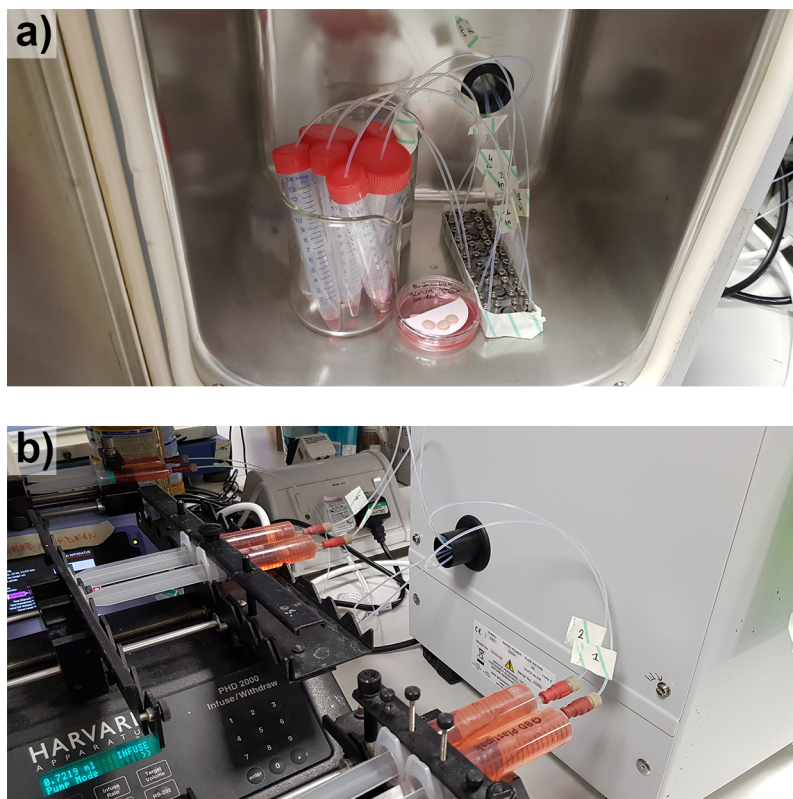
Figure 2.2.2: *Incubation set-up.* a) The V4.0 chips connected to centrifuge tubes for effluent collection, and a tissue culture dish with the skin sample biopsies in static culture. The inlet tubing can be seen entering through the back of the desk-top incubator the set up can be seen located in. B - A Harvard syringe pump connected to the inlet tubing supplying the V4.0 devices with the tissue culture medium.

2.2.12 On-Chip culture of the skin samples

Skin biopsy samples were inserted into the microfluidic devices. 20 mL syringe was filled with the culture medium, placed onto a syringe pump and connected to the microfluidic device with PTFE tubing equipped with a luer adapter. Harvard PHD 2000 syringe pumps were used to control the perfusion of the samples with the tissue culture medium. Up to three pumps were operated in parallel, wherever three different flow rates were required. Each device was always connected to an individual syringe. The culture medium was a high glucose DMEM (4.5 g/L D-Glucose, Gibco; 11960-044) supplemented with 2 mM L-Glutamine (Gibco; A2916801), 10% FBS (Gibco; 10500-064), 1% Pen Strep (Gibco; 15140-122), 1% Amphotericin B (Gibco; 15290-026), 25 mM HEPES (Sigma; H0887-100mL). The flow rate was set to the desired value. The samples were incubated at 37°C.

2.2.13 Preparation of microscopy slides for histology

Vectabond slide coating reagent was prepared by creating a 2% Vectabond solution by adding 7 mL of Vectabond reagent to 350 mL of acetone. Clean slides to be coated were placed in a metal rack, and immersed in acetone for 5 min. Next, the slides were removed from acetone, drained, and moved into the prepared vectabond reagent for 5 min. The slides were removed from from the solution, drained, and then dipped several times in ddH$_2$O over the period of 30 s to remove excess of the treatment reagent. The slides were drained again and moved into a 37°C oven to dry. Once dry, the slides were ready to be used with tissue sections.

2.2.14 Fixing of the skin samples

Once the culture experiment ended, the skin samples were placed in labelled histology cassettes, and submerged in the fixative solution for 24 h, after which they were

moved into 70% ethanol solution where they were kept until the embedding stage. 70% ethanol solution was used as a post-fixation storage medium.

2.2.15   Embedding of the skin samples

The fixed skin samples were dehydrated by moving them up ethanol gradient, whilst placing them for 30 min in 90%, 95% and 100% ethanol solutions, and then for 50 min in another 100% ethanol solution. Next, the samples were moved into xylene for 30 min and then again into fresh xylene for further 45 min. This was followed by the samples being placed in 60 °C melted parafin wax for 1 h, and again in fresh wax for further 1 h. Finally, the tissue samples were positioned on their sides in the embedding moulds in such way that both dermis and epidermis were facing up. The wax was poured in, and the mould was closed off with the labelled part of the histology cassette. The moulds were then placed on a cooling stage to facilitate wax solidification. Once set, the wax blocks were sectioned on a microtome set to 5 µm, and the sections were moved onto slides with the aid of a water bath.

2.2.16   Wholemount staining

The skin biopsies were collected after the culture experiment, and placed in the fixative overnight at 4°C. The fixative was removed the following day, and the samples were washed twice in PBST (PBS with 0.5% Triton X-100). Next, the tissue was rinsed 3 x 10 minutes in PBST and blocked for 1 hour in goat serum containing 0.2% sodium azide. The blocking buffer was then replaced with primary antibody made up in serum (plus PBST and 0.2% sodium azide) and incubated overnight at 4°C. Three sets of one hour washes were carried out using PBST containing 0.2% sodium azide. The samples were then washed three more times, 10 min each time, with PBST and incubated in appropriate fluorescently-tagged secondary antibody overnight at 4°C. Finally, the samples were washed 3 x 10 minute in PBS and then they were imaged

on a confocal microscope.

2.2.17 TUNEL staining

The slides with tissue sections on them were dewaxed in xylene for 20 min and rehydrated through a descending ethanol gradient (2 min in 100%, 100%, 90%, 70%, and 50%). After rinsing the slides in ddH_2O and drawing hydrophobic barriers around two tissue sections per slide, proteinase K solution was pipetted onto the tissue sections which were left in a dark humidified box for 20 min at 37°C. All the subsequent steps also involved the use of light-impenetrable humidified box for the incubation steps. The slides where then washed in PBS 2x 5 min. Next, 50 µL of the label solution from the TUNEL kit was pipetted on one of the bottom sections as a negative control. All other bottom sections received PBS. Then, the TUNEL solution was prepared by mixing 450 µL of the label solution and 50 µL of the enzyme solution and 30 µL of the mixture was pipetted onto each of the sections, and these were incubated for 30 min at 37°C. This was followed by three 5 min PBS washes. Lastly, the slides were mounted with in Mowiol. The mounting medium was allowed to cure by leaving it overnight in dark at 4°C.

2.2.18 Immunohistochemistry staining for K6 and K14

Firstly, the slides were dewaxed in xylene for 20 min and rehydrated by moving through ethanol gradient, with the samples spending 2 min in 100%, 100%, 90% 70%, and 50% ethanol solutions. Next, antigen retrieval was performed by microwaving the slides on full power in the citrate buffer for 1 min. Then, they were allowed to cool down for 20 min on ice. The slides were then rinsed in ddH_2O for 5 min and hydrophobic barriers were drown around three samples. Next, the samples were incubated in a 0.3% solution of H_2O_2 for 30 min at room temperature, which was followed by a 15 min wash step in PBS. The sections were then blocked in goat serum for 20 min

also at room temperature. K6 antibody was diluted at 1:500 in PBS, and K14 was diluted 1:1000 also in PBS, and 30 µL of the antibody solutions was pipetted onto appropriate tissue sections, and the slides were left overnight at 4°C in a humidified box. Next day, the slides were washed in PBS for 15 min and then they were incubated with the 2° goat anti-rabbit antibody provided with the ABC kit (1 drop in 5 ml of PBS) for 30 min. The slides were then washed again in PBS for 15 min. This was followed by an incubation with the ABC reagent for 30 min, and another 15 min wash in PBS. The ABC reagent was prepared by combining two drops of reagent A, and two drops of reagent B in 5 mL PBS). Then, NovaRed solution was applied onto the tissue sections until staining was achieved. The same timing was applied to all the slides to ensure comparability of the results. NovaRed was prepared by combining three drops of reagent 1 with two drops of reagent 2, two drops of reagent 3, and two drops of hydrogen peroxide. These were added into 5 mL ddH_2O. After the staining time, the slides were quickly washed in ddH_2O. The tissue sections were then briefly counter-stained with haematoxylin by quickly dipping the slides in the solution and then immediately washing off the counterstain with tap water and then rinsing them again with ddH_2O. Next, the stained slides were dehydrated by moving them up ethanol gradient, with the slides spending 30 sec in 50%, 70%, 90%, and then 1 min in 100%, and 100% ethanol solutions. Finally, the tissue sections were cleared in xylene for 10 min, and mounted in pretext. The slides were left overnight to allow pertex to cure, after which they were ready for imaging.

2.2.19 Immunohistochemistry staining for Ki67

The non-sustaining for Ki67 followed the same methodology as the protocol for immunostaining for K6 and K14, with a few modifications. These involved the antigen retrieval step which took 10 min in microwave on full power, then 10 min of cooling at room temperature, and then 10 min microwaving on full power again. The

blocking step was also different. Immediately after the PBS wash following a 30 min room temperature H_2O_2 (0.3% v/v, dH_2O) incubation, the samples were blocked in Mouse-on-Mouse (M.O.M.) Block for 1 h at room temperature. The M.O.M. block was prepared by combining two drops of the blocking reagent with 2.5 mL of PBS. The volume used per tissue section was 30 µL. Next, the sections were washed for 15 min in PBS wash, and another block step was performed in M.O.M. diluent which took 5 min. Preparation of M.O.M. Diluent required combining 400 µL of Protein Concentrate in 5 mL of PBS. 30 µL of M.O.M. Diluent were used per section. The M.O.M. diluent was then removed from the sections and 1:100 dilution of Ki67 antibody was prepared in M.O.M. diluent. The samples were incubated with the Ki67 antibody overnight at 4°C. Another protocol modification was the secondary antibody incubation step. The 2° M.O.M. antibody was prepared in the M.O.M. diluent and the incubation time was 40 min.

2.2.20 LDH assay

Lactate dehydrogenase (LDH) is an enzyme of high clinical significance, typically measured to asses cardiac damage. LDH analysis can also be used to investigate viability in cell cultures. Since LDH is found in the cytosol of almost all living cells, cell damage and rupture of the cellular membrane will lead to LDH release. This is the principle behind the use of LDH for cell damage monitoring.

The commercial kit (ThermoSCIENTIFIC, 88953) relies on the reaction where LDH converts Lactate into Pyruvate whilst reducing NAD+ to NADH, which is then used to reduce INT salt to Formazan. Formazan is red and can be measured at 490 nm. 680 nm measurement corresponds to the background signal from the instrument.

The LDH assay analysis required preparation of 24 skin biopsies, as per protocol 2.2.9. Fifteen of these were wounded in accordance with the method outlined in sec-

tion 2.2.10. The static controls consisted of D0 Normal Skin, D0 Wounded Skin, D3 Normal Skin, D3 Wounded Skin, D7 Normal Skin, and D7 Wounded Skin. These were compared to D3 Wounded skin, and D7 Wounded skin. The number of biological repeats was three for all the sample types. The flow rate for the on-chip samples was 10 µL min^{-1}. The control samples were placed on 6 cm petri dishes in a 37°C, 5% CO_2 incubator and the medium was changed every two days. The effluent was collected daily from the on-chip samples and every two days (and on the day of sample collection) from the control samples. The effluent collected from a device over a period of 24h was 14.4 mL, and the volume collected from the static cultures was 2 mL. LDH assay was carried out on the triplicates of all the samples in accordance with the manufacturer's guidelines. The manufacturer did not provide the details of the Limit of detection (LOD) for the kit.

In order for the LDH results to be analysed, the absorbance reading at 680nm was subtracted from the readings at 490nm, giving the LDH activity. This result was then normalised by subtracting the blank absorbance (0.1423) and dividing by the volume of the effluent collected. The end result is an LDH activity normalised to 1 mL of the effluent collected, in order to make the values easily comparable and informative. Equation 2.1 summarises the calculation used to achieve that result.

$$LDH_{norm} = \frac{(LDH_{490nm} - LDH_{680nm}) - 0.1423}{V} \tag{2.1}$$

2.2.21 Whole skin dissociation

The skin samples were collected at the end of the culture experiment and they were washed in PBST. Next, the samples were cut into small pieces. The digestion cocktail was prepared by mixing 435 µL from Buffer L, 50 µL from Enzyme D and 12.5 µL from Enzyme A in a sterile 50 mL centrifuge tube, and the cut skin samples were added to the mixture, and moved into a 37°C incubator for an overnight incubation.

This closely followed the recommendations of the kit manufacturer. Enzymes D, A, and Buffer L are proprietary components of the kit and the manufacturer does not disclose their identity. Enzyme D is likely to be Collagenase D as it is similar in appearance to it. Collagenase D is a protease enzyme commonly employed in tissue dissociation procedures. A pulse centrifugation was then performed to spin down the skin fragments to the bottom of the tube. The cell suspension was then passed through a 70 μm cell strainer positioned over a 15 mL centrifuge tube. The filter was then washed with 4 mL of cold cell culture medium to collect the remaining cells.

2.2.22 FACS

The following steps took place on ice.

Once cells have been isolated from the tissue samples as per protocol detailed in section 2.2.21, 10×10^6 cells were re-suspended in 1 mL of FACS staining buffer. These were then centrifuged at 1500 rpm, 4°C for 5 min. The supernatant was discarded, and the cells were re-suspended with 1200 μL of the FACS staining buffer. This was then subdivided into 8 FACS tubes, each with 150 μL of the sample per tube, and the respective antibodies were added with volumes specified in Table 2.4.

The FACS tubes were then wrapped in aluminium foil to minimise light exposure, and left to incubate for 20 min at 4° C. After that time, 1 mL of FACS staining buffer was added to the tubes, which were then centrifuged at 1500 rpm for 5min at 4° C. The supernatant was decanted.

The fixing solution was then prepared by preparing a 1:10 dilution of the 10x Lysing Solution Concentrate in ddH_2O. 400 μL of the solution was then added to each FACS tube, which were then incubated for 10 min in the dark at room temperature. Next, the samples were centrifuged and 1 mL of FACS staining buffer was added. These were then centrifuged again at 4° C 1700 rpm 6 min, the supernatant was decanted. This was followed by FACS acquisition.

Table 2.4: The antibodies used for FACS acquisition.

Target	Reporter	Manufacturer	Ref	Dilution
CD56	FITC	BD Biosciences	562794	1:30
CD4	PerCp	Biolegend	317432	1:75
CD25	PeCy7	Biolegend	302612	2:75
CD8	APCH7	BD Biosciences	560179	1:150
CD14	PB	Biolegend	325616	1:100
CD3	Qdot	Biolegend	317322	1:60

2.2.23   Image analysis and statistics

Wound area analysis

A wholemount-stained sample was placed on the stage of Zeiss LSM710 Laser Scanning Confocal Microscope in a 6 cm Petri dish containing 1 mL of PBS, and then it was visualised with green, red, and blue fluorescent filters, corresponding to KRT14, KRT1, and DAPI (nuclei) markers. Transmitted light detector was used to capture a bright-field image.

Once the images were acquired, they were imported into FIJI. For wound area analysis, the images were scaled using a scale bar added in the confocal microscope acquisition software. The polygonal selection tool was then used to select the area of the wound to be measured. Next, "Area" was selected in the parameters to be measured, and the measurement was produced using the "measure" function. K14 staining was used to calculate the outer wound area. In order to calculate the wound closure, the average wound area for a given sample was subtracted from the average wound area in D0 uncultured control samples. The result was subtracted from one. Equation 2.2 summarises the calculation.

$$WoundArea = 1 - \frac{averageAreaOfX}{D0averageArea} \tag{2.2}$$

Wholemount keratin expression analysis

In order to analyse keratin expression, the images were imported into FIJI. The measurement parameters were selected to area, mean grey intensity, and integrated intensity. The polygonal selection tool was used to select the wound area to be analysed. The measure function was used to acquire the measurements. Next, three small selections were made in the background around the wound, where no visible signal was present in the given channel. The measure function was used to acquire the parameters again. Corrected total fluorescence (CTF) was calculated using equation 2.3.

$$CTF = IntegratedDensity - (WoundArea \cdot BackgroundMeanFluorescence) \quad (2.3)$$

IHC image acquisition and analysis

The images of the IHC sections were acquired on Olympus IX 71 inverted microscope with a 20x objective. The images of K14 stained sections that were used for quantification of the epidermal thickness were imported into FIJI, the images were scaled using a slide graticule image acquired with the same objective, and a line tool was used to draw a line spanning the thickness of the epidermis. Seven such measurements were taken per image, at equal distances from each other.

TUNEL image analysis

Firstly, the images were stitched together using FIJI's grid/collection stitching plugin. The stitching was performed separately for the DAPI and FITC channels. The stitched images were used to perform total cell count, and the count of the apoptotic cells. In order to find the total cell count, the DAPI stitched image was imported into FIJI, the file was converted into an 8 bit image format, and auto local threshold

with the Phansalkar method was used to find the nuclei. The resulting image was inverted, and the "Fill holes" feature was used to fill in any gaps. The watershed feature was then used to break up grouped cells. "Set parameters" function was used to select Area and shape descriptors. The file was duplicated, and the copy was the "analyse particles" function was then used to produce an overlay mask with the list of identifiable particles with their areas and circularity coefficients. Particles that were clearly too small to be a cell, or groups of cells that were clustered together were noted, and their sizes and circularities were used to set the size and circularity cut-offs for further measurements. These cut offs were 100-700 pixels for size, and 0.5-1.0 for circularity. Next, the results were cleared and the polygonal selection tool was used to draw a selection around the epidermis of the sample on the other copy of the opened file. "Analyse particles" was used with the identified cut offs. The number of identified particles was the total epidermal cell count for the sample. The procedure was followed again on the same DAPI image from the point of drawing a polygonal selection, but this time it was drawn around the dermal section. The resulting count was the total dermal cell count. The entire procedure was then repeated with the FITC stitched images. Particle analysis used the same cut offs as for the DAPI samples. In order to find the percentage cell death, the apoptotic (TUNEL) cell count was divided by the total cell count (DAPI) for the section.

Statistics

One skin donor was always used to produce individual biopsies. One biopsy was used per microfluidic device. The error bars were produced using the standard error from data from multiple repeats. This approach has the benefit of minimising the impact of cross-donor biological variability, making it easier to observe the results of the culture conditions used.

All the statistical analysis and graphing were performed in R language (4.0.4) with

the use of R studio (1.4.1743).

Epidermal thickness analysis

Analysis of epidermal thickness in static control samples and the samples originating from V2.0 and V3.0 devices was performed on samples originating from separate patients. In both cases the repeats were biological replicates, as the results originated from separate explants. The biological replicates used for the procedures included: V2.0 D0 n= 3, V2.0 D7 = 4, V2.0 D7 - static control n = 3, V3.0 D0 n = 3, V3.0 D7 n = 3, V3.0 D7 - static control n = 2. V2.0 samples came from patient p56 - 43 years old female. The collection site was the abdomen. V3.0 samples came from patient p61 - 50 year old female. The collection site was the abdomen. T test was carried out on V2.0 D7 vs V3.0 D7 samples.

TUNEL analysis

Analysis of apoptosis in samples from V2.0 and V3.0 devices was performed on samples originating from p56 (V2.0) and p61(V3.0) patients. In both cases the repeats were biological replicates, as the results originated from separate explants. The biological replicates used for the procedures included: V2.0 D0 n= 3, V2.0 D7 = 4, V2.0 D7 - static control n = 3, V3.0 D0 n = 3, V3.0 D7 n = 3, V3.0 D7 - static control n = 2.

Analysis of apoptosis in samples from V4.0 was carried on on samples from patients HS74R and HS79 - both 51 year old females. The sample collection site in both cases was the abdomen. The biological replicates used for the procedures included: HS74R: D0 static control n = 3, D7 static control CO_2 n = 3, D7 static control HEPES n = 3, D7 V4.0 2.5 μL min^{-1} n = 2, D7 V4.0 5 L min^{-1} n = 1, D7 V4.0 10 μL min^{-1}HS79: D0 static control n = 2, D10 static control n = 2, D10 V4.0 2.5 μL min^{-1} n = 1, D10 V4.0 5 ul min^{-1} n = 1, D10 V4.0 10 μL min^{-1}

Wound closure

Analysis of wound closure was carried out on samples collected from patient HS112

- a 28 year old female. The collection site was the abdomen. The repeats prepared from the patients samples were biological replicates, as the results originated from separate explants. The biological replicates used for the procedures included: V4.0 D0 n= 3, V4.0 D3 = 3, V4.0 D3 - static control n = 3 , V3.0 D0 n = 3, V4.0 D7 n = 3, V4.0 D7 - static control n = 3. Two-way between-groups factorial ANOVA was carried out on the samples, and the results were compared using Tukey's Honest Significance Test.

LDH analysis was carried out on samples collected from patient HS93 - a 57 year old female. The sample collection site was the abdomen. The repeats prepared from the patients samples were biological replicates, as the results originated from separate explants. The biological replicates used for the procedures included: D0 no-wound n = 3, D0 wound n = 3, D3 no-wound static control n = 3, D3 wound static control n = 3, D3 V4.0 wound n = 3, D7 no-wound static control n = 3, D7 wound static control n = 3, D7 V4.0 wound n = 3.

Immunological profiling

cell analysis was carried out on samples collected from patient HS112. There were no biological replicates as n = 1 for all the samples.

Chapter 3

Results

3.1 Device design, fabrication, and testing

As part of the quest for a novel wound-on-a-chip flow-cell, four attempts were made at creating a microfluidic device for maintenance and analysis of human skin samples. In addition to that, two modifications of the final wound on a chip were designed and tested in order to adapt the wound-on-a-chip device to cell-based experiments. This section details the designs of those chips, and their assembly.

The CAD designs of the microfluidic flow-cells, the CAM tool paths, and the corresponding G-codes were produced in Fusion360 (Autodesk). The machining of the device parts was carried out on Datron M7 CNC machine (Datron Dynamics, Inc) unless specified otherwise. The manufacturers, and additional information on the materials used in this project are given in the Materials section on page 68.

The method of irrigating the skin samples with the tissue culture medium in the devices presented in this work utilised a microfluidic channel positioned below the tissue culture chamber. Fig. 3.1.1 shows a simplified graphical representation of this concept. A skin sample is placed in a sample retainer, which is then inserted into the body of the microfluidic device. The sample retainer utilises a porous membrane

on which the sample rests. The membrane prevents the sample from falling into the microfluidic channel, whilst allowing for a diffusion of the medium into the sample, and diffusion of the metabolites out into the medium.
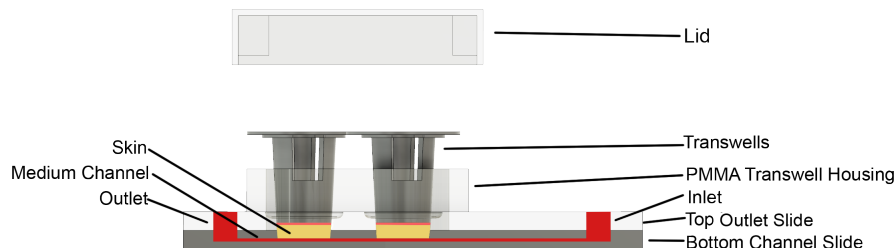
Figure 3.1.1: *The flow concept.* The conceptual schematic of V1.0 device showing the medium channel running under the tissue samples placed in Transwell inserts. This concept of medium flow under the samples was applied to all devices for human skin maintenance presented in this work.

3.1.1   Device V1.0

The first generation microfluidic wound-on-a-chip device (V1.0) was designed to work with Transwell inserts as sample retainers. This was inspired by the solution presented in Wagner et al. (2013a) study.

A schematic overview of the assembled device can be seen in Fig. 3.1.2. The device was made of four parts: bottom fluidics part, top glass part, Transwell housing, and the lid. The bottom fluidic part and the top glass part were thermally bonded (see section 2.2.2 for the method) to form a single glass body containing the fluidics system. A schematic diagram of the two glass parts constituting the fluidics system of the V1.0 device can be seen in Fig. 3.1.3. The choice of glass for manufacturing of the fluidic component of the device was favoured for its resistance to cleaning methods such as furnacing and Piranha treatment. This meant the device could be easily cleaned and reused. More specifically, the glass fluidics part can be cleaned in furnace, or using Piranha solution, whilst the PMMA parts can be ethanol cleaned. Being able to dismantle the device is allows the user to use furnacing or Piranha cleaning without

destroying the PMMA part.

The channels were designed to be 100 μm deep and 1000 μm wide, however the width of the channel increased to 6.5 mm under the skin sample, matching the diameter of the Transwell membrane.

When designing the microfluidic channels, the dimensions were chosen in the following way: firstly, the dimensions of the channel underneath the culture chamber were determined. The size of commonly used skin biopsies is 6 mm. V1.0 device was supposed to be used in conjunction with the Transwell inserts. The closest internal Transwell size to 6 mm is 6.5 mm. This defined the diameter of the channel underneath the culture chamber. Next, the channel diameter was pre-determined by the limitations of CNC machining. The smallest diameter of diamond coated CNC milling bit suitable for glass is 1 mm, which ended up being the channel width of choice. Channel depth of 100 um was because it was desired to ensure that the channel is sufficiently shallow to allow for fast diffusion of molecules. The time required for the same glucose molecule to diffuse 100 μm in a microfluidic channel is only 8.5 s. The residence time of the medium under the skins sample at the flow rate of 10 μm min -1 is 20 s. This means that glucose has sufficient amount of time to diffuse from the bottom of the channel to the skin sample interface within the time it resides underneath it. At the same time, the depth isn't so shallow that the membrane supporting the skin sample would cave in causing channel blockage.

The channel architecture was designed in a branching fashion, where one inlet channel branched off into three channels supplying three samples with tissue culture medium. This was to allow for one syringe to supply three samples with the medium and therefore to triple the number of samples that can be studied in parallel. The microfluidics system was milled out of 3 mm thick stock of B-270 glass.

Transwell inserts (6.5 mm membrane diameter, 10 μm thickness, 3 μm pore size) were chosen as sample holders. The choice was motivated by Transwell's standing
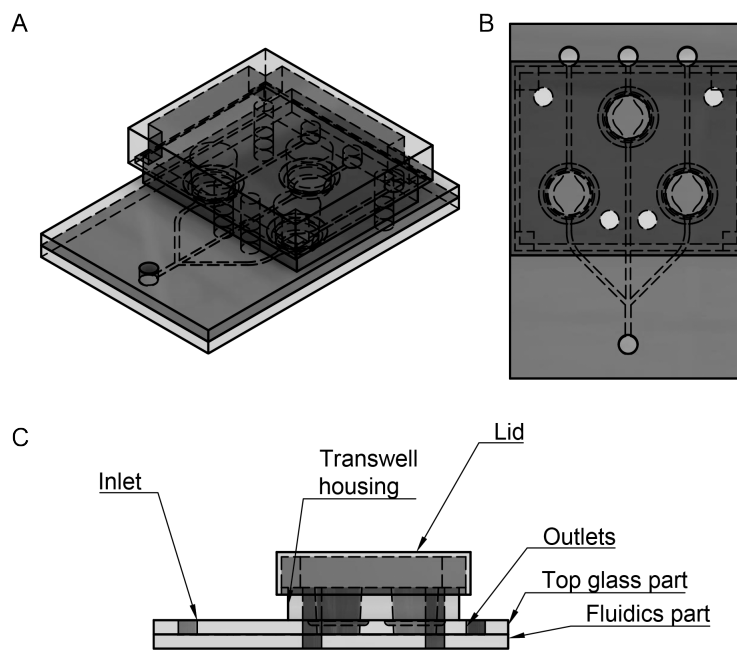
Figure 3.1.2: *The overview of the assembled V1.0 device.* A) Overview of the assembled chip, B) Top-down view of the chip, C) Right-hand side view of the chip

reputation within the scientific community. They have been widely used and their quality has been thoroughly tested.

The plastic "Transwell housing" part was designed as an add-on onto the glass fluidics system, which was then attached using M4 bolts, with a BS-012 O-ring placed in the O-ring grove in between the two parts to prevent medium leakage. (see Fig. 3.1.3-b, and **??** for the Transwell housing and the top glass part, with the O-ring grove detailed). The Transwell housing's task was to ensure that the Transwells were secured in place. It also acted as a support platform for the device lid (see Fig. 3.1.5) which rested on top to prevent dust and contaminants from falling onto the samples. The lid was designed to be wide enough to allow for a small gap to let air into the samples.

Interfacing of the V1.0 device with inlet and outlet tubing was performed with the help of inverted P200 pipette tips that were pushed onto cut-off luer locks from plastic syringes. These were then forced into the inlets and outlets of the device (see

(a) The bottom fluidics part   (b) The top glass part
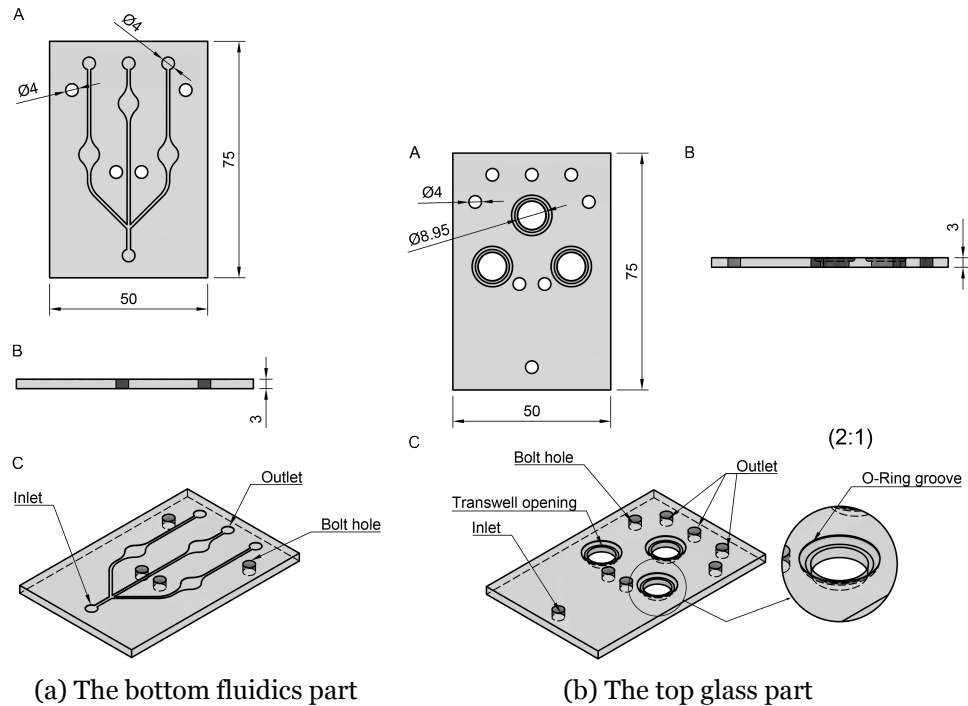
Figure 3.1.3: *The glass fluidic parts of V1.0 device.* a: A) Top down view of the fluidic part, B) Right hand side view of the fluidic part, C) Overview of the fluidic part. b: The top glass part. A) Top down view of the top glass part, B) Right hand side view of the top glass part, C) Overview of the top glass part, with the O-Ring grove clearly visible. The dimensions provided in mm.
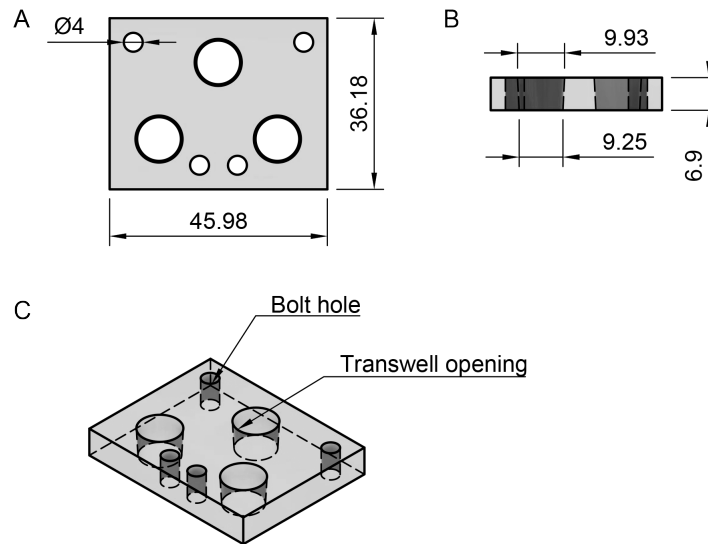
Figure 3.1.4: •label fig: transwell housingV1 A) The top down view, B) the side view, C) the overview. The dimensions provided in mm.

fig. 3.1.6). PTFE tubing (0.3 mm ID, 58698-U Sigma Aldrich) was then connected to those pipette tips by interfacing with a short piece of TYGON tubing that connected both parts. Pumping of red food dye showed an obvious problem with this design (see Fig. 3.1.6). Namely, the liquid was raising through the Transwell inserts, and nothing was entering the outlet tubing.

It was hypothesised that the skin sample placed in the Transwell insert would be able to seal off the Transwell membrane, and at the same time prevent the liquid from raising. To assess this, pig skin samples prepared with a 6 mm biopsy punch were placed in the Transwell inserts (see Fig. 3.1.8-A). Pig skin was used during the initial optimisation process due to its availability. It quickly became apparent that the samples produced with the 6 mm biopsy punch did not seal off the membrane properly, and the liquid was still raising through the inserts, and very little was reaching the outlet tubing. Fig. 3.1.7 shows a pig skin sample cut out with a 6 mm biopsy punch. There is a lot of visible space around the sample, not covering the surface of the membrane.

In order to troubleshoot the sample size issue, it was decided to use a larger 8
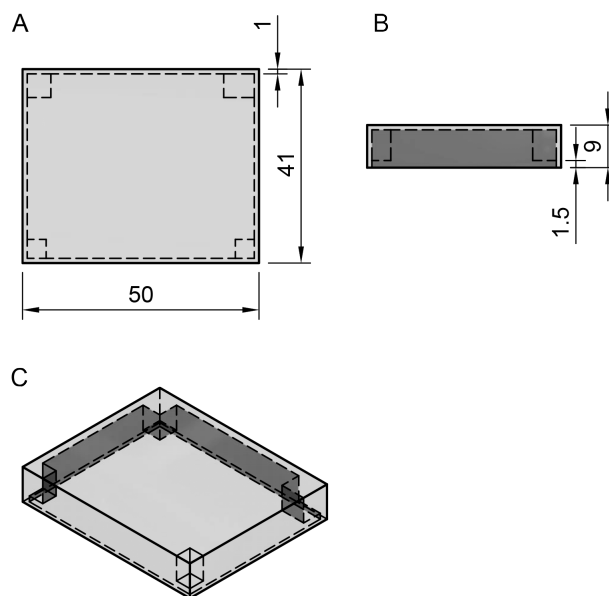
Figure 3.1.5: The Lid for V1.0 device. A) The top down view, B) the side view, C) the overview. The dimensions provided in mm.

mm biopsy punch to prepare the samples. In addition, the pipette tips used as connectors were replaced by cut-off luer slips from syringes, which were pushed into 4 mm wide outlet openings in the device. Then, a 5 mm long piece of a TYGON tubing (ID 1.27mm, OD 2.29mm, WZ-06419-05, Cole-Parmer) was pushed onto an end of PTFE tubing, and that was then insert into the luer locks positioned in the outlets of the device. This approach was successful, and it was possible to establish stable flow through the microfluidic channel system (see Fig. 3.1.8-B).

Flow analysis was performed to assess homogeneity of the flow output from the three channels. Water was pumped through the microfluidic channels at a range of flow rates for a controlled amount of time, and the effluent was collected in pre-weighted tubes.

The perfusion was established using Harvard PHD 2000 pumps. A range of flow rates between 10 and 60 μL/min were tested.

The perfusion lasted exactly 60 min per repeat. Each flow rate was repeated three times. It is possible that some evaporation occurred, however that would have not af-
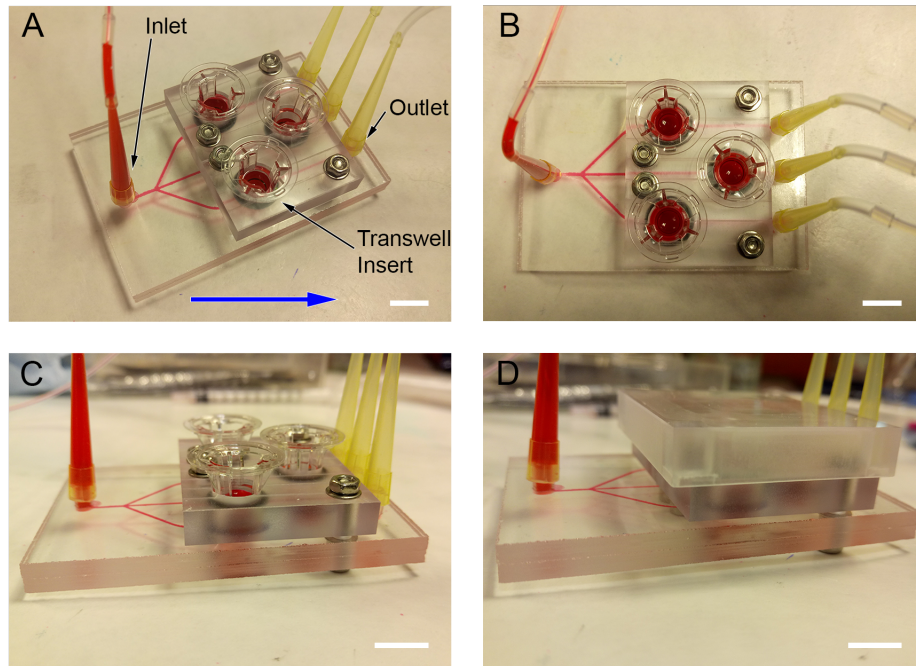
Figure 3.1.6: *Testing of V1.0 device with red food dye.* The white scale bars represent 1 cm. The blue arrow indicates the direction of flow. A) At an angle view of V1.0 device, B) Top down view of V1.0 device, C) Side view of V1.0 device, D) Side view of V1.0 device with the lid on. Red food dye has been used to fill up the channels. It can be clearly seen raising up the Transwell inserts in A) and B).

fected the output ratio of the three channels, as the evaporation would be expected to occur at a similar rate in every case. As a result, the results would be still comparable.

The results were then plotted on a graph shown in Fig. 3.1.9. As much as 25% discrepancy was observed in the flow outputs in-between the channels. Also, the middle channels was consistently receiving a higher flow rate than the side channels. Such a large difference in medium flow could lead to significantly different biological behaviour in the samples maintained on the device.

One possible explanation for the higher flow output in the middle channel is that it has a smaller hydrodynamic resistance than the side channels. The difference in channel length can play a role in this. Since the middle channel is shorter than the side channels, it would have less resistance to flow, which could cause the higher flow output. Additionally, the roughness of the channel walls could also influence
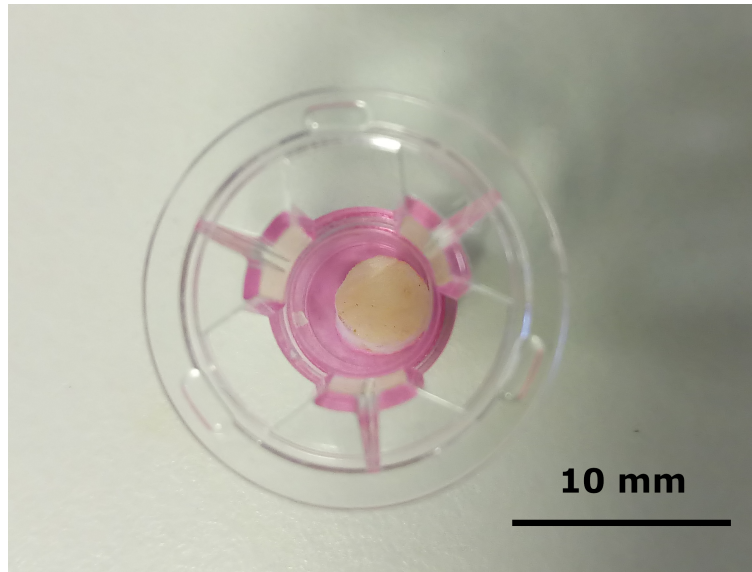
Figure 3.1.7: *A pig skin sample produced with a 6 mm biopsy punch.* The membrane was stained with red food dye. The diameter of the membrane is 6.5 mm, only 500 µm larger than the diameter of the biopsy punch. The gap between the side of the insert and the sample is around 1.5 mm.

the resistance to flow. This is a likely explanation for the flow discrepancy between the flow outputs from the side channels. The fabrication accuracy is almost certainly not the cause of the deviation, as the CNC accuracy is around 10 µm.

Furthermore, besides the inconsistent flow profile, it was found that the V1.0 device is unsuitable for human skin experiments due to it not being able to accommodate the mechanical properties of human skin. Despite being able to establish a flow under pig skin samples, no reliable flow could be maintained with human skin samples as human skin is much thinner than the pig equivalent, and so it was being lifted off by the liquid in the Transwell, and the liquid raised inside of the Transwells instead of entering the outlet tubing. V2.0 and V3.0 devices were proposed as potential solutions to the problem. These will be discussed in details in the upcoming sections.
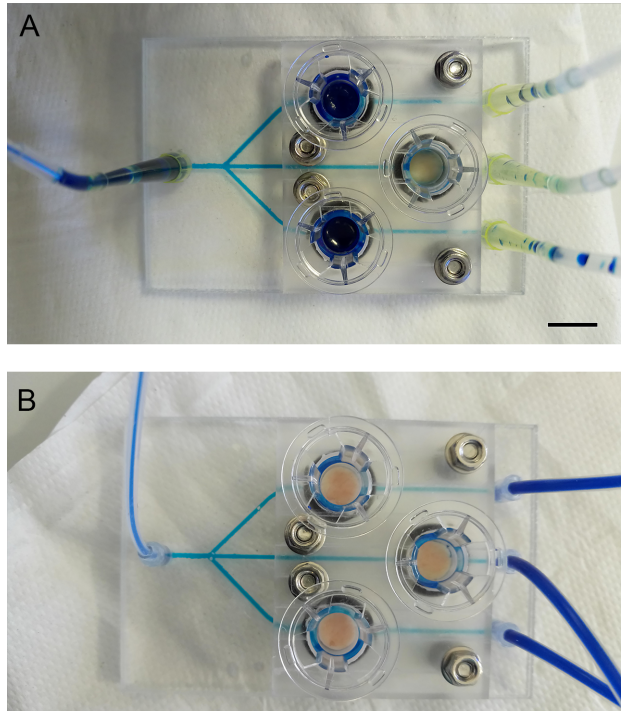
Figure 3.1.8: Testing of V1.0 device with pig skin. The scale bar represents 1 cm. Blue food dye was pumped through the system. A) First attempt at pumping the blue dye through the device, with pig skin samples prepared using a 6 mm biopsy punch. Liquid raising through two Transwell inserts can be observed, B) second attempt at pumping the blue dye through the device, with pig skin samples prepared using 8 mm biopsy punch. Additionally, the outlet tubing has been changed to wider TYGON tubing. No leakage can be seen here. One device was used for these experiments. Three pig skin samples were used per each experiment, and both attempts with 6 mm and 8 mm biopsy punches were carried out on the same day.
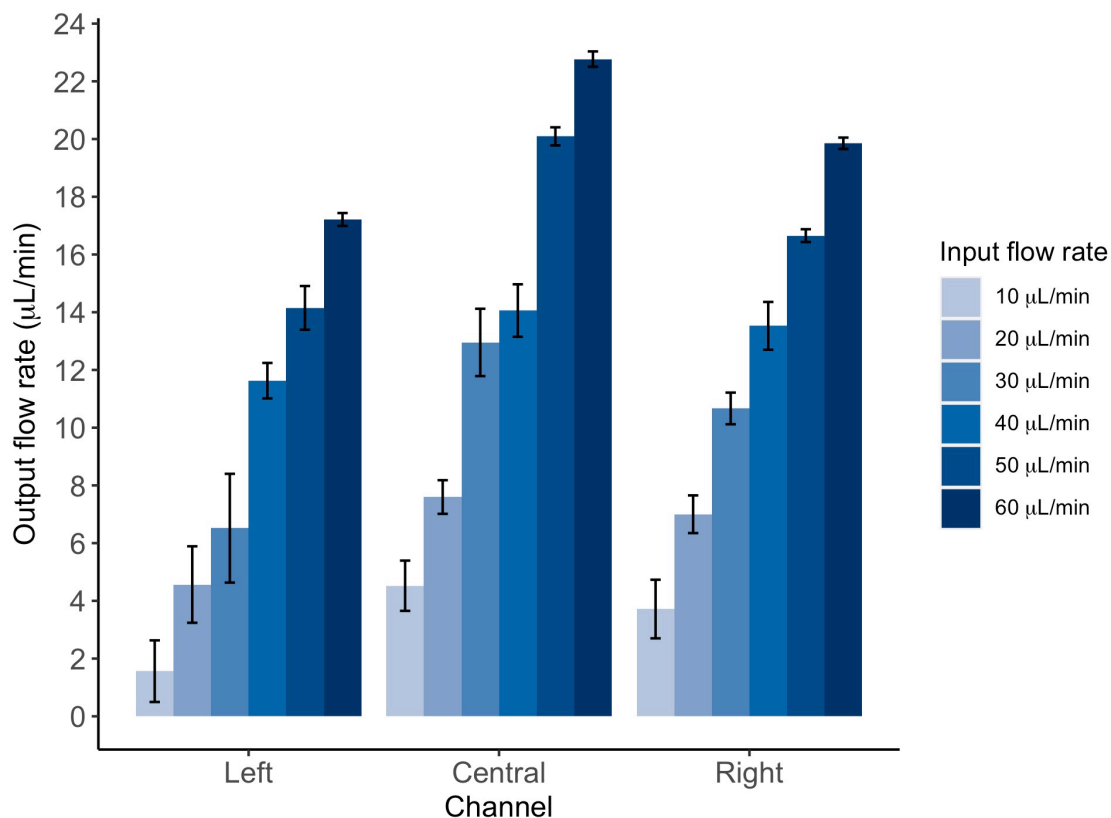
Figure 3.1.9: *V1.0 flow stability analysis.* Water was pumped at six different flow rates through V1.0 device, and then it was collected at the outlets of the channels over a fixed period of time in pre-weighted Eppendorf tubes,and the liquid volume was determined by weighing. The results show that the flow is not equal across the channels. The central channel produced higher output flow rate than the side channels. In addition, the deviation between the output flow rates can reach as much as 25%. The experiment was repeated three times, on three different occasions, with one device. The perfusion time per experimental repeat was 60 min. The error bars represent the standard error of the mean.

3.1.2   Device V2.0

The second generation wound on a chip microfluidic device was designed to resolve the flow issues encountered in the V1.0 device. Several new solutions were introduced into this design. First of all, PC was chosen as the material for fabrication of the parts, instead of glass. This was meant to reduce the fabrication time, as milling the parts out of glass requires considerably longer machining times. Making the parts out of plastic also means it is possible to tap threads directly in the material. Threads can be used to add additional components into the body of the device, such as tubing connectors and sample retainers.

Next, the microfluidic system was completely redesigned to benefit from the symmetrical branching system, to ensure equal flow rates under each of the samples, and to avoid the uneven flow reported with V1.0 device. Fig. 3.1.11 presents the design of the new fluidic channel design. The channel width was varied in this model to keep the flow velocity constant. As the channel splits in two, the width of the daughter channels is halved, maintaining the flow velocity constant. The tubing connection system was also changed from the luer-slip based system to a custom-made mechanism where a nitrile BS-004 O-Ring is pushed onto the outlet TYGON tubing, which was then sandwiched between the chip and a custom-designed connector piece which was held down using M3 screws. Fig. 3.1.12 demonstrates the design of the top part of V2.0 device, and Fig. 3.1.18 the design of the tubing connector. Fig. 3.1.10 shows the assembled tubing connector.

The bottom fluidic part, and the top part of the device were fused using a hot press to produce an enclosed fluidic section. See section 2.2.3 for the details.

Furthermore, the Transwell-based tissue culture system was replaced with a custom-made sample retainer. The sample retainers were designed with threads on their outer edge (M10 x 1.5 mm) that would screw into the device's body. These
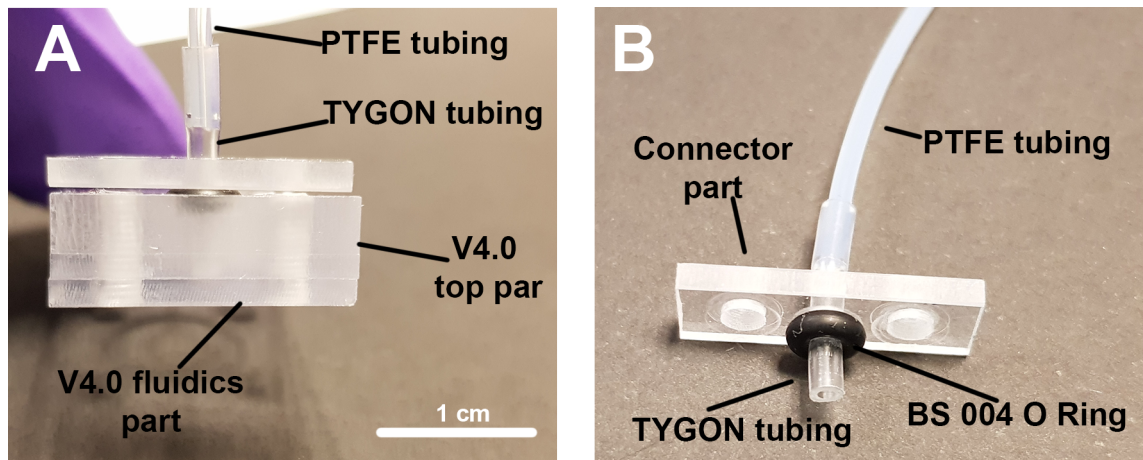
Figure 3.1.10: *V4.0 tubing connector.* A - the side view of the device demonstrating how the tubing is interfaced with the device body. B - A photo presenting the connector part, with the tubing and the BS 004 O-ring. The scale bar represents 1 cm.

were manufactured by the mechanical workshop staff from a cylindrical stock of PC, and then a nylon membrane was attached to the part's bottom by partial dissolving with chloroform as described in section 2.2.6. Matching threads were installed on the tissue culture compartments which would then receive the sample retainers by screwing them in. Additionally, a thread was added in place of the inlet, to allow for screwing in a flangeless connector with 1/4"-28 port size.

The custom sample retainer made use of a polycarbonate pin that was applying a small amount of force onto the sample from the top, preventing it from being lifted off by the culture medium flowing underneath. See Fig. 3.1.13 for overview of V2.0 device. This device made it possible to flow liquid under a human skin sample without it lifting off and causing leakage through the inside of the sample retainer. The leakage visible in fig. 3.1.14 was caused by a manufacturing artefact not allowing correct positioning of an O-ring seal. This was remedied with PTFE tape applied to the threads.
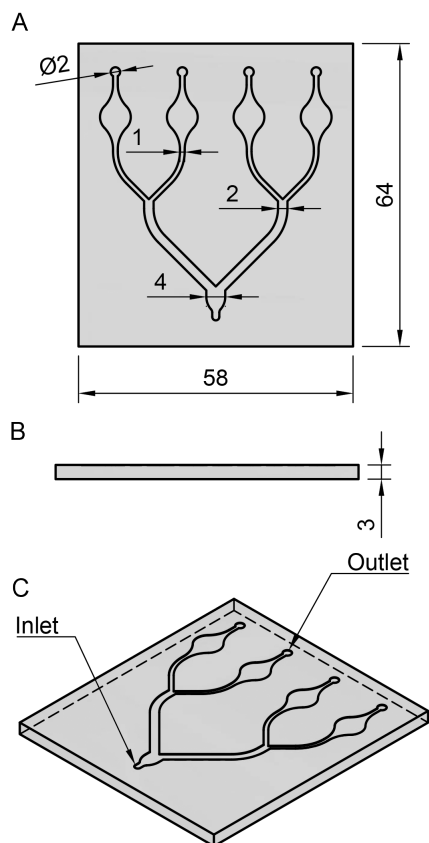
Figure 3.1.11: *The fluidics part of V2.0 device.* A) The top down view, B) the side view, C) the overview. The dimensions provided in mm.
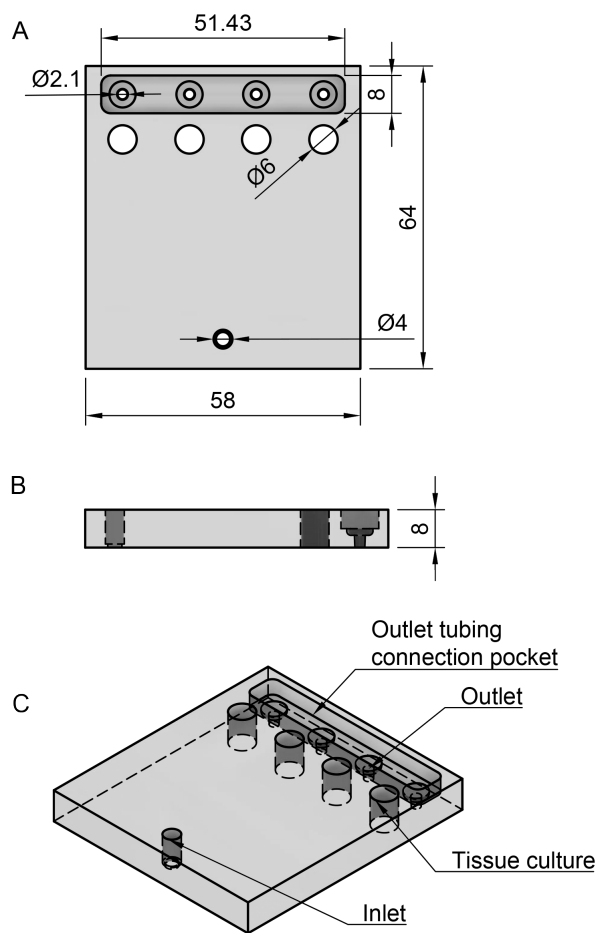
Figure 3.1.12: *The top part of V2.0 device.* A) The top down view, B) the side view, C) the overview. The dimensions provided in mm.
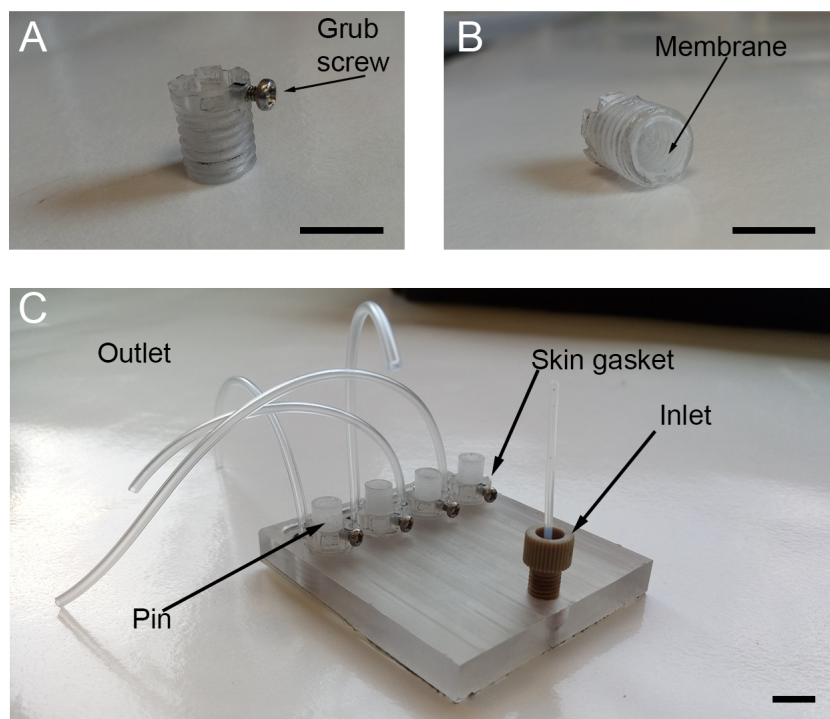
Figure 3.1.13: *Assembled V2.0 device.* A) and B) Skin gaskets at different angles, B) Skin gasket with visible nitrile membrane, C) Overview of V2.0 device. The scale bar represents 1 cm.
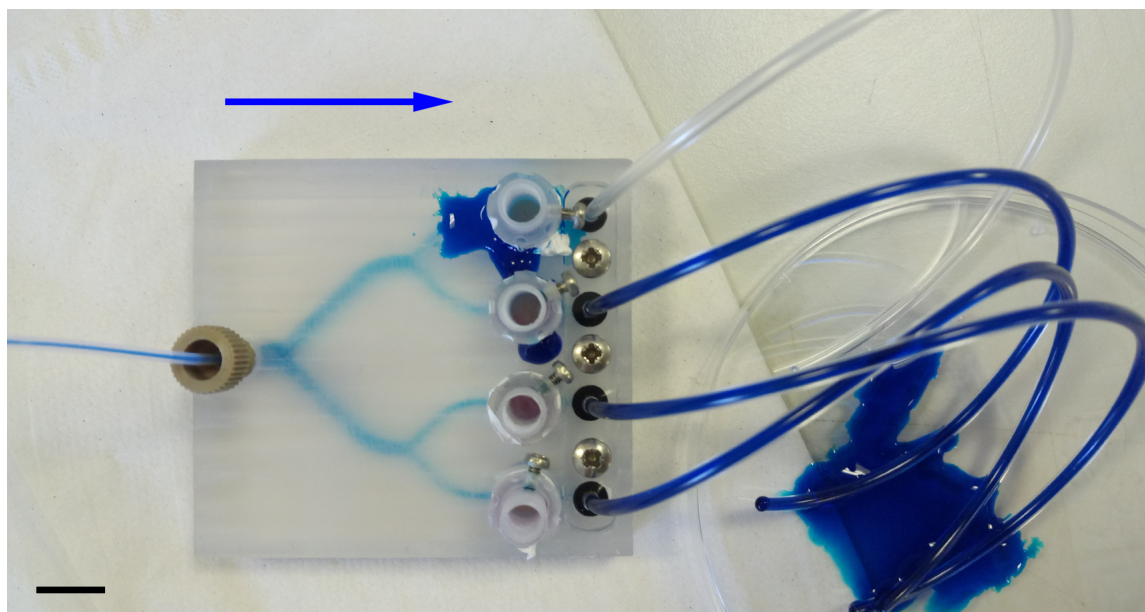
Figure 3.1.14: *Testing of V2.0 device with human skin and blue dye.* The scale bar represents 10 mm. The blue arrow indicates the direction of flow. No O-Ring groves were manufactured in the skin gaskets, therefore PTFE tape had to be used to seal the threads. Despite of the use of the PTFE tape, leakages can be still observed. One of the outlets appeared to be blocked.One device was used for this experiment.

3.1.3   Device V3.0

The third generation wound on a chip device is a modified version of the V2.0 device. This iteration of the platform was designed to troubleshoot the problems caused by the mechanical pressure applied to the skin sample by the pin of the custom sample retainer (see section 3.2.3 for more information). The shared features of the two devices are the same fluidics system design concept, and the same inlet and outlet tubing connection mechanisms. Although the overall design of the fluidics system remained similar, the length of the channel between the area under the maintained samples and the outlet was increased to allow for space for a new lid that will be used to enclose the system.

The key advantage of this microfluidic chip, over the previous models, comes from the way the skin biopsies are kept on the device. First of all, the sample retainer was completely redesigned, and it no longer relies on a pin pushing down onto the skin

sample to prevent it from lifting off. Fig. 3.1.19 demonstrates the new gasket which, in V3.0 device, is simply lowered into the tissue culture compartment. This system does not require any threads on the sample retainer. Instead, a BS-011 O-Ring is placed in the grove. The lid (see Fig. 3.1.17) of the device then pushes down onto the O-Rings and seals of the device. The lid itself is assembled by interfacing a 1 mm thick layer of PDMS onto the CNC-milled PC lid part. The PDMS sheet was casted as described in section 2.2.5, and then a scalpel was used to cut out openings for the bolts to pass through. When the lid is placed onto the device, the PDMS part is sandwiched between the chip body and the PC lid. The lid was designed with vents positioned above the skin culture retainers. They allow for oxygen diffusion through PDMS into the cultured skin samples.

The V3.0 device was manufactured using CNC milling, and the threads were installed in the post processing. This design was significantly easier to assemble in a BSL2 laminar flow hood, than the V2.0 device. The assembly of V3.0 device resulted in no leakages, and the pumped food dye was not raising within the skin culture gaskets. The drawbacks of this system, and the V2.0 device was channels being blocked at random. The threaded sample retainers needed to reach the same depth in the device when screwed in. Once the retainer reached the bottom of the channel, the weight of the sample and the force applied by the pin to the sample can cause the membrane to cave into the underlying fluidic channel. This increases the required pressure to maintain the same flow rate through the channel, which leads to uneven flow through the device, and is likely to create an opportunity for air bubbles to gather in that region and shut-off the channel all together. Fig. 3.1.20 demonstrates such case of air trapped in the middle channel of V1.0 device. The same behaviour was observed in V3.0, making it unreliable. It was hoped that removal of the thread-based system would get rid of this issue by reducing the likelihood of the sample retainer membrane protruding into the channels.
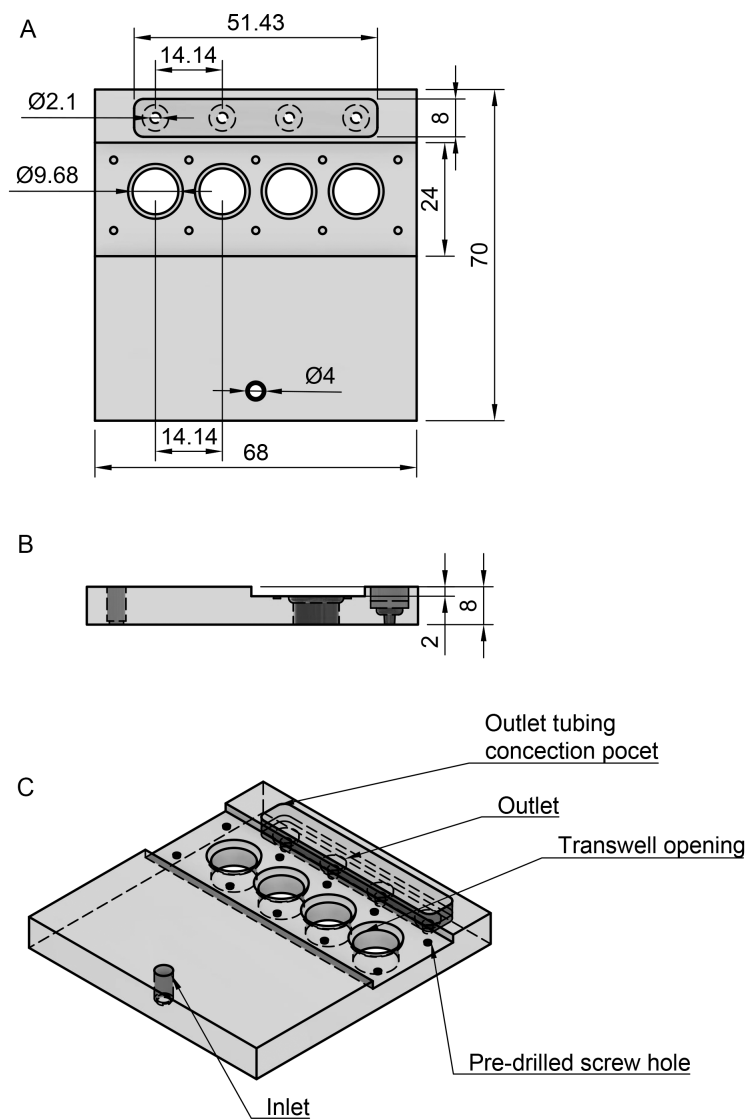
Figure 3.1.15: *The top part of V3.0 device.* A) The top down view, B) the side view, C) the overview. The dimensions provided in mm.
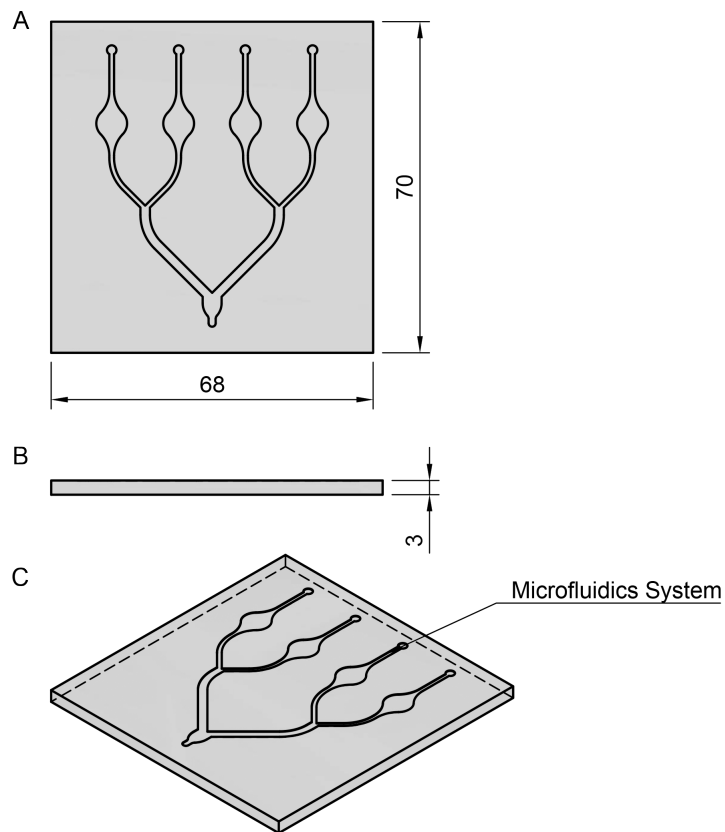
Figure 3.1.16: *The fluidics part of V3.0 device.* A) The top down view, B) the side view, C) the overview. The dimensions provided in mm.
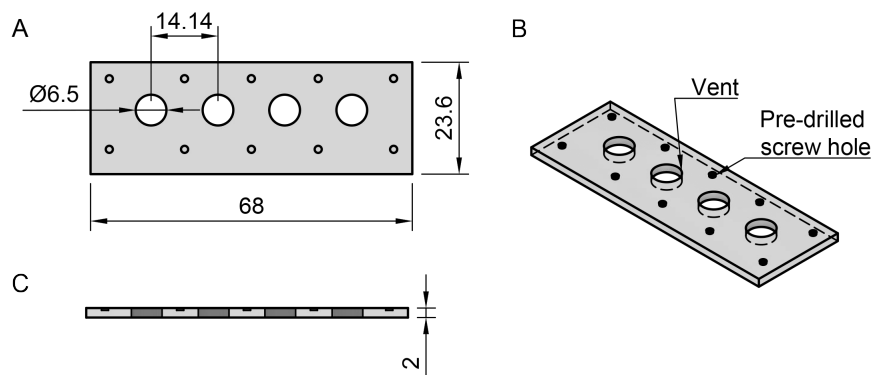

Figure 3.1.17: *The lid for V3.0 device.* A) The top down view, B) the overview, C) the side view. The dimensions provided in mm.
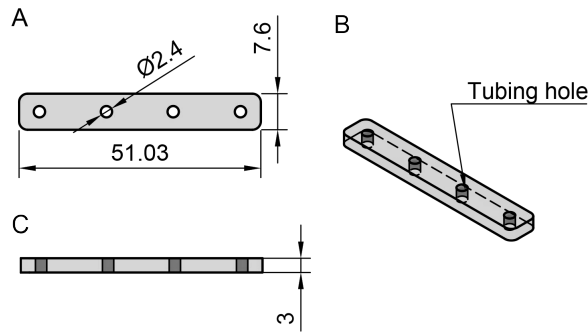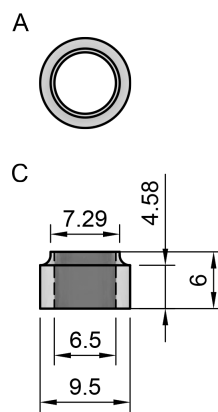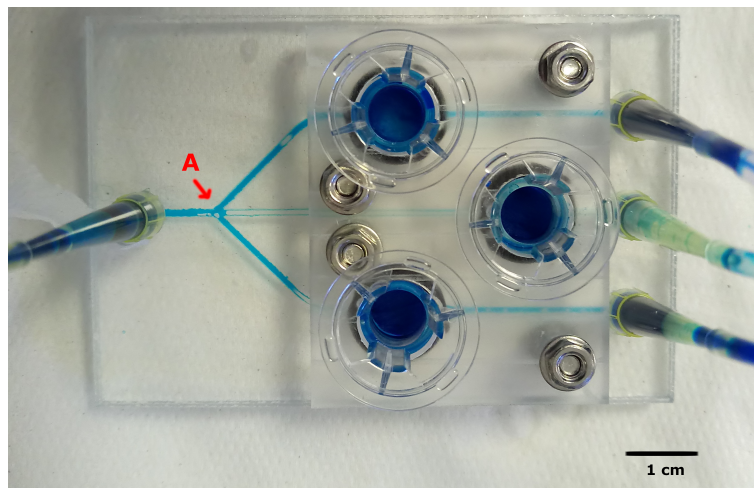
Figure 3.1.18: *The tubing connector for V2.0 and V3.0 devices.* A) The top down view, B) the overview, C) the side view. The dimensions provided in mm.

Figure 3.1.19: The skin gasket for V3.0 device. A) The top down view, B) the overview, C) the side view. The dimensions provided in mm.

Figure 3.1.20: *Air trapped in the channel of V1.0 device.* This spontaneous behaviour caused unreliable functioning of them device. The scale bar represents 1 cm. One device was utilised for this experiment, with three pig skin samples.
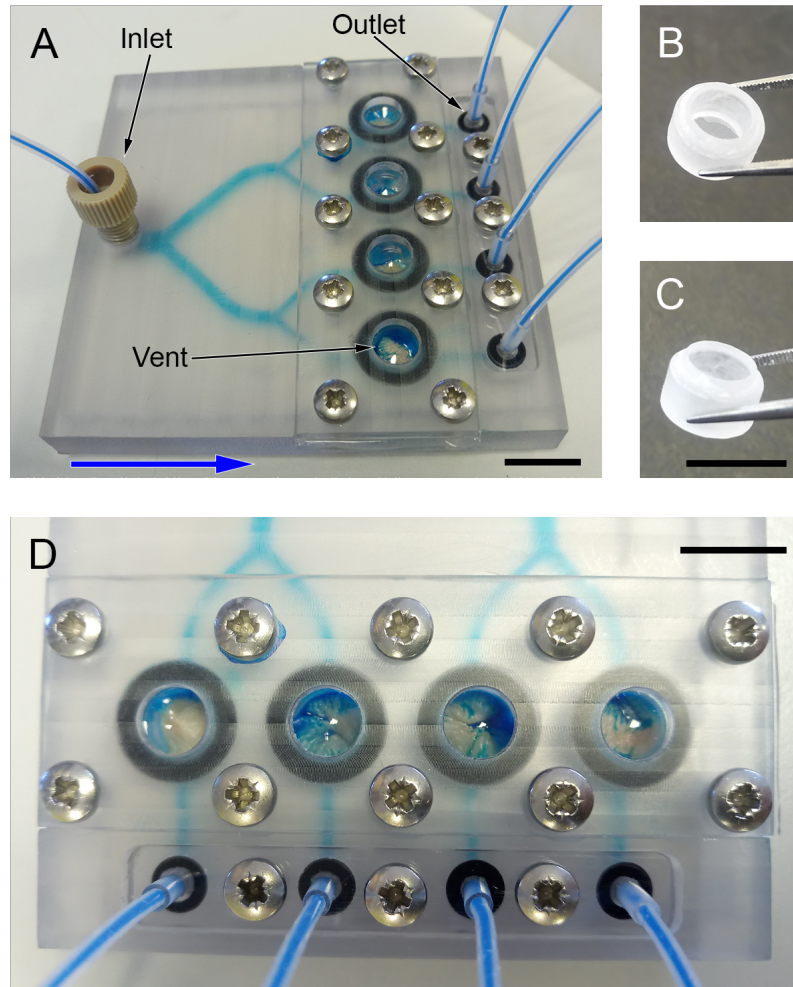
Figure 3.1.21: *Testing of V3.0 device with human skin and blue dye.* The scale bars represent 1 cm. The blue arrow indicates the direction of flow. A) An overview of the assembled V3.0 device. B) and C) Skin gasket at two angles, with the nylon membrane visible in B, D) A close-up on the lid of the V3.0 device. The skin samples are visible through the PDMS layer. The blue dye is not raising in side due to balanced pressures, however it can be seen that the dye is reaching some of the top parts of the epidermis.

3.1.4   Device V4.0

The fourth generation wound-on-a-chip device was designed to resolve the problems V3.0 device encountered. All parts of this iteration were designed to be manufactured out of PC, apart from the nylon and PDMS membranes. The branching fluidic system that originated with V2.0 device was replaced by a single channel of the dimensions that were the same as in the previous devices (100 μm deep by 1000 μm wide). Fig. 3.1.23 presents the fluidic part of the device with the design of the channel. The fluidic part was then hot-press bonded to the top part of the device (Fig. 3.1.24) to create a closed microfluidic channel with open access points for the inlet, outlet and the sample holder (Fig. 3.1.27). A thin layer of PDMS was prepared as described in section 2.2.5 on page 74, and it was placed under the PC part of the lid (Fig. 3.1.25). When held down by the bolts, the pressure kept the PDMS layer securely in place. The sample retainer (Fig. 3.1.27) was completed by bonding a nylon membrane (60 μm pore size) to the bottom of the skin retainer using chloroform. See section 2.2.6 for the method. M3 sized threads were installed in the top part of the device. The tubing connector working principles are the same as the ones in V2.0 and V3.0 devices.

The final form of the wound-on-a-chip device (V4.0) inherited the PDMS containing lid from V3.0, aimed at creation of small pressure in the tissue culture compartment, whilst allowing for an influx of oxygen. The design footprint was reduced, allowing for a faster fabrication time and reduced cost per device. The single-channel design eliminated the problems of air bubbles obstructing and shutting of channels that the previous versions faced. The overall device performance allows for successful culture of skin samples. Fig. 3.1.28 presents the V4.0 flow cell after assembly. The skin sample can be seen through the PDMS membrane in the lid, however condensation gathered on it during incubation experiments, meaning that wound healing assays cannot be monitored by imaging through the lid.
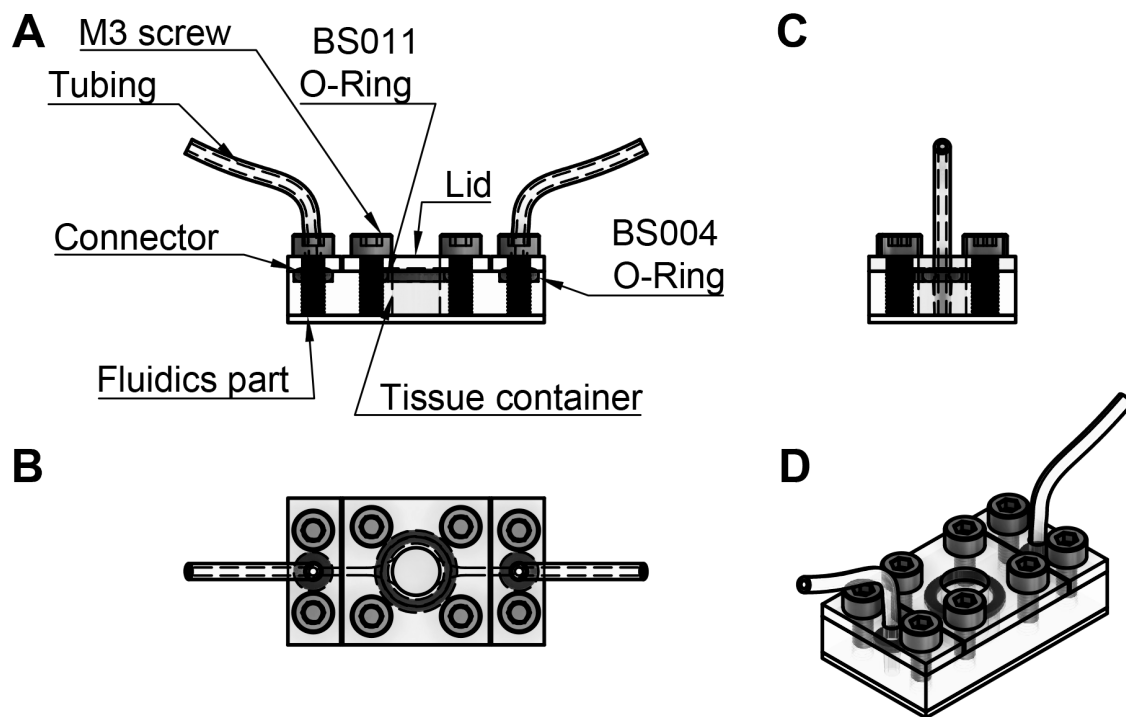
Figure 3.1.22: *Schematic of assembled V4.0 device.* A) The side view, B) the top down view, C) the front view, D) the overview.
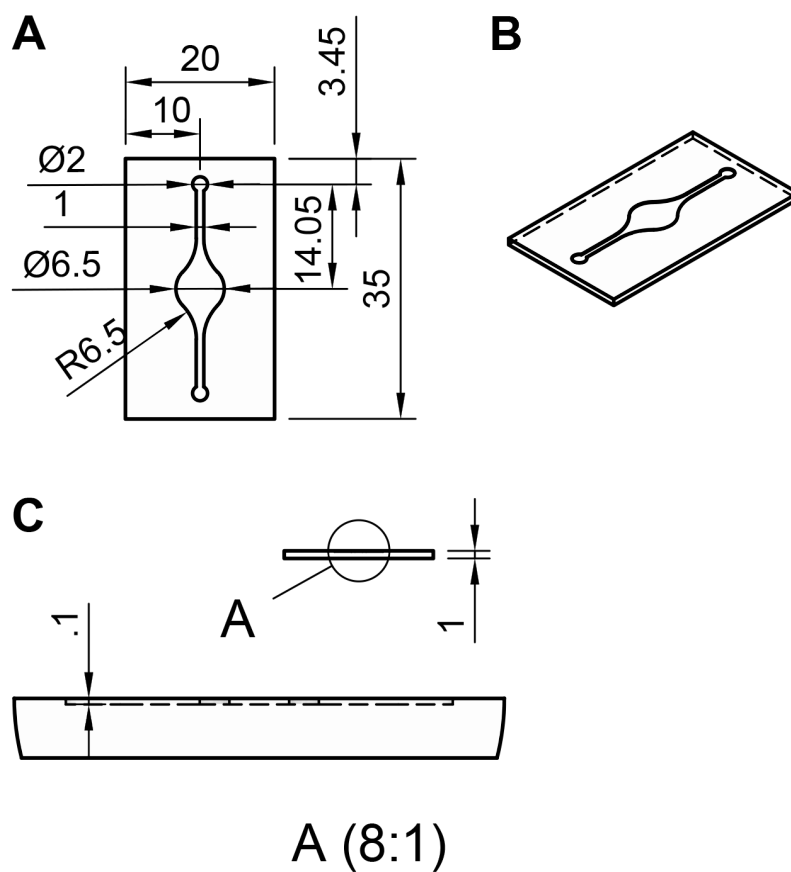
Figure 3.1.23: *V4.0 fluidics part.* A) The top down view, B) the overview, C) the front view at a scale 8:1 showing the depth of the channel. All measurements are given in mm.
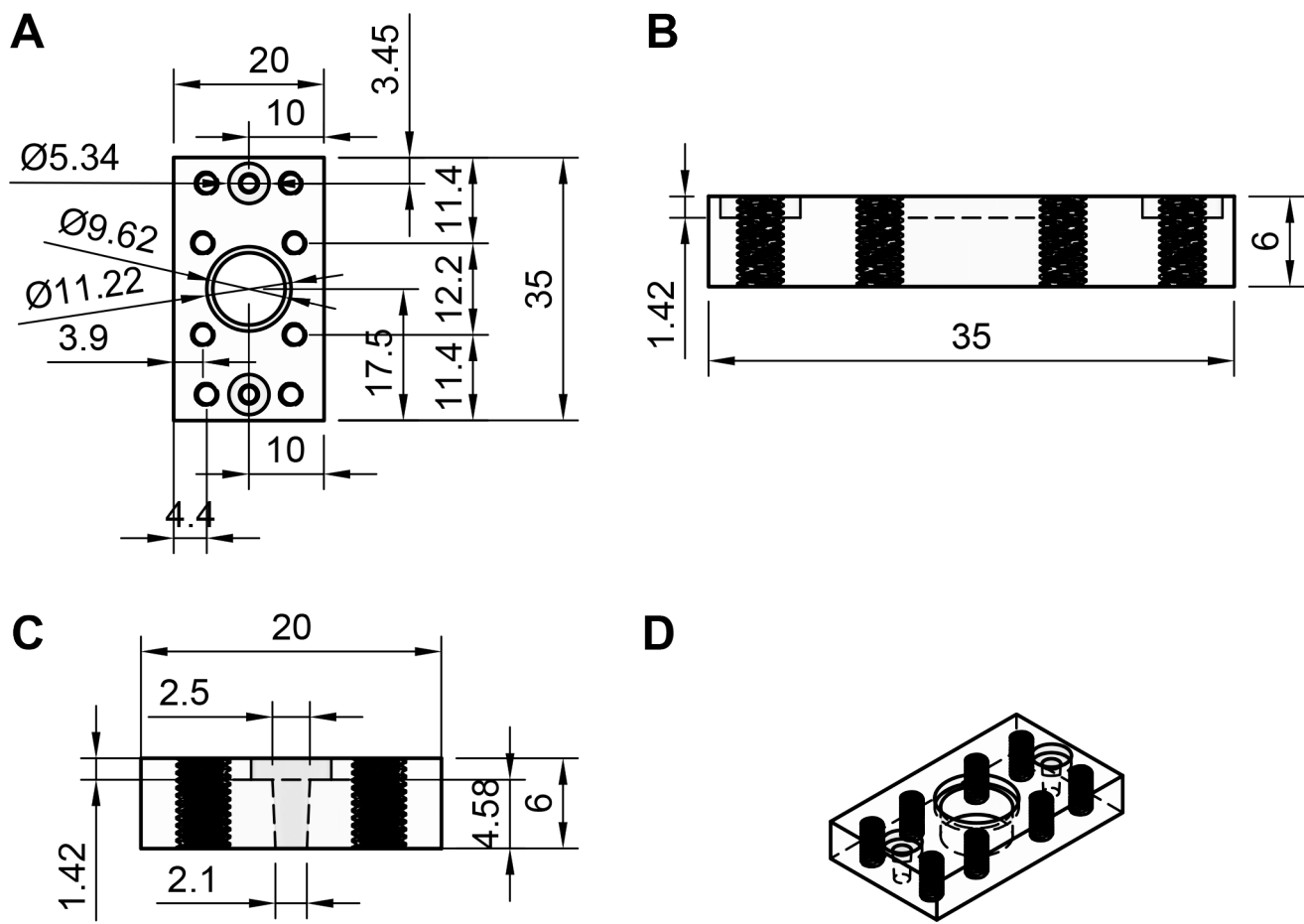
A

B

C

D

Figure 3.1.24: *V4.0 top part.* A) The top view, B) the side view, C) the front view, D) the overview. All measurements are given in mm.
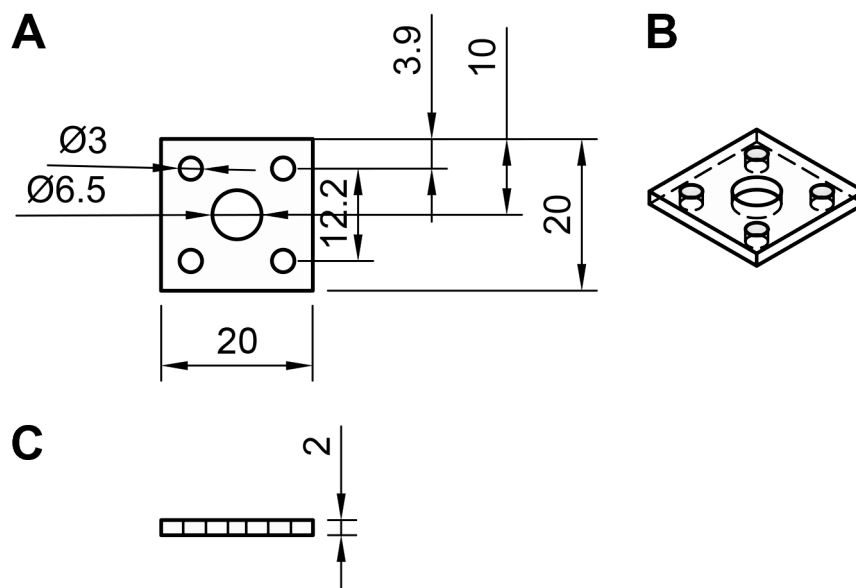
Figure 3.1.25: *V4.0 lid.* A) The top down view, B) the overview, C) the front view. All measurements are given in mm.
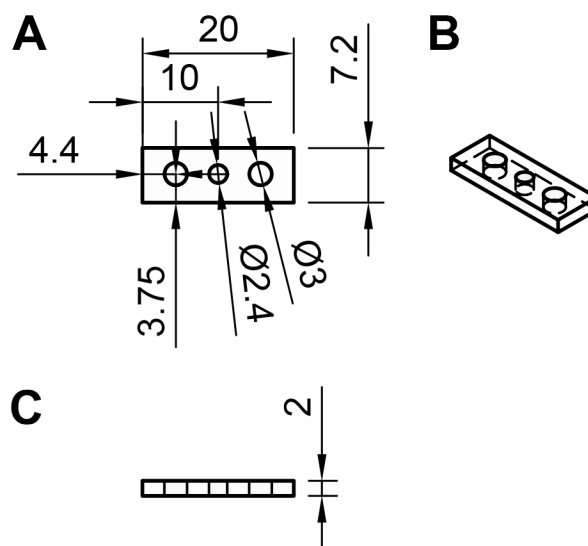

Figure 3.1.26: *V4.0 tubing connector.* A) The top down view, B) the overview, C) the front view. All measurements are given in mm.
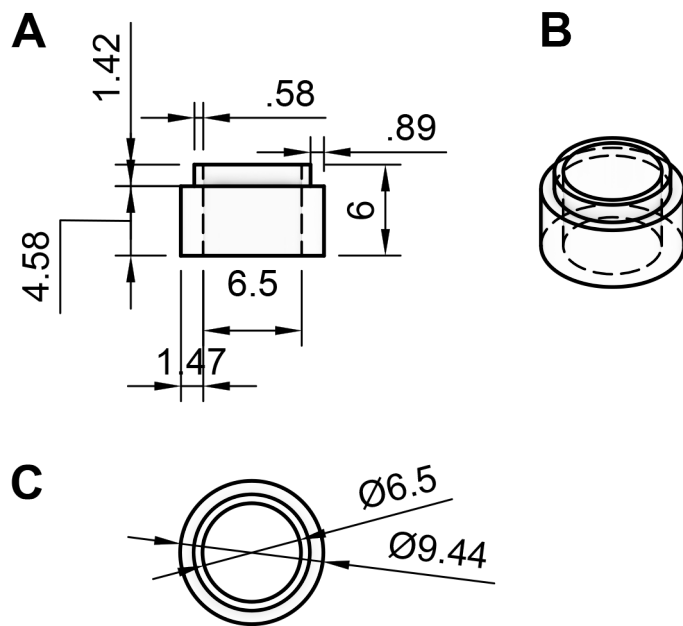
Figure 3.1.27: *V4.0 sample retainer.* A) The top down view, B) the overview, C) the front view. All measurements are given in mm.
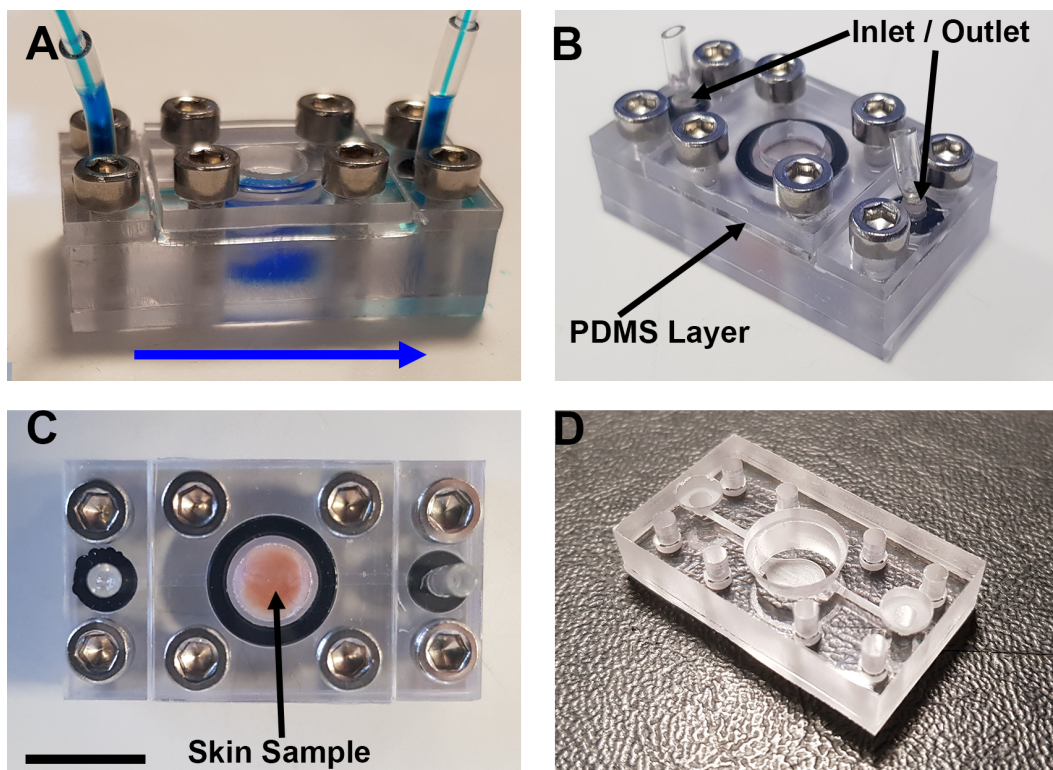
Figure 3.1.28: *V4.0 Device.* A) The blue dye was flown through the flow cell to test for leakages and to make the channel structures easier to see. The blue arrow indicates the direction of the flow. B) Assembled empty V4.0 device. C) The skin sample can be observed through the PDMS layer. D) The view of the fluidics and top parts of the device without the lids. The scale bas represents 1 cm.

3.1.5   Device V4.C1

In order to allow the researcher to work with cell-based wound healing models, a modified version of V.40 was produced.

The device uses the same chip top, lid, and the tubing connector system that V4.0 did, however the bottom fluidics system part was changed to allow for microscopic analysis of the grown cells. CNC milling of the fluidics part results in a cloudy surface appearance which makes it unsuitable for microscopic imaging on the device. Instead, Fused Deposition Modelling (FDM) 3D printing was used to print the outlines of the microfluidic channels on a glass wafer. These were then used as moulds to cast the channels using PDMS, as described in section 2.2.4. Fig. 3.1.29 shows a photo of the glass wafer on which the moulds of the channels were printed. Once printed, the surface was cleaned with isopropanol, and then PDMS was cast following the method described in section 2.2.5. A glass microscope slide was then pressed onto the uncured PDMS, so that once cured, it would be possible to peel it off the slide containing the microfluidic section identical to that of V4.0 device presented in section 3.1.4. Fig.3.1.30 shows a photo of such slide with the PDMS channel. The PDMS film was then transferred onto a rectangular coverslip. Coverslip was chosen over the sturdier microscopy slide to obtain the best possible image quality during confocal imaging.

The top part of the V4.0 device (see Fig. 3.1.24) was then aligned with the PDMS channel section on the slide, and placed in a 3D printed clamp to keep both parts together. Fig. 3.1.31 shows the 3D printed clamp design, and Fig. 3.1.32 shows the assembled V4_C1 device already in the clamp.

Once assemble it was found that high pressure applied by the 3D printed holder was needed to prevent leakages from between the PDMS layer and the PC body of the device. This force was strong enough to crack the coverslip glass used as the cell culture surface. Fig.3.1.32 shows two examples of the catastrophic breakages that

occurred during attempts to set up microfluidic cell culture with V1.C1 device. These prevented continuation of the experiment.

V4.C2 device was designed to troubleshoot the problems with glass cracking.
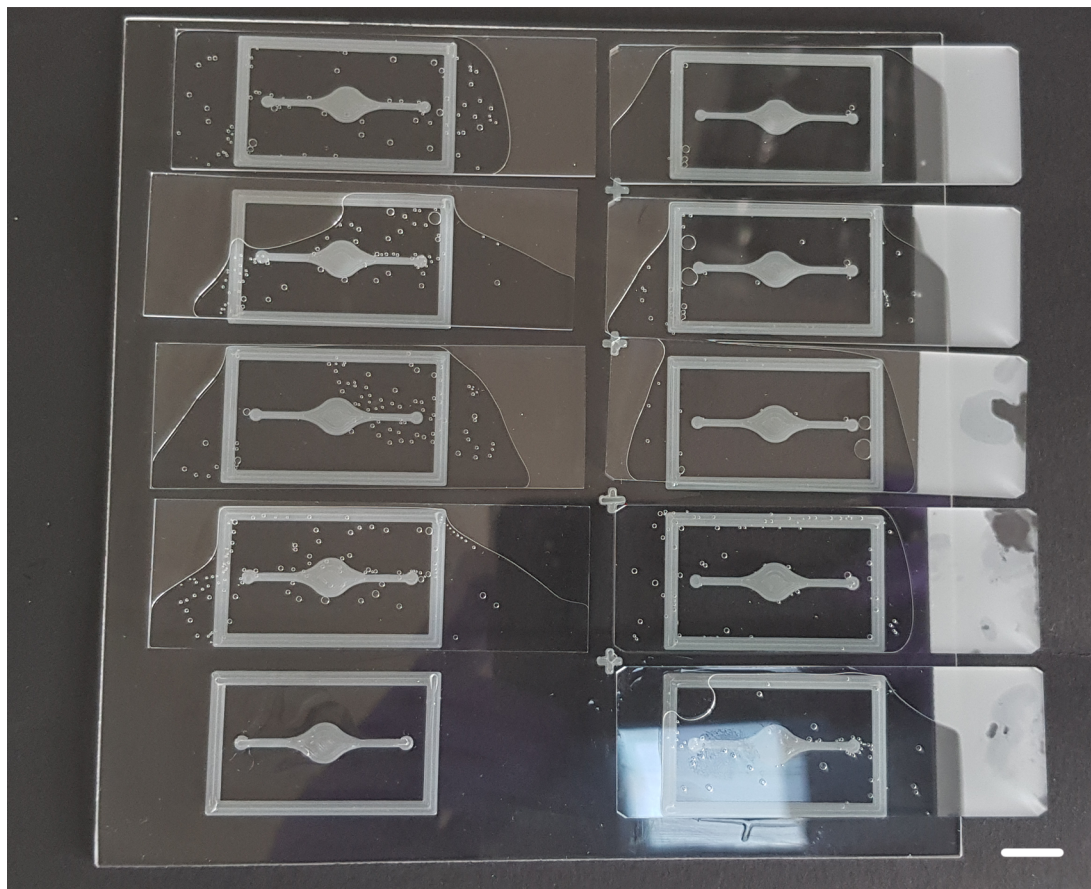

Figure 3.1.29: *Glass wafer with the 3D-printed channel moulds.* A layer of PDMS was poured into the microfluidic outlines printed on a glass wafer. These were then covered with microscopy slides, and gentle pressure was applied to push out the excess PDMS prior to curing in an oven. The scale bar represents 1 cm.
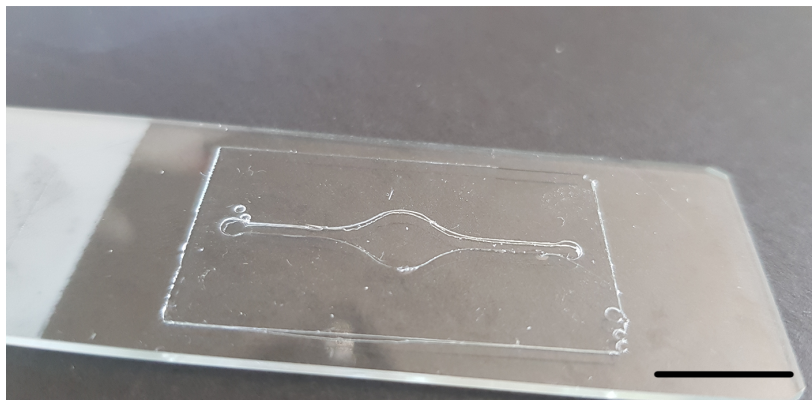
Figure 3.1.30: *The PDMS channel made using the 3D printed mould.* The casted PDMS mould of the channel section. This is identical to the channel design used in V4.0 device. The scale bar represents 1 cm.
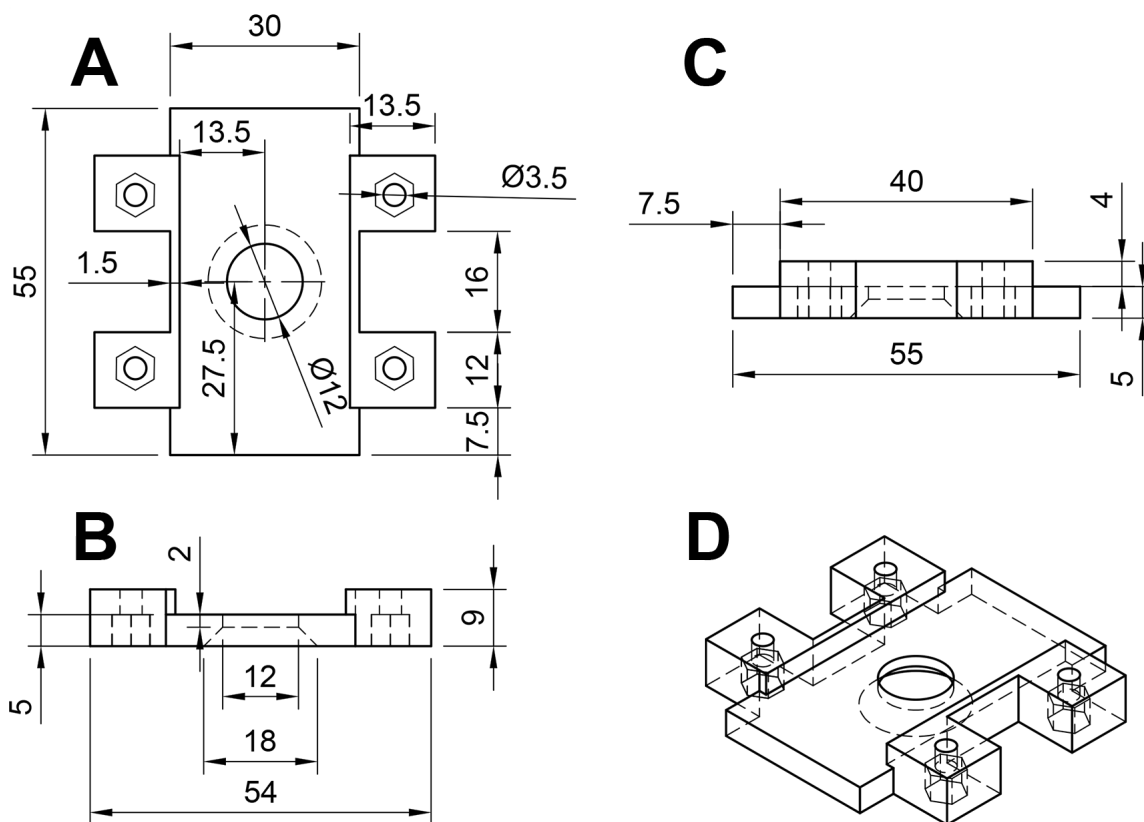

Figure 3.1.31: *V4.C1 clamp design.* A) The top view, B) the front view, C) the side view, D) the overview. All measurements are given in mm.
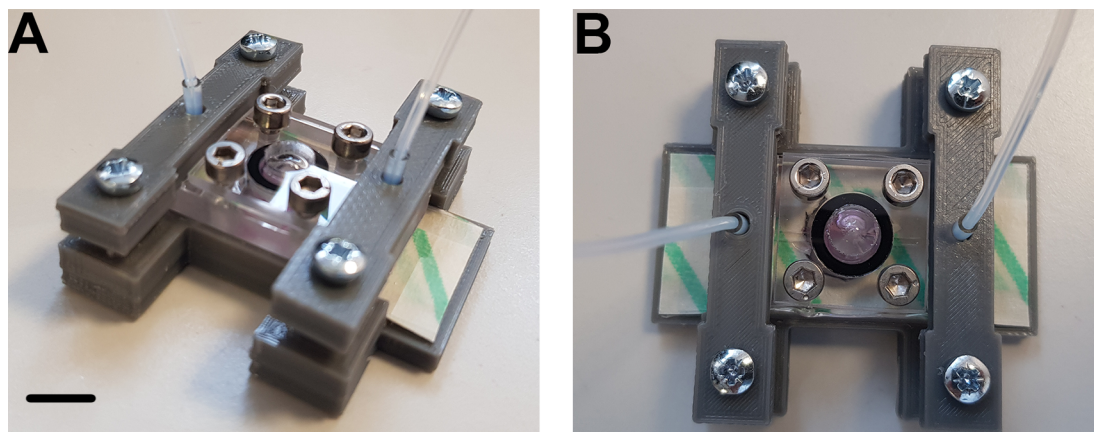
Figure 3.1.32: *Assembled V4.C1 device.* The overview (A), and the top view (B) show the fully assembled device together witht he tubing in place. The scale bar represents 1 cm.
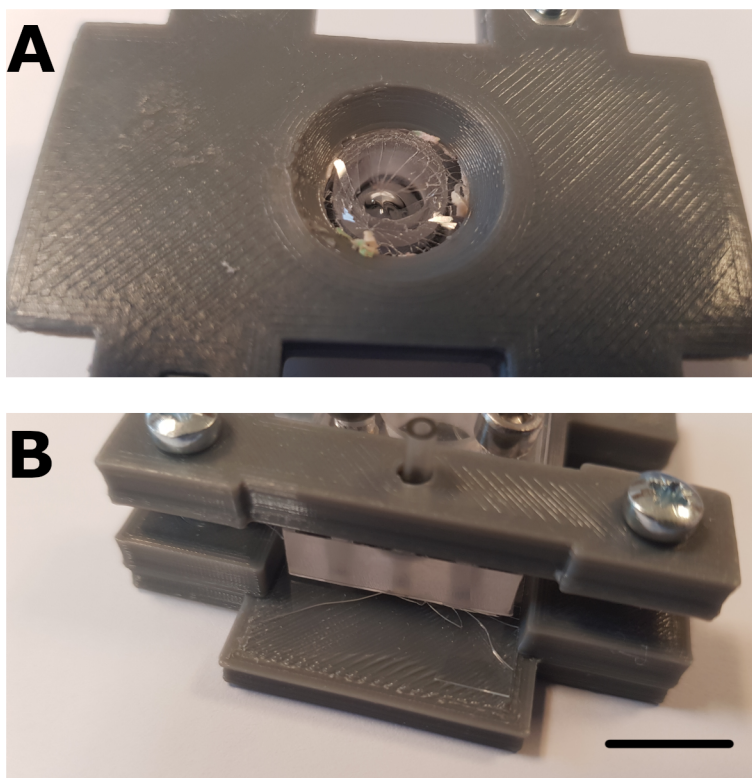

Figure 3.1.33: *The problems with V4.C1.* A) the cracked coverslip underneath the cell culture chamber, B) The crack at the side of the device. The scale bar represents 1 cm.

3.1.6   Device V4.C2

V4.C2 device was based on the concepts used for V4.C1. Its aim was to troubleshoot the problems observed with V4.C1 device, namely cracking of the glass coverslips. The main modifications introduced included replacement of the glass coverslip with a sturdier glass slide. Initial tests were carried out with the 3D printed holder, however no reliable sealing was achieved, and leakages were occurring between the PC part and the PDMS layer. As a result, the plastic holder was removed, and instead it was decided the PDMS layer would be bonded to the PC body of the device, in order to prevent leakages. Plasma bonding was chosen as the method of choice.

Plasma bonding optimisation

Four bonding strategies were tested, before an optimal bonding outcome was achieved. The general procedure was described in full in section 2.2.8. This was then modified to achieve best possible bonding outcome. Table 3.1 contains the specific conditions used in the four protocol variations.

Protocol A led to formation of a strong bond, however air pockets were visible between the PC part and the PDMS layer. The bond disappeared within an hour of exposure to water. Protocol B wasn't very successful either. No bonding was achieved. Protocol C was more successful than A and B, allowing for a strong bond to be formed, however it would disappear after around 3 h of water exposure. Finally, protocol D allowed for formation of a strong and lasting bond which didn't deteriorate under liquid exposure.

Table 3.1: *The silanisation conditions.* The protocol specific conditions were outlined for the key protocol procedures - PC Plasma and PDMS Plasma - referring to Plasma treatment of the surfaces, Silanisation - referring to the silane treatment details, incubation - referring to the conditions of incubating of the treated surface with the particular silane, the wash off procedures referring to the method used to remove the excess silane from the surface, and to optionally clean it prior to interfacing, which is the final procedure where the surfaces are brought together to achieve bonding.

| Procedure	Protocol			
	A	B	C	D
PC Plasma	1 min	1:30 min	1:30 min	1 min
Silanisation	5% APTMS (EtOH, v/v)	5% APTMS (EtOH, v/v)	5% APTMS (EtOH, v/v)	1% v/v APTES
Incubation	60°C, 1:20 h	80°C, 30 min		RT, 20min
1st wash off	N/A	Rinse with EtOH, dry with air gun	Shake off the solution, air gun dry.	Rinse with ddH2O, dry with air gun.
PDMS Plasma	PDMS + PC for 1 min	PDMS for 1:30 min	PDMS for 1:30 min, PC for 15 s	PDMS for 1 min
2nd wash off	N/A	Air gun to blow off potential dust	N/A	N/A
Interfacing time	30 min	30 min	60 min	60 min
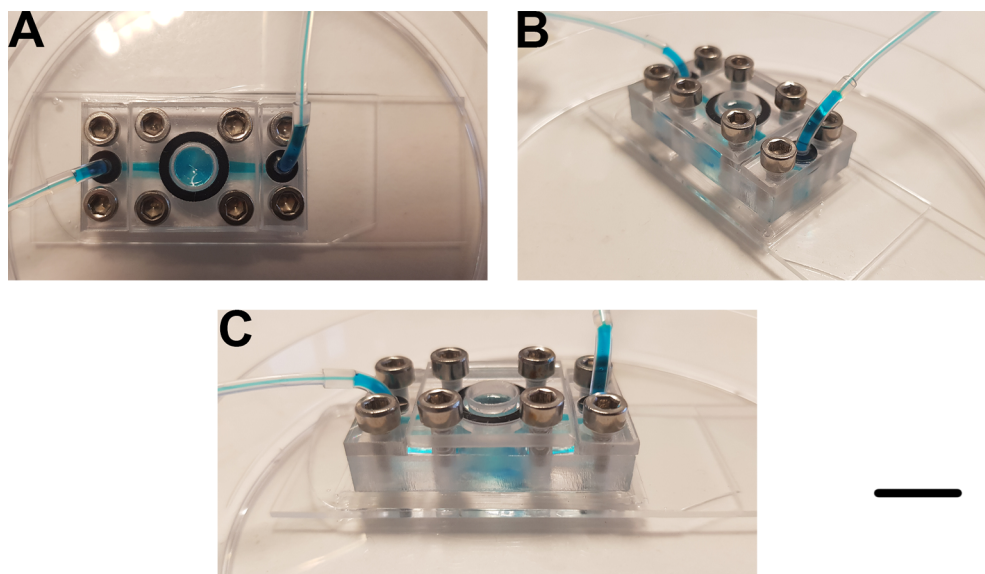
Figure 3.1.34: *Assembled V4.C2 device.* A) The top view, B) the overview, C) the side view. Blue dye was used to make the fluidic structure visible. The scale bar represents 1 cm.

Device iteration summary

Figure 3.1.35 summarises all the microfluidic devices produced as part of this project, and presented in the thesis. The encountered problems and the improvements are also enumerated.
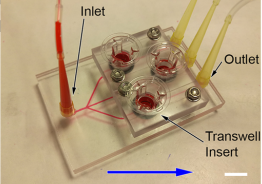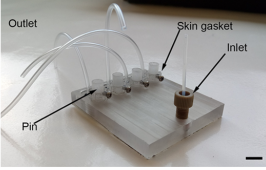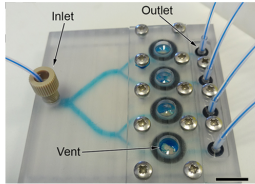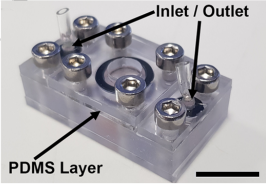
Figure 3.1.35: *Comparison of device versions.* All the microfluidic wound-on-a-chip devices produced as part of this work, and their issues encountered, and the improvements. The scale bars represent 1 cm.

3.2   Biological validation of the devices

The devices presented in section 3.1 were then put through biological validation to asses their impact on tissue viability.

3.2.1   V3.0 device improved tissue viability when compared to V2.0

In order to compare V2.0 and V3.0 devices and the extent of apoptotic cell death associated with the culture system used, a seven-day long culture experiment was set up. The static control ex-plants, and microfluidic explants were set up and carried out as described in sections 2.2.11 and 2.2.12 respectively. The culture duration was seven days, and the microfluidic samples were supplied with the medium at 10 μL min^{-1}. Seven-day culture period was chosen for the initial experiments as the classical off-chip static culture experiments are often carried out for such time period. This makes it easier to draw comparisons, as the microfluidic model should be able to maintain the tissue samples alive for at least that period of time. The flow rate of 10 μL min^{-1} was chosen as the starting point, as this value was well thin the flow rate values reported in the literature on the skin-on-a-chip studies. This value was then to be further optimised, as presented in section 3.2.4. TUNEL staining was performed on the skin samples to investigate the impact of the device type on the apoptotic cell death in the samples. TUNEL staining was carried out as described in section 2.2.17. The analysis revealed that the upgraded V3.0 device is significantly better at maintaining the skin samples alive than V2.0 device, due to reduced apoptosis levels observable in the V3.0 samples. This was confirmed by performing a one-way ANOVA analysis, which returned $p < 0.001$, $f(3) = 19.67$ (f-value for a test with three degrees of freedom). The post-hoc Tukey HSD multiple comparison of means analysis further specified that the mean of apoptotic cell death from the samples collected from V2.0 devices

is significantly different than that of samples from V3.0 devices. As evident from Fig. 3.2.2, the skin samples collected form V3.0 device presented with over 2x lower levels of apoptosis. These levels were also comparable with those of the static culture samples, and a little higher than the levels observed in the uncultured Day 0 samples. Fig. 3.2.1 presents a montage of fluorescent microscopy images that were used to produce Fig. 3.2.2. For the V2.0 device, the apoptotic cell death is most likely to be present in the epidermis and the distal dermal section close to the epidermis. This is due to the pin used to hold the samples in place exerting mechanical force on the tissue. In comparison, the V3.0 device is likely to present with a greater proportion of apoptotic cell death in the dermis. V3.0 device was suffering from uneven flow due to the channels shutting off randomly. This is likely to lead to reduced sample perfusion. In such instance the dermis will suffer both suboptimal nutrient and oxygen delivery, whereas the epidermis will still be able to receive some oxygen through the PDMS layer in the chip lid, with glucose delivery still being suboptimal.
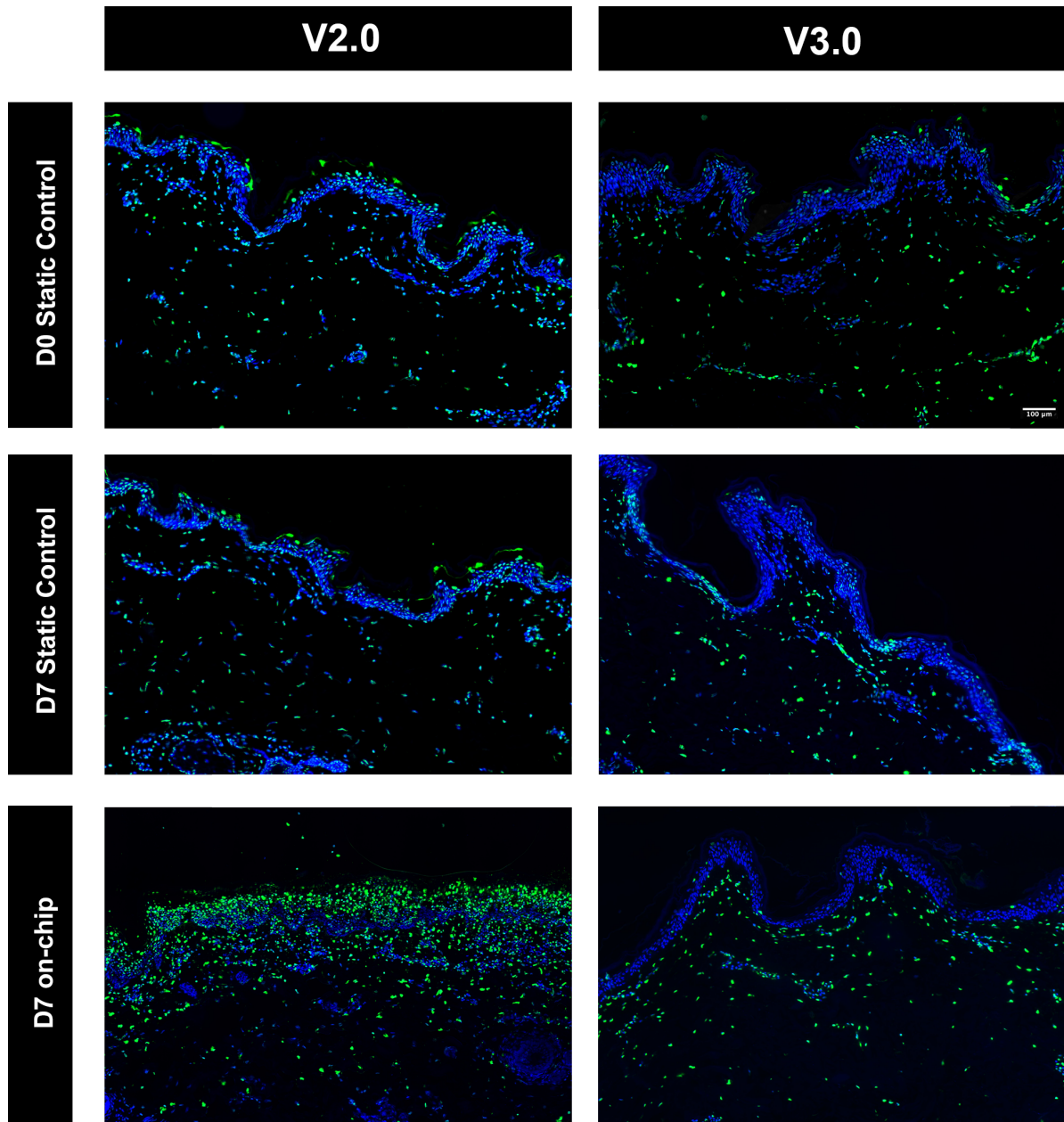
Figure 3.2.1: *TUNEL micrographs comparing V2.0 and V3.0 devices.* The skin samples were maintained on V2.0 and V3.0 devices, and in static culture, for seven days. They were then fixed, sectioned, stained using TUNEL assay to visualise the double-stranded DNA breaks indicating apoptotic cell death, and counterstained with DAPI to visualise the nuclei. The tissue sections were then imaged on a fluorescent microscope with a 20x objective. The samples used for the experiment came from p56 (V2.0) and p61 (V3.0) patients, both females who donated skin samples from their abdomen. The experiments were carried out on separate days. textcolorblueDAPI - blue, TUNEL - green. The scale bar represents 100 μm.
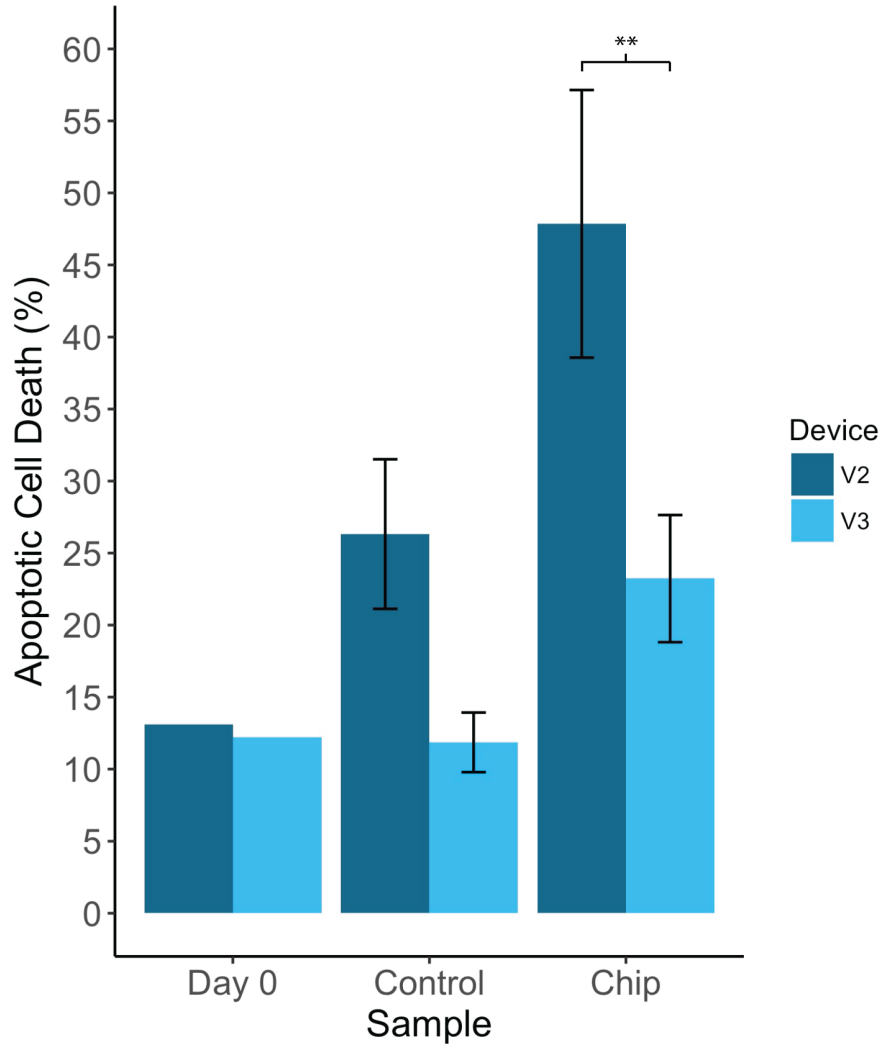
Figure 3.2.2: *Comparison of apoptosis in samples from V2.0 and V3.0 devices*. The skin samples were maintained on V2.0 and V3.0 devices with flow rate of 10 μm min⁻¹, and in static culture. The samples used for the experiment came from p56 (V2.0) and p61(V3.0) patients, both females who donated skin samples from their abdomen. V2.0 and V3.0 experiments were carried out on separate days. The sample numbers for V2.0 and V3.0 experiments are n = 4 and n = 3 respectively. These were biological replicates. The culture duration was seven days. They were then fixed, sectioned, stained using TUNEL assay to visualise the double-stranded DNA breaks indicating apoptotic cell death, and counterstained with DAPI to visualise the nuclei. The tissue sections were then imaged with a 20x objective on a fluorescent microscope. ImageJ was used to count the DAPI and FITC stained cells, and the ratio was used to calculate the percentage of apoptotic cell death. R was used to plot the results and carry out one-way ANOVA. ** - $p < 0.01$. The results suggest that there is a clear reduction in apoptotic cell death in the V3.0 samples when compared to V2.0. The error bars represent the standard error of the mean.

3.2.2 V3.0 helps to reduce cell stress, when compared to V2.0

Next, keratin IHC staining was carried out to gain a better understanding of the progress of the healing process in the studied systems. The static control cultures, and microfluidic cultures were set up and carried out as described in sections 2.2.11 and 2.2.12 respectively. The overall culture duration was seven days. The microfluidic samples were supplied with the medium at 10 μL min^{-1}. Keratin 6 (K6) and Keratin 14 (K14) staining was carried out as described in section 2.2.18. The analysis of the stained samples revealed very little expression of K6 in the Day 0 (D0) control samples associated with V2.0 device experiment. As evident from Fig. 3.2.3, the Day 0 controls for the V3.0 device experiment displayed some atypical nuclear staining, as K6 is typically expressed in the cell cytoplasm. Interestingly, Static Control for the V2.0 device showed even more condensed nuclear staining. The biggest change can be observed in the on-chip maintained samples. The skin sections from the V2.0 device show very intense staining and significantly increased thickness (see section 3.2.3 for more details) of the epidermis compared to the controls. Another very obvious feature is a large number of cells with the nuclei separated from the cytoplasm and apparently dead. Fig. 3.2.3 presents the holes that can be seen in the epidermis of the on-chip cultured samples from V2.0 devices (see label A). This tissue damage is likely to have been caused by the pressure applied onto the sample by the sample retaining pin used in V2.0 device. This might suggest that V2.0's tissue retention design creates a worse environment for the sample, leading to its deterioration, however such claim cannot be made with certainty due to lack of biological repetitions.

Gaps between constricted nuclei and what would be the cells can also be seen in the same panel; example has been labelled (label B). This might be a sign of apoptotic cell death, however this would have to be further verified with a separate test such as TUNEL assay.

On the other hand, the K6 staining in the samples from the V3.0 device seems to be much weaker, with no visible cells with nuclei separating from the cytoplasm. The weaker staining in the V3.0 samples is not an artefact, but a genuine result. Three different samples were considered in the case of each device type. Furthermore, the staining result matches the expectation that V4.0 device, which did not utilise the pin mechanism mechanically holding the skin sample in place, would not cause mechanical stress leading to hyper-proliferation, which could be inferred from increase in K6 staining.

p56 and p61 specified in Fig. 3.2.3 refer to two different patient samples used as part of this study. This unfortunately is an additional variable. The results are still very informative about the detrimental impact of the retention system used in V2.0, however the lack of sufficient replication makes it impossible to confirm it with a degree of statistical certainty.

Figure 3.2.3: *Comparison of K6 staining of tissue samples from V2.0 and V3.0 devices.* The skin samples were maintained on V2.0 and V3.0 devices with flow rate of 10 um min^{-1}, and in static culture. The samples used for the experiment came from p56 (V2.0) and p61(V3.0) patients, both females who donated skin samples from their abdomen. V2.0 and V3.0 experiments were carried out on separate days. The sample numbers for V2.0 and V3.0 experiments are n = 4 and n = 3 respectively. These were biological replicates. The culture duration was seven days. They were then fixed, sectioned, and stained with NovaRED for K6 (brown-red), and counter-stained with Haematoxylin (blue), which stains the nuclei and the collagen in the skin sections. The tissue sections were then imaged with a 20x objective on an inverted microscope. Label A - hole in the epidermis. B - potential sign of cell death. In black, the strata annotations: c - *Stratum corneum*; s,g - *Stratum spinosum* and *Stratum granulosum*, b - *Stratum basale*, d - Dermis. The scale bar represents 50 μm.

3.2.3 The V3.0 device prevented epidermal thickening, when compared to V2.0 device

The staining for Keratin 14 (K14) revealed that, in the uncultured Day 0 sample which acted as a D0 control for the V2.0 device, K14 was expressed in the basal layer of the epidermis (see Fig. 3.2.5). The thickness of that layer then increased in the static control samples, and took up the entire thickness of the dermis in the samples cultured on the device. The samples collected from the V3.0 device showed a different staining profile. The D0 control samples did not present with a distinct band of stained cells in the basal layer. Instead, the entire epidermis showed K14 expression. This did not change in the static controls or the samples cultured on the chip. The epidermal thickness was quantified in the K14 stained samples, and the results can be seen in Fig. 3.2.4. The average epidermal thickness in the samples from the V2.0 device was 98 ±22 μm. This was only 39 ±1 μm for the samples grown on the V3.0 device. A two-sample T-test performed on the samples collected from the microfluidic devices confirmed that the difference in the means of the dermal thickness is not due to chance, and it returned t(3) = 4.3223, p = 0.0208. This means that maintaining human skin samples V3.0 microfluidic device yielded significantly lower epidermal thickness than it was the case with V2.0 device.

Although this data might suggest that V2.0 device contributed to the increase in epidermal thickness, it is impossible to conclude with certainty that this is what happened. It is possible that the compressive force coming from the pin holding the skin sample down could have induced thickening of the sample, possibly by inducing cellular proliferation. A recent study demonstrated that mechanical stimulation can up regulate the proliferation of fibroblasts (Wahlsten et al., 2021).
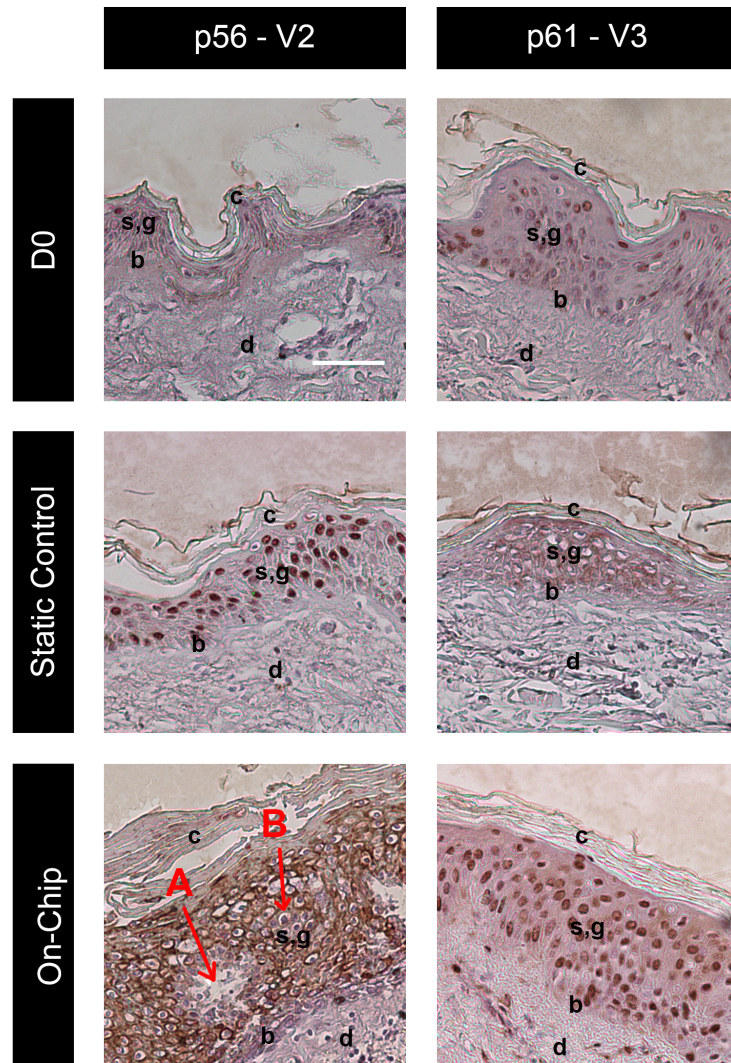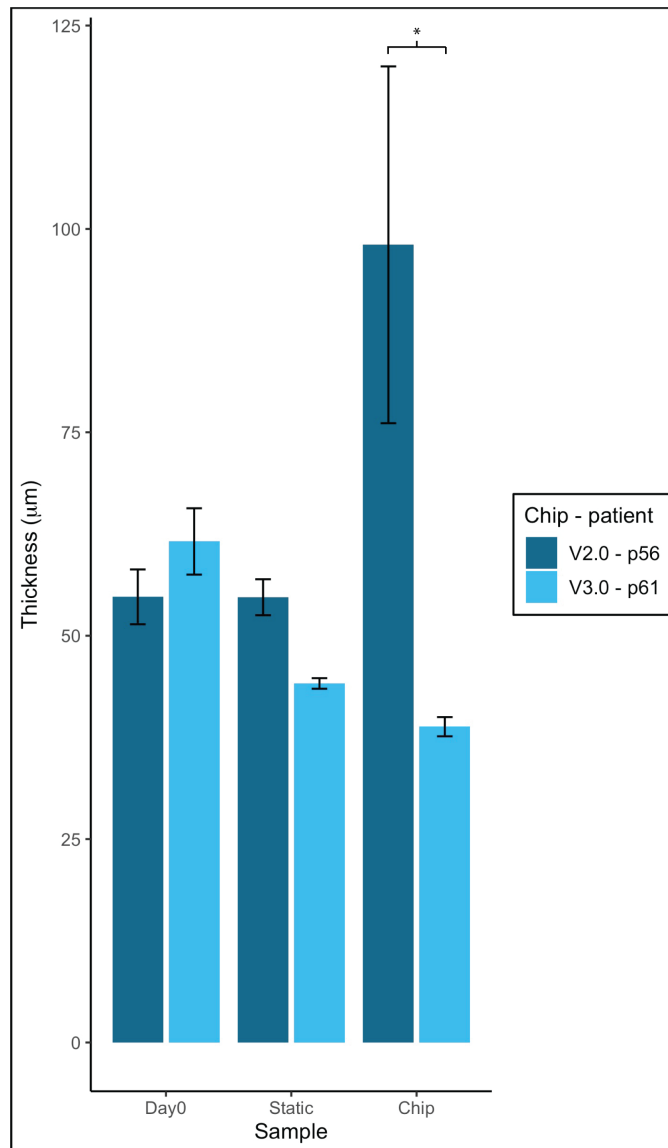
Figure 3.2.4: *Comparison of epidermal thickness in samples from V2.0 and V3.0 devices.* The skin samples were maintained on V2.0 and V3.0 devices with flow rate of 10 µm min⁻¹, and in static culture. The samples used for the experiment came from p56 (V2.0) and p61(V3.0) patients, both females who donated skin samples from their abdomen. V2.0 and V3.0 experiments were carried out on separate days. The sample numbers for V2.0 and V3.0 experiments are n = 4 and n = 3 respectively. These were biological replicates. The culture duration was seven days. They were then fixed, sectioned, stained using NovaRED for K14, and counter-stained with Haematoxylin which stains the nuclei and the collagen in the skin sections. The tissue sections were then imaged with a 20x objective on an inverted microscope. ImageJ was used to measure the thickness of the epidermal layer. R was used to plot the results and carry t-test. * - $p < 0.05$. The results suggest that the samples from V2.0 device have significantly thicker epidermis. The error bars represent the standard error of the mean.
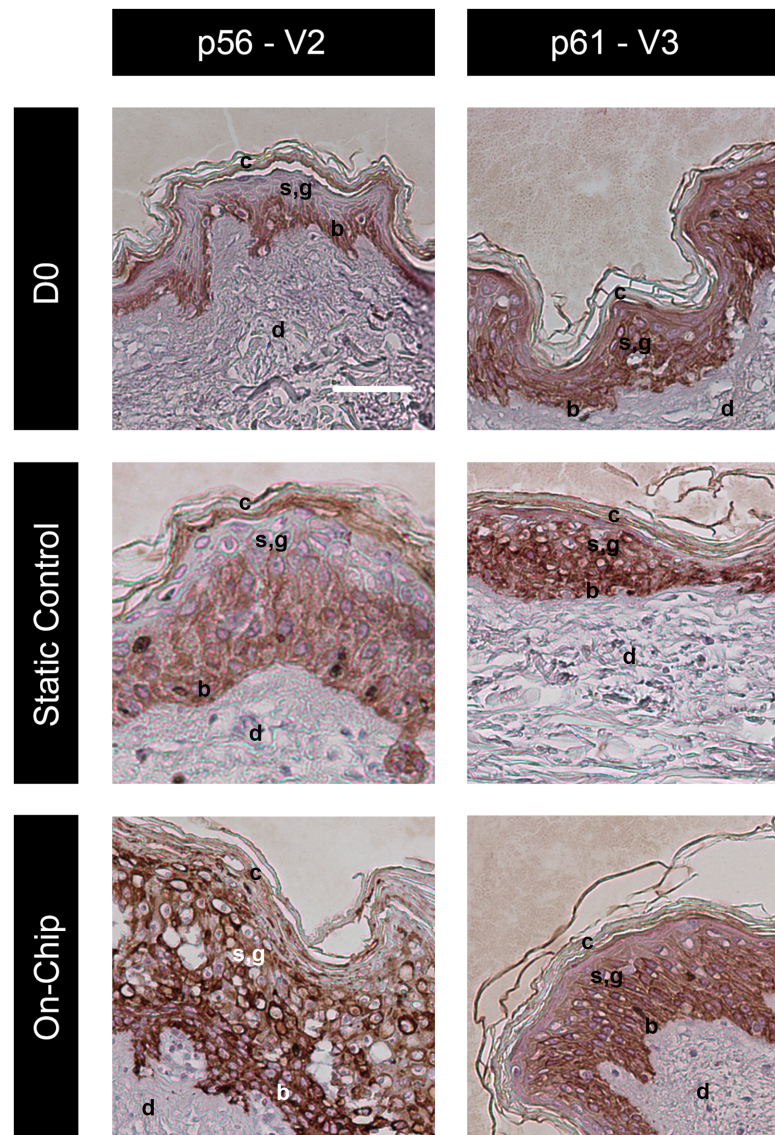
Figure 3.2.5: *Comparison of K14 staining of tissue samples from V2.0 and V3.0 devices.* The skin samples were maintained on V2.0 and V3.0 devices with flow rate of 10 um min⁻¹, and in static culture. The samples used for the experiment came from p56 (V2.0) and p61(V3.0) patients, both females who donated skin samples from their abdomen. V2.0 and V3.0 experiments were carried out on separate days. The culture duration was seven days. The samples were then fixed, sectioned, and stained with NovaRED for K14 (brown-red), and counter-stained with Haematoxylin (blue), which stains the nuclei and the collagen in the skin sections. The tissue sections were then imaged with a 20x objective on an inverted microscope. In black, the strata annotations: c - *Stratum corneum*; s,g - *Stratum spinosum* and *Stratum granulosum*, b - *Stratum basale*, d - Dermis. The scale bar represents 50 μm.

3.2.4   The V4.0 device outperforms the controls in tissue survival

The assessment of the V4.0 device involved a seven, and fourteen day long culture periods, with the end-point samples being collected on days zero and seven for the seven-day-long experimental set up; and days zero, ten, and fourteen for the fourteen-day-long experiment. The static and microfluidic cultures were set up and carried out as described in sections 2.2.11 and 2.2.12 respectively. Three flow rates of 2.5 μL min^{-1}, 5.0 μL min^{-1}, and 10.0 μL min^{-1} were used to further investigate the impact of the flow rate on the tissue viability. End-point TUNEL staining was used to analyse apoptotic cell death in the samples. This was carried out as described in section 2.2.17. Different flow rates were tested to asses the relationship between the flow rate and tissue viability. The extended culture duration was aimed to investigate the viability changes in the samples for a time period longer than seven days. The flow rate naturally affects the delivery of nutrients to the sample, removal of the metabolic by-products, potential removal of the wound exudate, but it also exerts shear stress. The sample was not positioned in the channel, but it sat directly above it and it was separated by a membrane, therefore the impact of the shear force will be minimal, but because the pore size is 60 μm, there will be some shear force. Sharma et al. investigated the shear forces in a Testis-on-a-Chip device, where the sample was separated from the medium flow by a series of battlement structures with 250 μm pore size. The maximum shear stress observed did not exceed 0.02 Dyn cm^{-2}, with 0.1 Dyn cm^{-2} being the estimated standard shear stress for endothelial barriers (Sharma et al., 2022). Despite the differences in the designs of the fluidic systems, the Testis-on-a-Chip study can be used for cooperative purposes. The values observed with a 60 μm pore membrane would be expected to be even lower, and therefore well within the physiological values. The increase in the culture duration from seven to fourteen days was aimed to test the sample viability during a longer culture period.

The results from the seven day long culture experiment (see Fig. 3.2.6) showed that the samples maintained on the V4.0 device supplied with culture medium at 10.0 μL min^{-1} exhibited four-fold decrease in apoptotic cell death in the epidermis, when compared to the static control collected on the same day. (1.4% cell death for the on-chip sample vs. 6.1% for the static control). Furthermore, the dermal cell survival was significantly improved in the on-chip samples, with only 4.1% cell death detected in the samples from the flow chip vs. 8.3% for the static control. A dose-dependent relationship can be seen between the flow rate and the dermal apoptotic cell death. The highest death rate amongst Day 7 on-chip samples can be observed in the device with the flow established at 2.5 μL min^{-1}, and it reduced as the flow rate was increased. On the other hand, the epidermal cell death stayed very low, around 1%, irrespective of the flow rate, and always lower than the dermal cell death.

Maintaining the samples on the device for 14 days (Fig. 3.2.7) produced supporting results, confirming that the microfluidic devices were more successful at keeping tissue alive than the static culture systems. The average dermal cell death for the control samples collected on day 14 was 38.1% whilst the on-chip samples exhibited dermal cell death averaging 8.3%. Day 10 controls also produced epidermal and dermal cell deaths measurably higher than those of the on chip cultured samples, irrespective of the flow rate applied.

The presentation matches the expected results of the epidermis yielding higher levels of apoptotic cell death. This is most likely due to the fact that it is populated by a greater amount of respiring cells than the dermis, and it's further away from the irrigation channel, meaning the diffusion of the nutrients and oxygen to the epidermis would be suboptimal.

The number of samples used for the D0 uncultured control sample was n=3. These control samples were processed on the same day, and under the same conditions, and they all originated from the same patient. The variability demonstrated by the sample

is significantly greater than that of other samples. This is an indicator of intra-donor variation in the dermal thickness, even between samples originating from proximal sites.

Figure 3.2.6: *Apoptotic cell death results from the TUNEL analysis of 7-day culture experiment on the V4.0 devices.* The skin samples were maintained on V4.0 devices with flow rats ranging from 2.5 µL min^{-1} to 10 µL min^{-1}, and in static culture. HEPES and CO_2 controls were static controls collected on day seven. The samples used for the experiment came from patient HS74R - a female who donated skin samples from her abdomen. All the samples were run in parallel. The sample numbers for V4.0 samples of the following flow rates where: 2.5 µL min^{-1} n = 2, 5 µL min^{-1}n = 1, 10 µL min^{-1} n = 1. These were biological replicates. The culture duration was seven days. They were then fixed, sectioned, stained using stained using TUNEL assay to visualise the double-stranded DNA breaks indicating apoptotic cell death, and counter stained with DAPI to visualise the nuclei. The tissue sections were then imaged with a 20x objective on a fluorescent microscope. ImageJ was used to count the DAPI and FITC stained cells within dermis and epidermis, and the ratio was used to calculate the percentage of apoptotic cell death. The results suggest that the samples from V4.0 device demonstrated lower epidermal cell death than the static controls. The error bars represent the standard error of the mean.
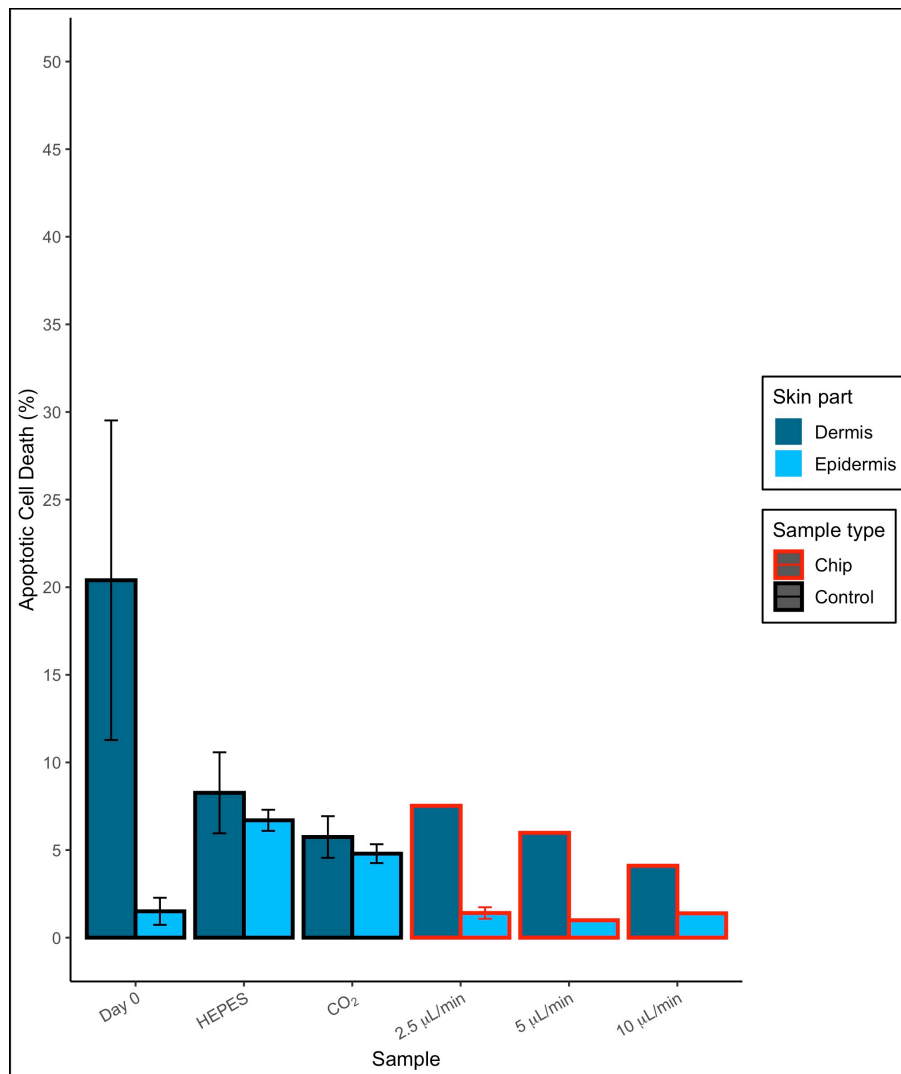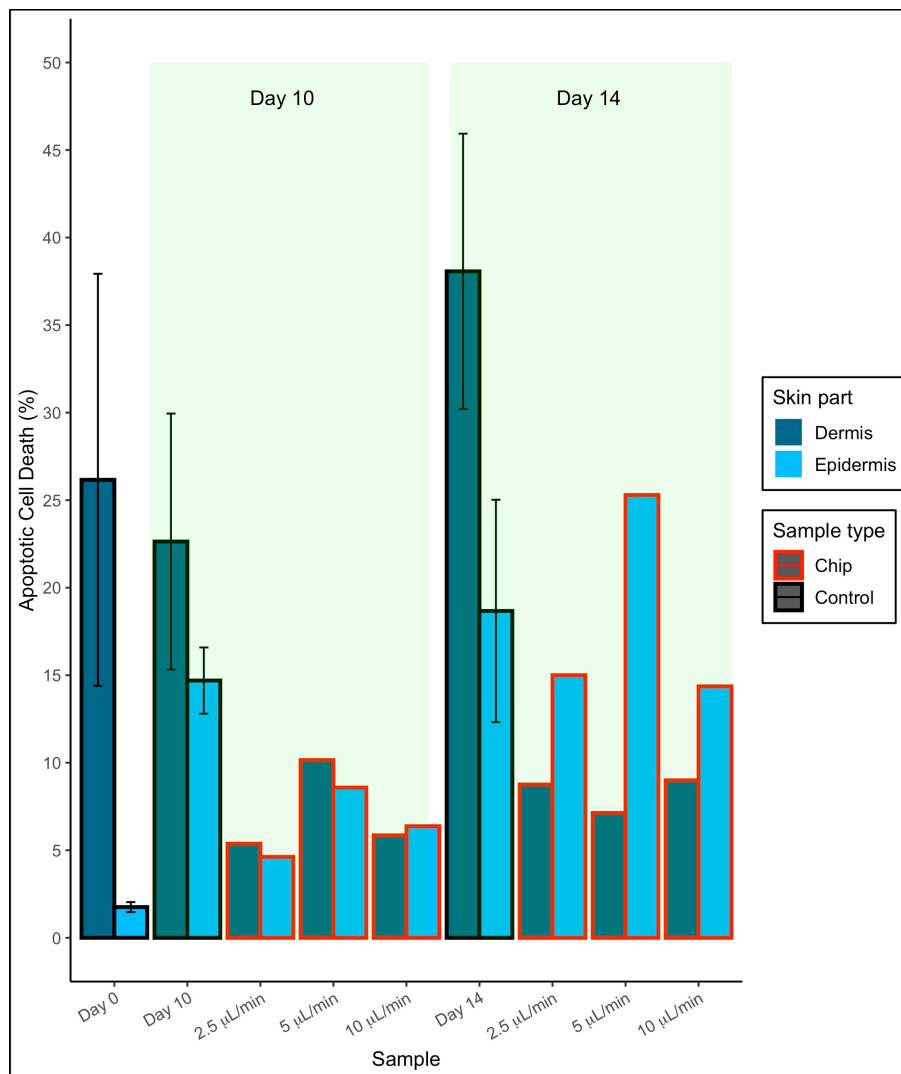
Figure 3.2.7: *Apoptotic cell death results from the TUNEL analysis of 14-day culture experiment on the V4.0 devices.* The skin samples were maintained on V4.0 devices with flow rats ranging from 2.5 μL min⁻¹ to 10 μL min⁻¹, and in static culture. The samples used for the experiment came from patient HS74R - a female who donated skin samples from her abdomen. All the samples were run in parallel. The sample numbers for V4.0 samples of the following flow rates where: D10 2.5 μL min⁻¹ n = 2, D10 5 μL min⁻¹n = 1, D7 10 μL min⁻¹ n = 1, D14 2.5 μL min⁻¹ n = 1, D14 5 μL min⁻¹n = 1, D14 10 μL min⁻¹ n = 1. These were biological replicates. The culture duration was seven days. They were then fixed, sectioned, stained using stained using TUNEL assay to visualise the double-stranded DNA breaks indicating apoptotic cell death, and counter stained with DAPI to visualise the nuclei. The tissue sections were then imaged with a 20x objective on a fluorescent microscope. ImageJ was used to count the DAPI and FITC stained cells within dermis and epidermis, and the ratio was used to calculate the percentage of apoptotic cell death. The results suggest that the samples from V4.0 device demonstrated lower epidermal cell death than the static controls on day 10, but lower dermal cell death on day 14. The error bars represent the standard error of the mean.
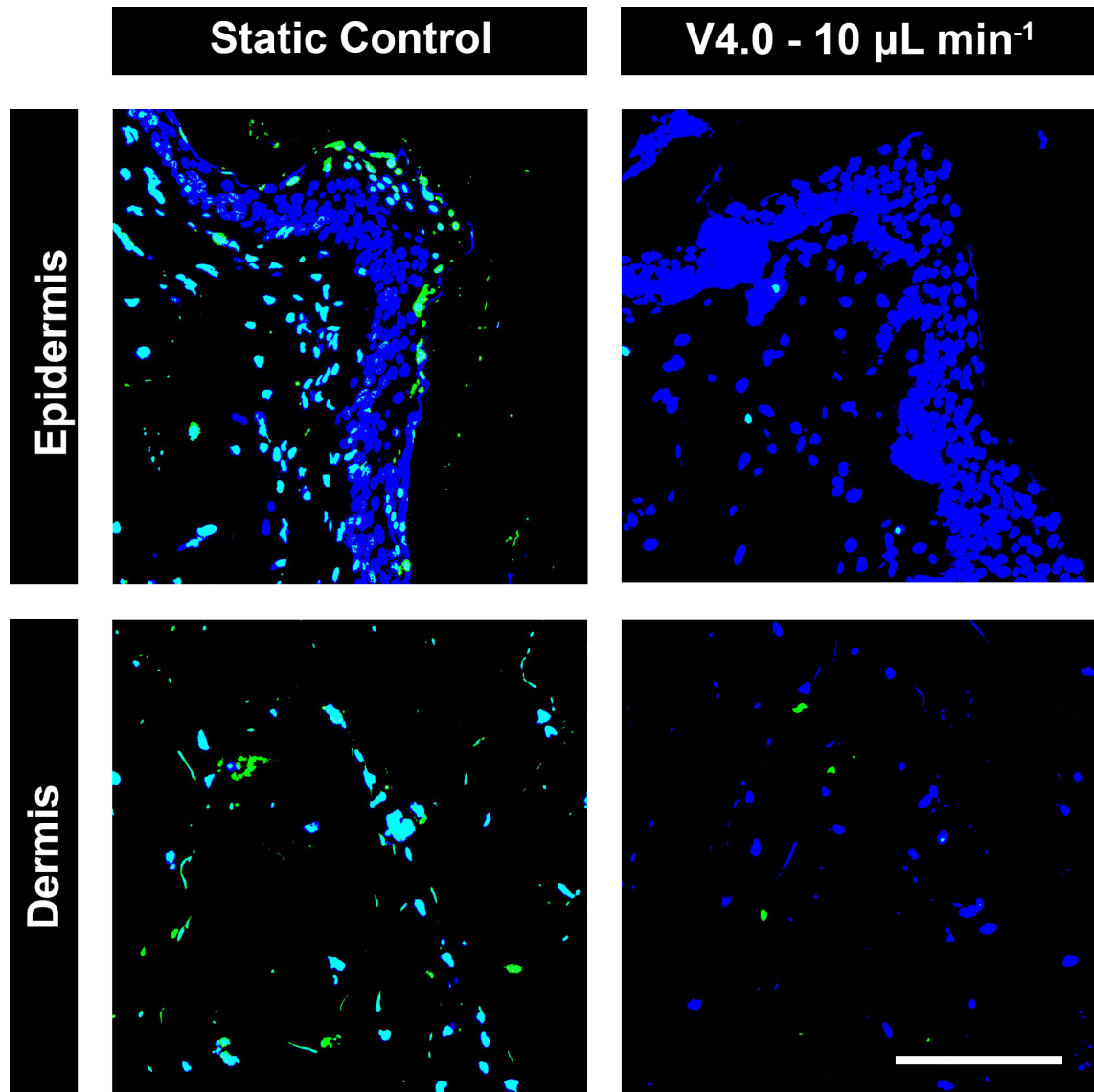
Figure 3.2.8: *Fluorescent TUNEL staining*. The skin samples were maintained on V4.0 devices at 10.0 µL min^{-1}, and in static culture, for ten days. They were then fixed, sectioned, stained using TUNEL assay to visualise the double-stranded DNA breaks indicating apoptotic cell death, and counterstained with DAPI to visualise the nuclei. The images were acquired using 20x magnification objective using a tile scan function on the IXM4 microscope. The samples used for the experiment came from patient HS79 who donated skin samples from her abdomen. Blue - DAPI, Green - TUNEL. The scale bar represents 100 µm.
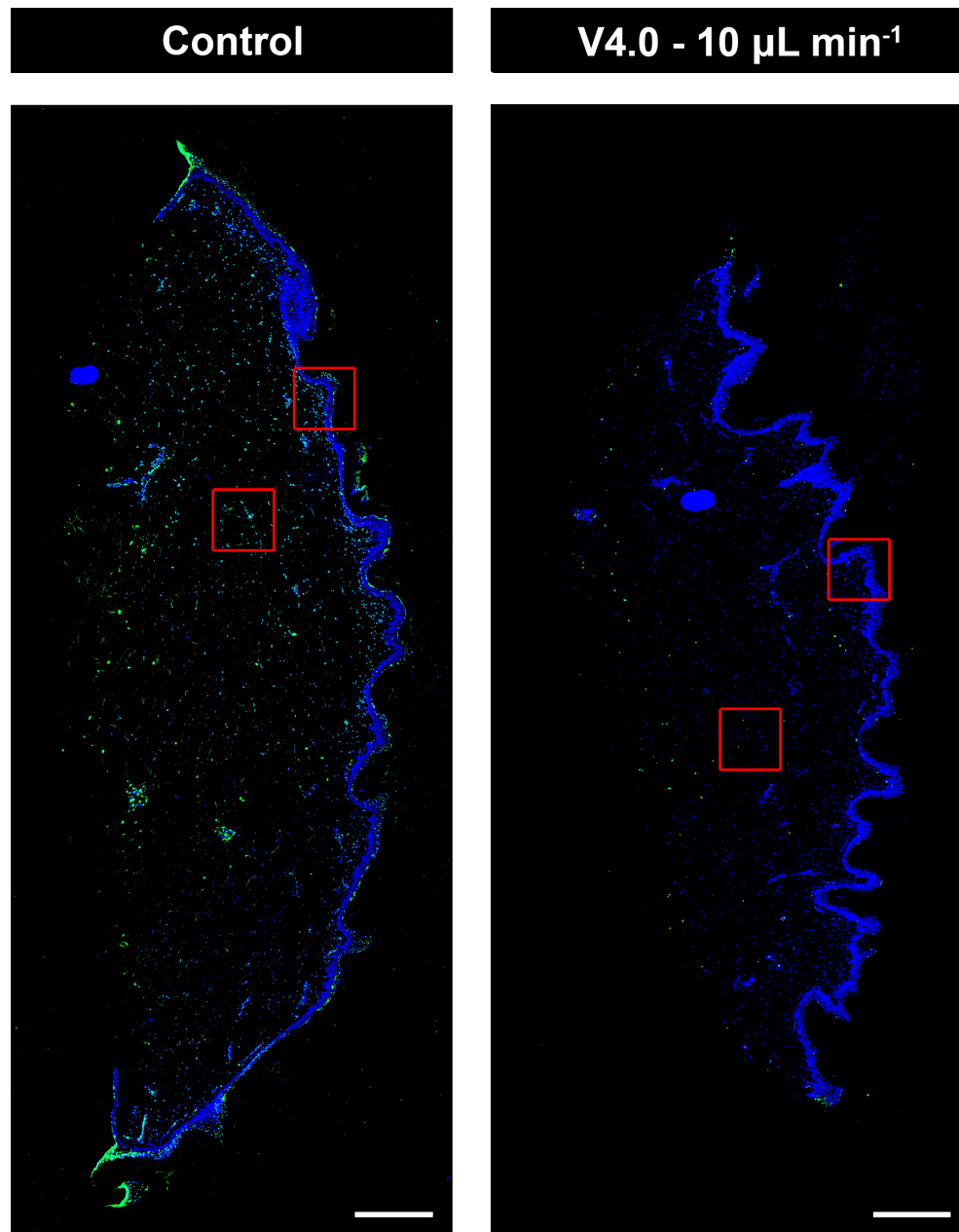
Figure 3.2.9: *Full TUNEL-stained section of skin samples.* The skin samples were maintained on V4.0 devices at 10.0 µL min^{-1}, and in static culture, for ten days. They were then fixed, sectioned, stained using TUNEL assay to visualise the double-stranded DNA breaks indicating apoptotic cell death, and counterstained with DAPI to visualise the nuclei. The images were acquired using 20x magnification objective using a tile scan function on the IXM4 microscope and then stitched together in ImageJ. The red squares represent the areas where magnified images were selected and presented in Fig. 3.2.9. The samples used for the experiment came from patient HS79 who donated skin samples from her abdomen. Blue - DAPI, Green -TUNEL. The scale bar represents 500 µm.

3.3 Wound Healing

The effectiveness of the V4.0 wound-on-a-chip device for wound healing studies has been assessed by performing a seven-day long healing assay and studying wound closure and the immunological profile of the tissue.

3.3.1 Wound closure and constriction analysis

A seven-day wound healing culture was set up using the V4.0 microfluidic device. The static and microfluidic culture experiments were set up and carried out as described in sections 2.2.11 and 2.2.12 respectively. The explants were wounded following the procedure outlined in 2.2.10. The wounding method, although easy, does not always produce round wounds wounds perfectly matching the size of the biopsy punch. The overall wound surface area will be reproducible, with little variability in-between the samples, as the wound diameter solely relies on the diameter of the biopsy punch. The wound depth is the key factor that that might be difficult to control, as the depth of the wound will depend on the sharpness of the punch, the amount of force applied to the sample by the operator, the thickness of the sample, and the physical properties of the sample such as it's stiffness. Wound area analysis and keratin expression measurement followed the protocol outlines in section 2.2.23. Samples were collected on days zero, three, and seven. Day zero sample was a fresh, uncultured tissue sample. The samples were then whole-mounted and immunostained for Keratins 1 (K1) and 14 (K14) as described in section 2.2.16. These biomarkers were chosen to visualise the distal wound edge (K1), and the leading wound edge (K14). Confocal images were then acquired to analyse the healing outcome, following the protocol outlined in section 2.2.4. Fig. 3.3.1 shows the confocal images captured. It is evident, especially from the bright-field and DAPI-stained images that the wound area was reducing in size over the period of seven days, in both cases of the V4.0 samples and the control

samples. The on-chip samples yielded reduced wound perimeter when compared to the static controls from the same day. Fig. 3.3.2 represents the quantified wound area values collected from the confocal images of the whole-mounted samples. It can be seen that the wound area in the uncultured samples on day zero was approximately 0.5 mm². This then dropped to around 0.3 mm² for the control samples, but the V4.0 samples produce only 0.18 mm². On the day seven, the static controls produce wound area of 0.28 mm², whereas the on-chip samples present a value of only 0.08 mm². This also means that the perimeter reduced in the day seven samples by around 80% in the on-chip devices, and only by 45% in the control samples (see Fig. 3.3.2). The result of a two-way between-groups factorial ANOVA show that the culture method has a very significant influence on the wound size ($f(1) = 75.684$, $p=5.61 \times 10^{-6}$). Interestingly, the same analysis showed that the culture method does have a greater impact on the wound closure than the assay day ($f(2) = 24.615$, $p = 0.012$). A post-hoc analysis by Tukey's Honest Significance Test confirmed that the on-chip samples produced a significantly different smaller wounds on day seven of the assay than the control static culture samples ($p = 0.012$), however the the difference between day-three on-chip and the control samples did not return a significant result ($p=0.108$).

As evident from Fig. 3.3.1, the on-chip samples expressed keratin 1 and keratin 14 ring around the wound area on day three. The control samples showed only limited amount of KRT1 and KRT14 expression. The difference in keratin expression between the control and the on-chip samples is around 3.5 fold (see Fig. 3.3.3). This is an indicator of unfinished healing process. The keratin expression in the on-chip samples is comparable to the control samples on the day 7.
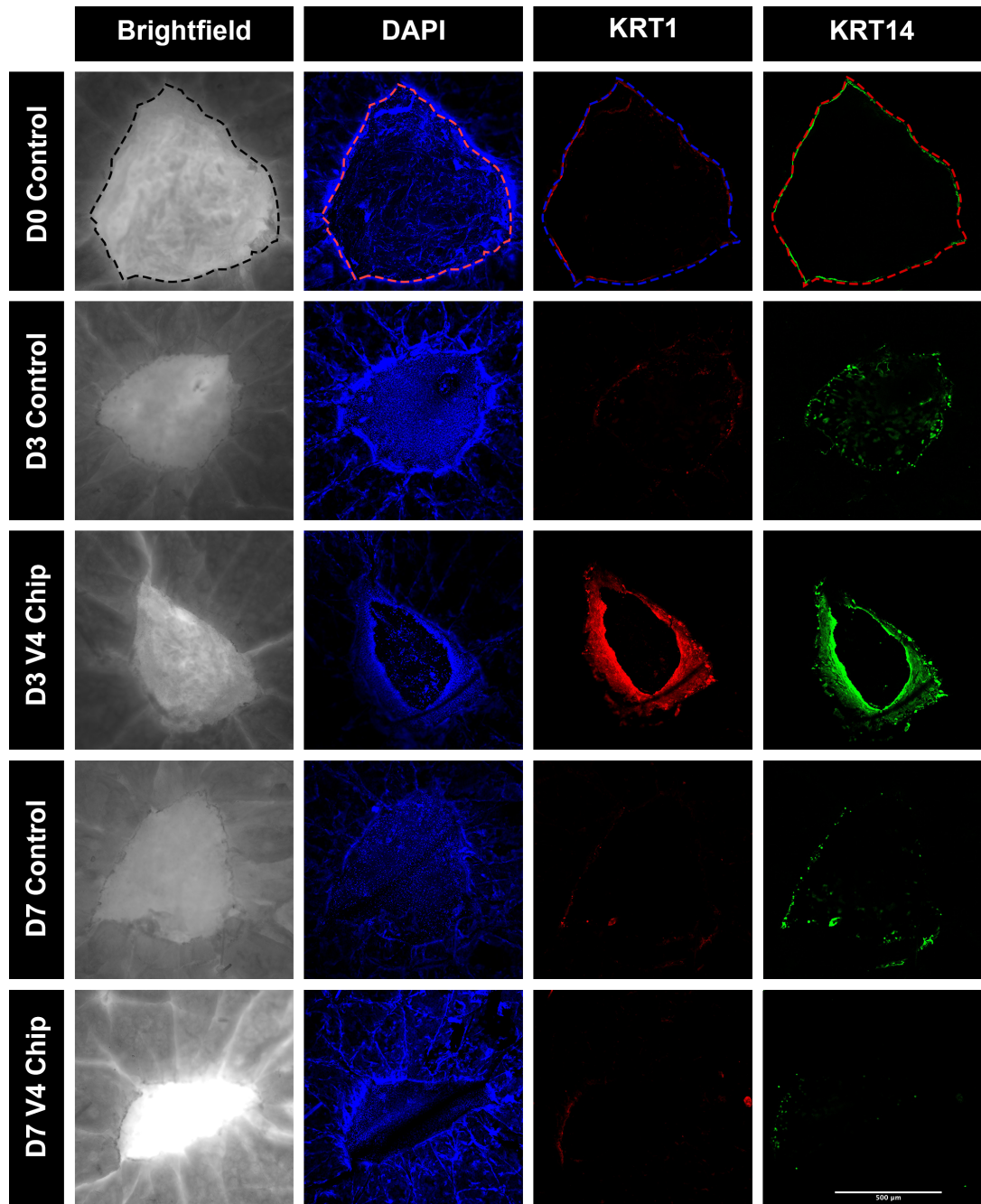
Figure 3.3.1: *Wholemount staining of wounded samples.* The human skin samples were cultured for seven days on V4.0 platforms, and in the static culture for comparison purposes. End-point samples were collected on days 0, 3 and 7, and then wholemounted and stained with DAPI, Keratin 1 (KRT1), and Keratin 14 (KRT14). The dashed lines represent the wound position. Biological replicates: n=3 for each sample. The scale bar represents 500μm.
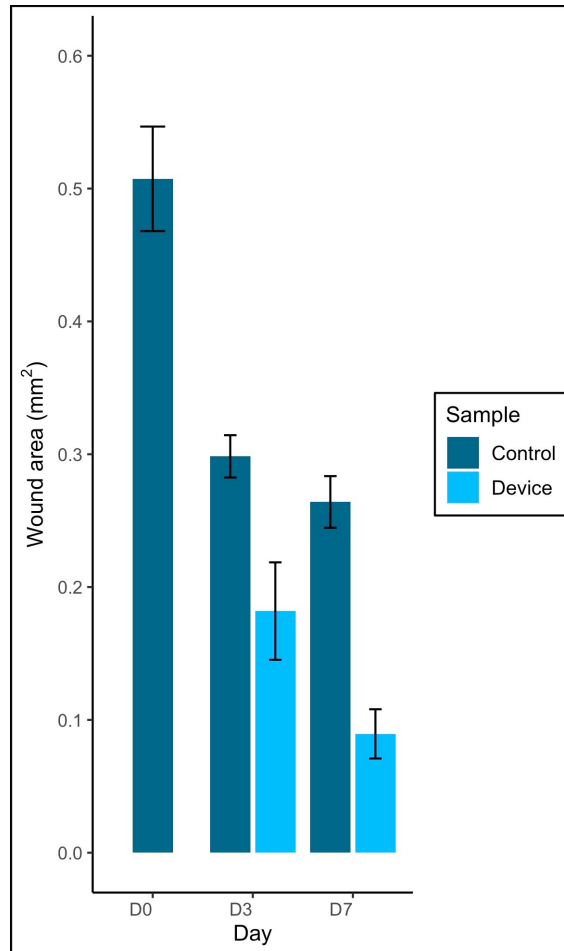
Figure 3.3.2: *Wound area.* Quantified wound area values collected from the confocal images of the whole-mounted samples. The human skin samples were cultured for seven days on V4.0 platforms, and in the static culture for comparison purposes. End-point samples were collected on days 0, 3 and 7, and then wholemounted and stained with DAPI, Keratin 1 (KRT1), and Keratin 14 (KRT14). Wound area was quantified using imageJ. Biological replicates: n=3 for each sample.
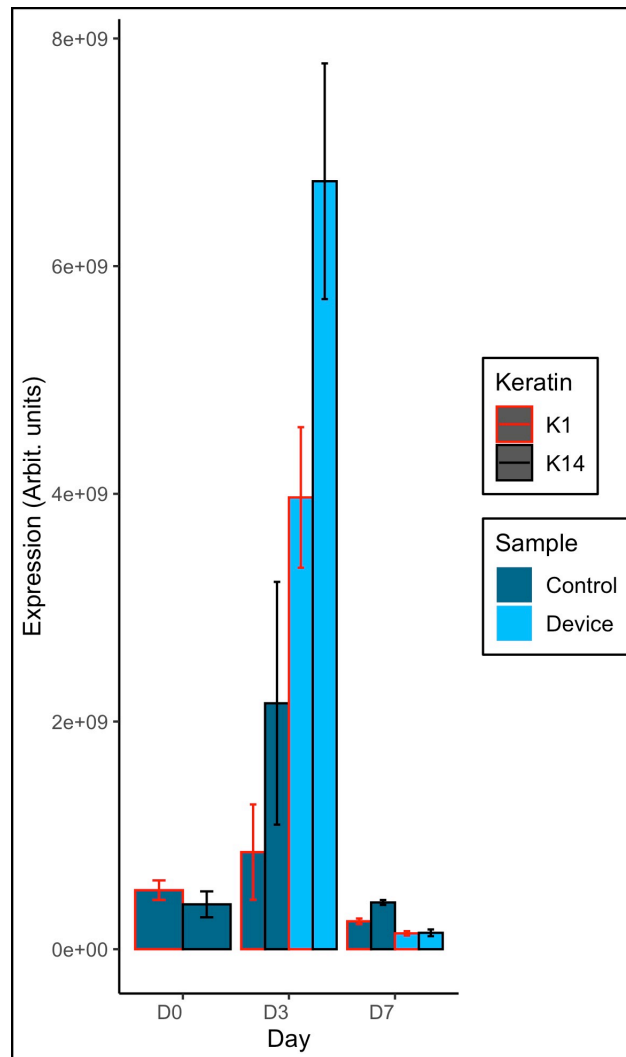
Figure 3.3.3: *Keratin levels.* Keratin1 and Keratin 14 expression in the control and the on-chip samples measured form the conforcal images. The human skin samples were cultured for seven days on V4.0 platforms, and in the static culture for comparison purposes. End-point samples were collected on days 0, 3 and 7, and then wholemounted and stained with DAPI, Keratin 1 (KRT1), and Keratin 14 (KRT14). Keratin expression quantified using imageJ. Biological replicates: n=3 for each sample.

3.3.2   The Immunobiology of wound healing

The immune response is a crucial part of the wound healing process, but it is also the part that is often missing from the wound healing assays and models. Here we have profiled and compared the populations of the immune cells in the samples used for the on-chip and the static control healing assays. For that purpose, a seven-day wound healing culture was set up using the V4.0 microfluidic device. The static and microfluidic cultures were set up and carried out as described in sections 2.2.11 and 2.2.12 respectively. The explants were wounded in a way outlined in 2.2.10. The samples were dissociated after collection, and FACS analysis was performed as described in section 2.2.22.

Table 3.2 lists the biomarkers that were stained for, and the corresponding immune cells that were investigated. The overall population changes are also presented for convenience. The biomarkers were selected to profile the populations of skin resident lymphocytes, many of which are macrophages and T cells. The selection of biomarkers covers Helper T cells - involved in recruitment of other lymphocytes, Cytotoxic T cells - responsible for pathogen lysis, Regulatory T cells and NK T cells - negatively regulating the immune response, and Macrophages - one of the key phagocytes, and antigen presenting cells. This selection covers the key immunological aspects of the immune involvement in the wound healing process such as chemotactic recruitment, pathogen destruction, and the control of the immune intervention.

The overall theme seen from the FACS data demonstrated that the wounded skin samples cultured on the V4.0 microfluidic devices yielded higher levels of immune cells than the static control samples collected on the corresponding days, however the controls still produced higher levels of the immune cells on days 3 and 7 with small exceptions (see Fig. 3.3.5).

This figure presents the relative expression changes in form of percentage difference. It was constructed from the raw FACS expression data, and the relative changes

Table 3.2: *Immune cell population changes.* Comparison of the changes of population sizes of the immune cells studied with regards to the culture method

Cell	Marker	Day 3 Change V4.0	Control	Day 7 Change V4.0	Control
Helper T cell	$CD4^+$ $CD3^+$	++	+	+	-
Cytotoxic T cell	$CD8^+$ $CD3^+$	++	+	++	+
Macrophages	$CD14^+$	++	+	++	+
T Reg	$CD25^+$ $CD3^+$	-	−	++	+
T Reg	$CD25^+$ $CD8^+$			++	+
NK T cells	$CD56^+$ $CD3^+$	-	-	−	-

between D0 and D3 or D7 were calculated for each of the markers. This was done by subtracting the D0 value from the new expression level, and dividing the result by the D0 value expression value. The negative values indicate reduction in expression relative to Day 0. Certain expression changes are very large, with the greatest reaching 6111% increase, equivalent to over 60-fold increase. A potential explanation could be cell loss during cell extraction from the D0 sample.

It was observed that the levels of populations of $CD8^+CD3^+$ cells and $CD14^+$ cells increased on both days three and seven, however the samples collected from the V4.0 devices always yielded a greater increase than the control samples. Interestingly, the populations of $CD56^+CD3^+$ cells decreased on both days regardless of the culture method. $CD25^+CD3^+$ cell populations changes were different on both assay time points. The expression levels decreased on day three, with the reduction being smaller in the V4.0 samples, and then the levels increased on day seven, with the increase being greater in the V4.0 samples. The population of $CD4^+CD3^+$ cells shows the expected pattern where the levels drop on the day seven in the static control samples, however they increase in the V4.0 samples.

Furthermore, it has been noticed that the relative changes in populations of the immune cells were much greater between days zero and three, than between zero and seven (see Figs. 3.3.4a and 3.3.4b).

Overall, the V4.0 device allowed for an increased number of cells to be collected on day seven in every single marker group, apart from in the CD56$^+$CD3$^+$group, where the levels dropped more in the V4.0 samples than in the control samples. The same relationship was noted on day three.

(a) Three Day experiment   (b) Seven day experiment
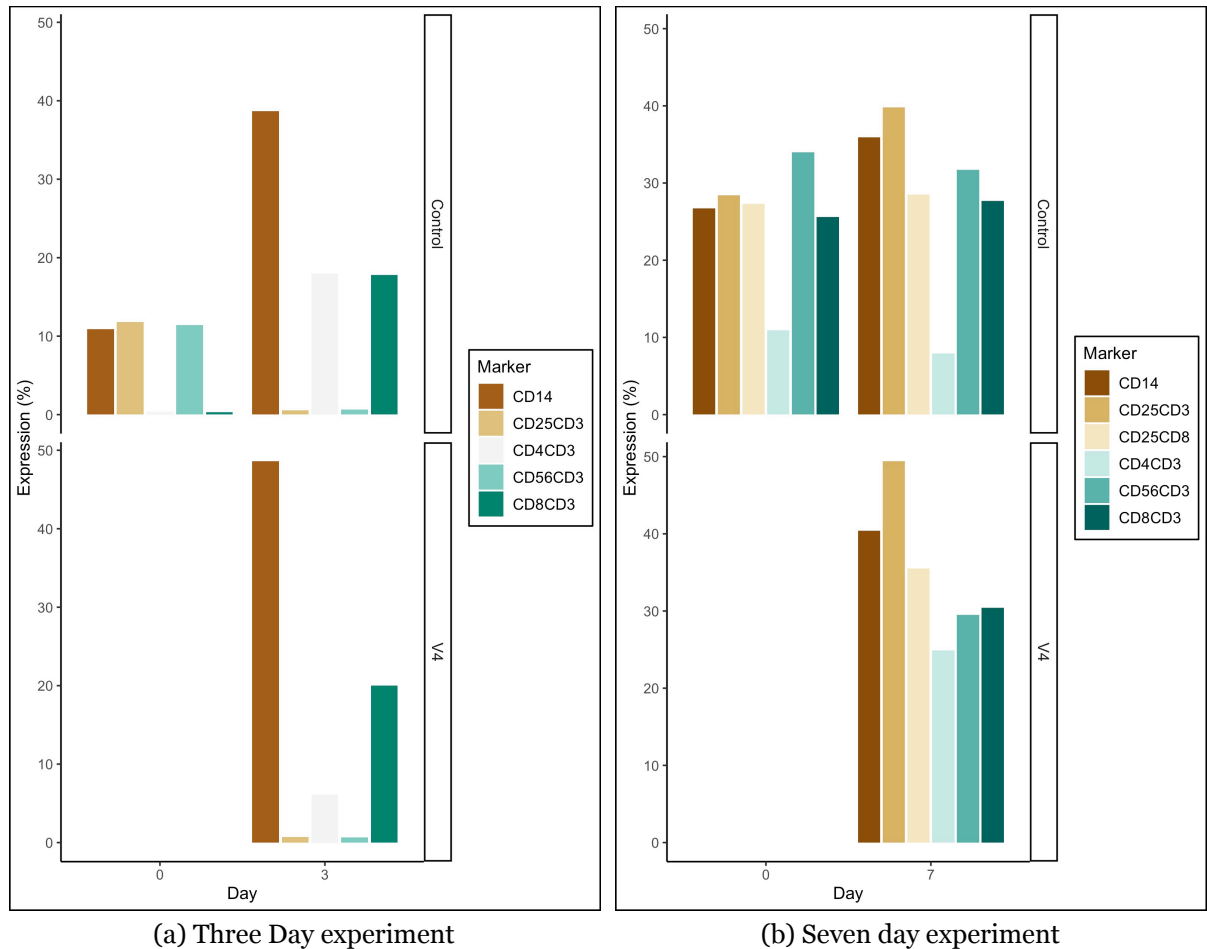
Figure 3.3.4: *Comparison of immune cell populations.* A set of bar charts comparing the expression the biomarkers studied in cells extracted from wounded skin samples cultured for three and seven days in static cultures. The skin samples were dissociated using a commercial kit produced by Miltenyi Biotec. The cells were then harvested, and stained with a range of fluorescently labelled antibodies against the antigens of interest, and analysed using flow cytometry. All the samples came from the same patient - HS112, who was a 28 year old female. The skin samples were collected from the abdomen. V4.0 was the version of the microfluidic device used for the experiment, with n = 1 for the biological repeats.
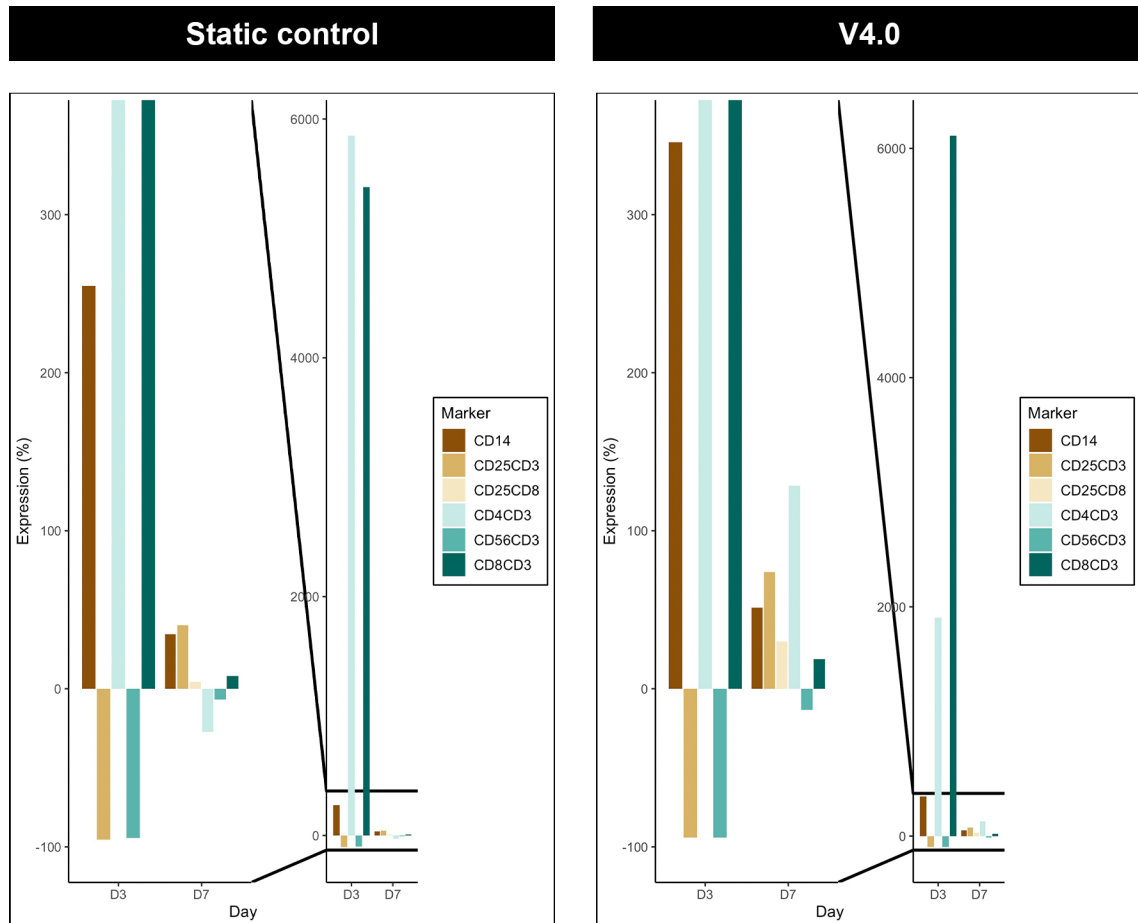
Figure 3.3.5: *Immune cell expression changes.* This figure presents the relative expression changes in the biomarkers studied, in form of percentage difference. It was constructed from the FACS expression data presented in Fig. 3.3.4, and the relative changes between D0 and D3 or D7 were calculated for each of the markers. The negative values indicate reduction in expression relative to Day 0. Certain expression changes are very large, with the greatest reaching 6111% increase, equivalent to over 60-fold increase. A potential explanation could be cell loss during cell extraction from the D0 sample.

A population analysis was carried out on the samples to understand the impact of the microfluidic culture on the overall immune cell population size. As seen from Fig. 3.3.6, the percentage of cells within the designated gate dropped significantly from the day zero to day three, however the on-chip grown samples retained 7.5x more immune cells than the control samples maintained under the static conditions.

These cells represented 13.4% of the cells found in the day-zero sample. The seven-day experiment yielded even better results, with the on-chip samples presenting as much as 75.6% of the cells found on day-zero. The device also allowed for 7.26% increase in the number of the immune cells recovered (Fig. 3.3.6).

Furthermore, upon closer examination, it is evident that the D0 uncultured control sample had much greater $CD3^+$ cell population than $CD4^+$ or $CD8^+$, for the three-day long culture experiment (see Fig. 3.3.7). The population of $CD4^+$ cells was also very small in the D0 control sample from the seven-day culture experiment, as evident from Fig. 3.3.7, however this time both $CD8^+$ and $CD3^+$ cells had distinct populations.

When analysing the $CD3^+$ cell populations (Fig. 3.3.8), it is evident that the V4.0 culture method led to much higher population of $CD3^+$ cells than the static control collected on the same day (Fig. 3.3.8). Day seven of the assay saw the samples $CD4^-$, however $CD3^+$ population was present, and it clearly favoured the on-chip culture, showing a three-fold higher numbers on the V4.0 device (Fig. 3.3.8). The same can be said about the populations of $CD8^+$ cells (Fig. 3.3.9) which seem to have equally benefited from the continuous flow culture system, yielding over 2x greater number than the static control. Similar increase in $CD8^+$ cells is observable on Day 7 of the assay, as seen in Fig. 3.3.9. The macrophage population ($CD14^+$ cells) was also shown to proliferate better on the V4.0 devices, with the control samples producing ~10% smaller populations size on day three, and ~5% smaller population size on day seven (Fig. 3.3.13). Interestingly, $CD25^+$ $CD3^+$ cell populations demonstrate a decrease on day
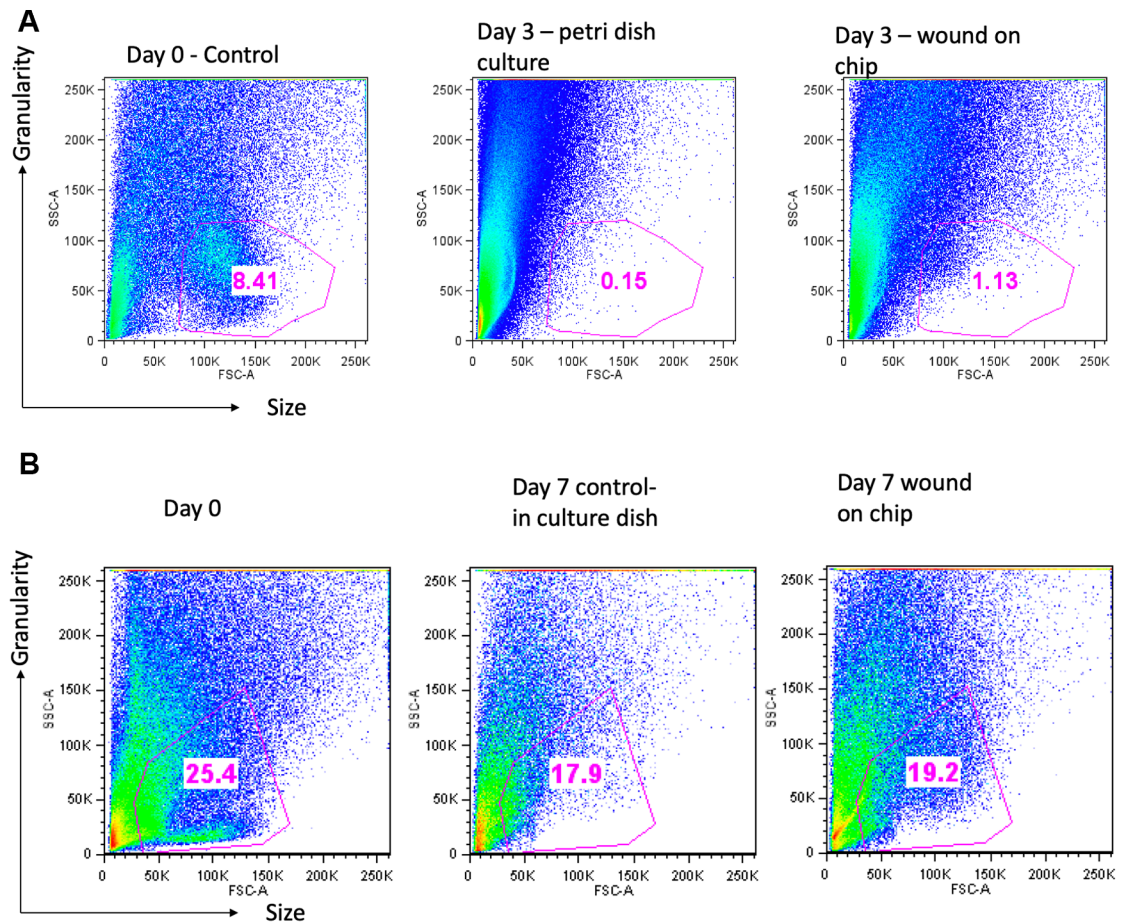
Figure 3.3.6: *Lympocytes identified by size and granularity.* A set of scatter plots comparing the expression of cells based on their granularity and size, in cells extracted from wounded skin samples cultured for three and seven days in static cultures. The skin samples were dissociated using a commercial kit produced by Miltenyi Biotec. The cells were then harvested and analysed using flow cytometry. All the samples came from the same patient - HS112, who was a 28 year old female. The skin samples were collected from the abdomen. V4.0 was the version of the microfluidic device used for the experiment, with n = 1 for the biological repeats. A - day zero vs day three samples, B - day zero vs day seven samples. The colour scale is from dark blue to red, with dark blue representing low cell density, and red representing high cell density. There is a clear reduction in cells identified just based on there granularity and size, both in day three and day seven samples, however the reduction was greater from day zero to three. The on-chip samples retained greater number of cells in both cases.
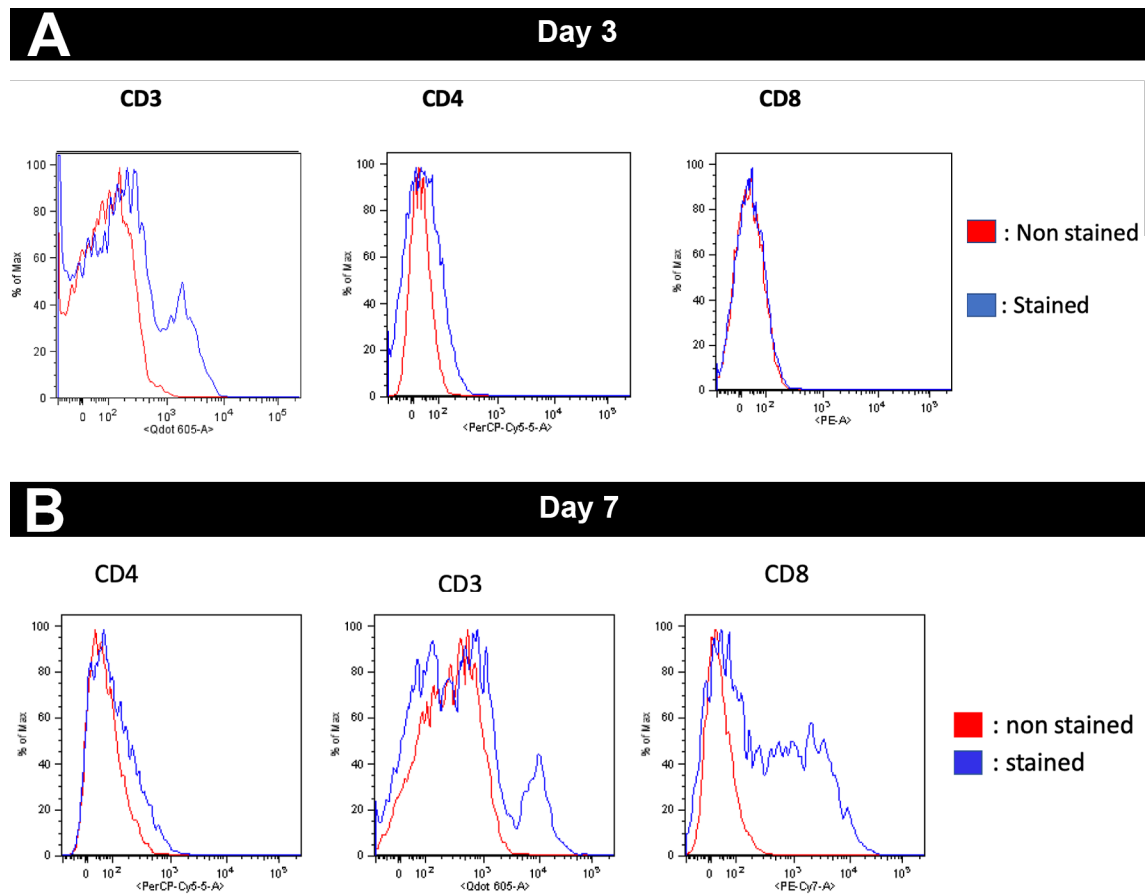
Figure 3.3.7: *T cell population size comparison.* A set of histograms comparing the expression of CD3, CD4, and CD8 antigens in cells extracted from wounded skin samples cultured for three and seven days in static cultures. The skin samples were dissociated using a commercial kit produced by Miltenyi Biotec. The cells were then harvested, and stained with Brilliant Violet (Qdot) 605 anti-human CD3 antibody, PerCP anti-human CD4 antibody, and PE-Cy7 anti-human CD8 antibody, and analysed using flow cytometry. All the samples came from the same patient - HS112, who was a 28 year old female. The skin samples were collected from the abdomen. V4.0 was the version of the microfluidic device used for the experiment, with n = 1 for the biological repeats. Clear CD3 population was visible on Day three, with a small CD4 population, and no detectable CD8 population. Day seven samples produced clear CD3 and CD8 populations, with a small detectable group of CD4 expressing cells.

Figure 3.3.8: *CD4+CD3+ T cell populations characterisation.* A set of scatter plots comparing the expression of CD3+ and CD4+ antigens in cells extracted from the skin samples cultured for three and seven days in static and microfluidic cultures. The skin samples were dissociated using a commercial kit produced by Miltenyi Biotec. The cells were then harvested, and stained with PerCP anti-human CD4 antibody, and Brilliant Violet 605 anti-human CD3 antibody, and analysed using flow cytometry. All the samples came from the same patient - HS112, who was a 28 year old female. The skin samples were collected from the abdomen. V4.0 was the version of the microfluidic device used for the experiment, with n = 1 for the biological repeats. NS indicates no-stain. There has been an increase in the expression of CD4+CD3+ cells on both days 3 and 7, with the microfluidic device presenting a greater increase on D7.

Figure 3.3.9: *CD8+CD3+ T cell populations characterisation.* A set of scatter plots comparing the expression of CD3+ and CD8+ antigens in cells extracted from the skin samples cultured for three and seven days in static and microfluidic cultures. The skin samples were dissociated using a commercial kit produced by Miltenyi Biotec. The cells were then harvested, and stained with APC-H7 Mouse anti-Human CD8 antibody, and Brilliant Violet 605 anti-human CD3 antibody, and analysed using flow cytometry. All the samples came from the same patient - HS112, who was a 28 year old female. The skin samples were collected from the abdomen. V4.0 was the version of the microfluidic device used for the experiment, with n = 1 for the biological repeats. NS indicates no-stain. There has been an increase in the expression of CD8+CD3+ cells on both days 3 and 7, with the microfluidic device presenting a greater increase on both days.
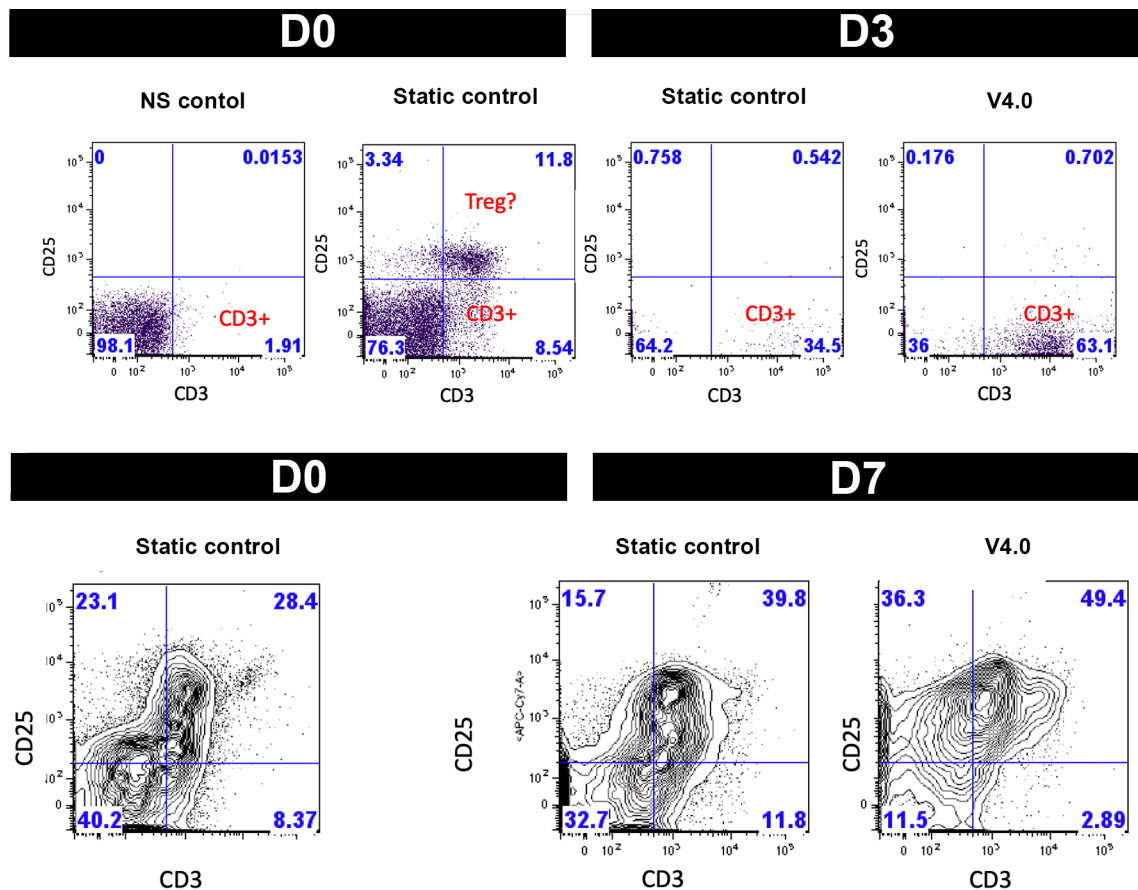
Figure 3.3.10: *CD25+ CD3+ cell populations characterisation.* A set of scatter plots comparing the expression of CD3+ and CD25+ antigens in cells extracted from the skin samples cultured for three and seven days in static and microfluidic cultures. The skin samples were dissociated using a commercial kit produced by Miltenyi Biotec. The cells were then harvested, and stained with PE/Cyanine7 anti-human CD25 antibody, and Brilliant Violet 605 anti-human CD3 antibody, and analysed using flow cytometry. All the samples came from the same patient - HS112, who was a 28 year old female. The skin samples were collected from the abdomen. V4.0 was the version of the microfluidic device used for the experiment, with n = 1 for the biological repeats. NS indicates no-stain. Interestingly, there has been a decrease in the expression of CD25+CD3+ cells on day three, with the microfluidic device sample presenting a lower decrease than the control. The levels however increased on day seven, with the microfluidic device presenting a greater increase than the control.
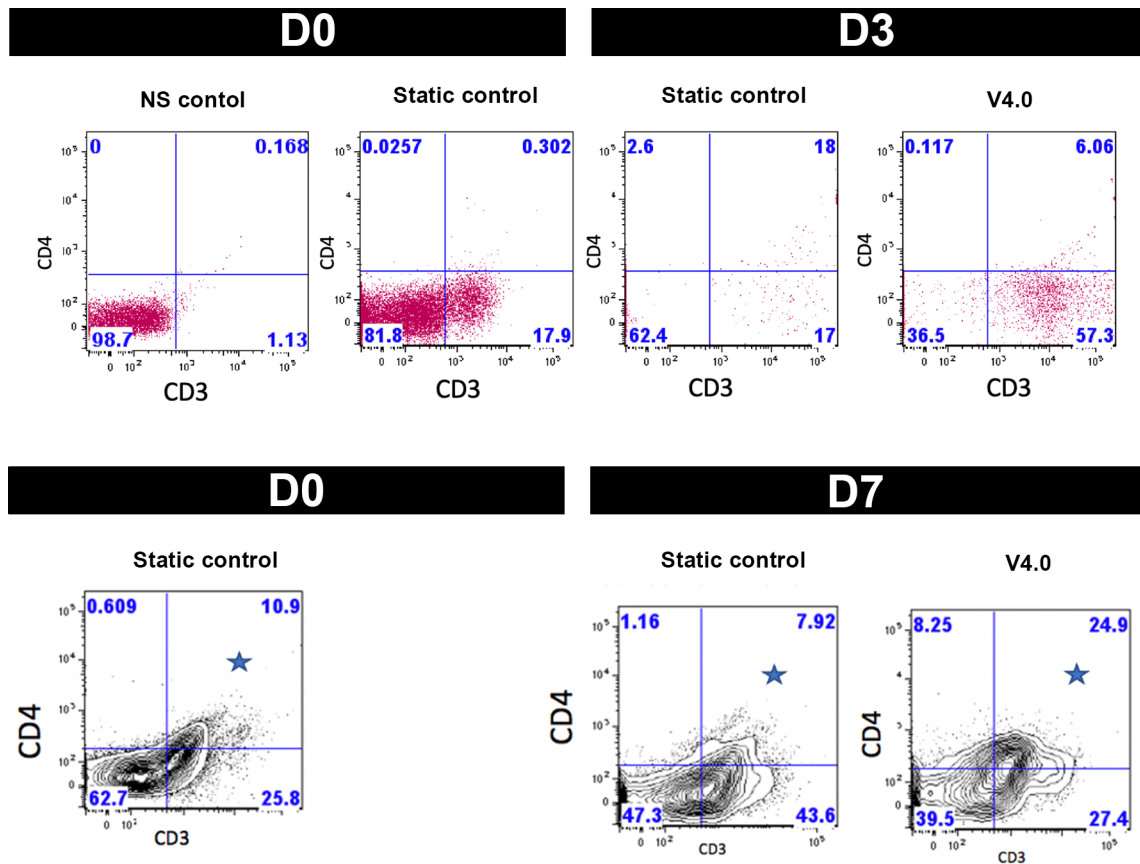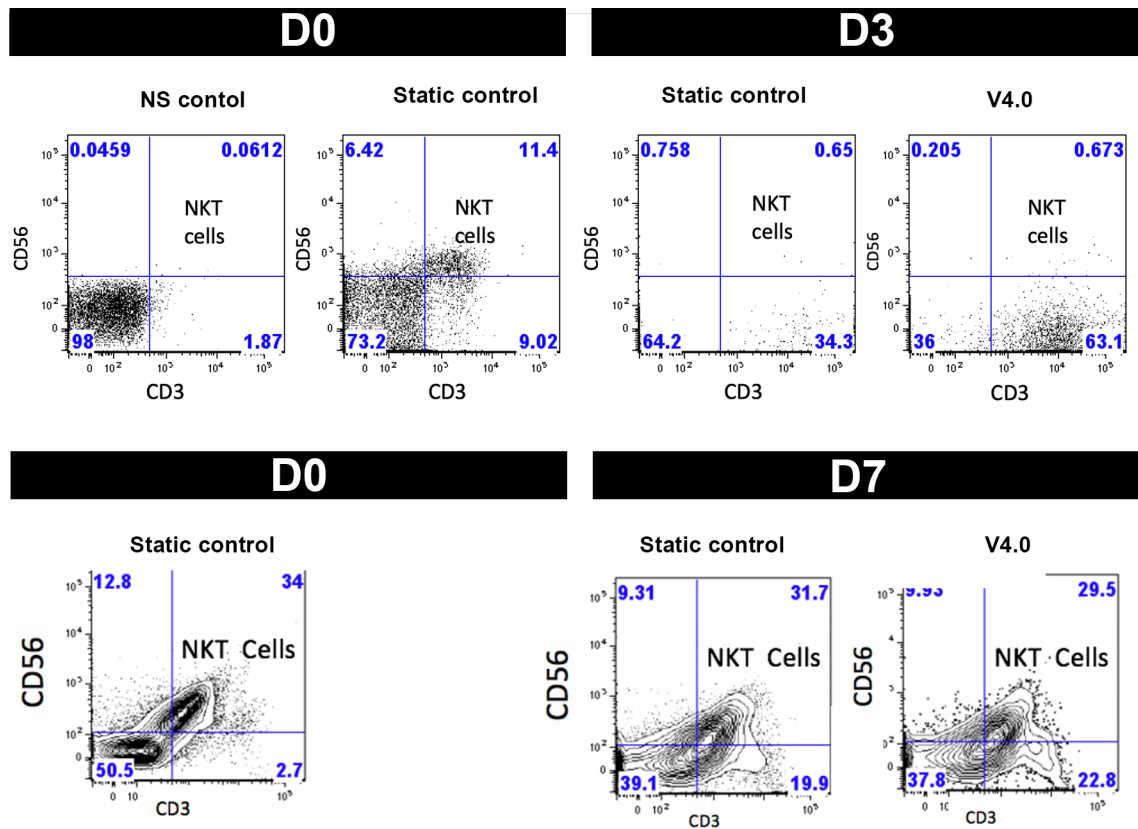
Figure 3.3.11: *CD56+ CD3+ cell populations characterisation.* A set of scatter plots comparing the expression of CD3+ and CD56+ antigens in cells extracted from the skin samples cultured for three and seven days in static and microfluidic cultures. The skin samples were dissociated using a commercial kit produced by Miltenyi Biotec. The cells were then harvested, and stained with FITC Mouse anti-Human antibody against CD56, and Brilliant Violet 605 anti-human CD3 antibody, and analysed using flow cytometry. All the samples came from the same patient - HS112, who was a 28 year old female. The skin samples were collected from the abdomen. V4.0 was the version of the microfluidic device used for the experiment, with n = 1 for the biological repeats. NS indicates no-stain. There has been a decrease in the expression of CD56+CD3+ cells on both days 3 and 7, with the microfluidic device presenting a greater reduction in expression on day seven.
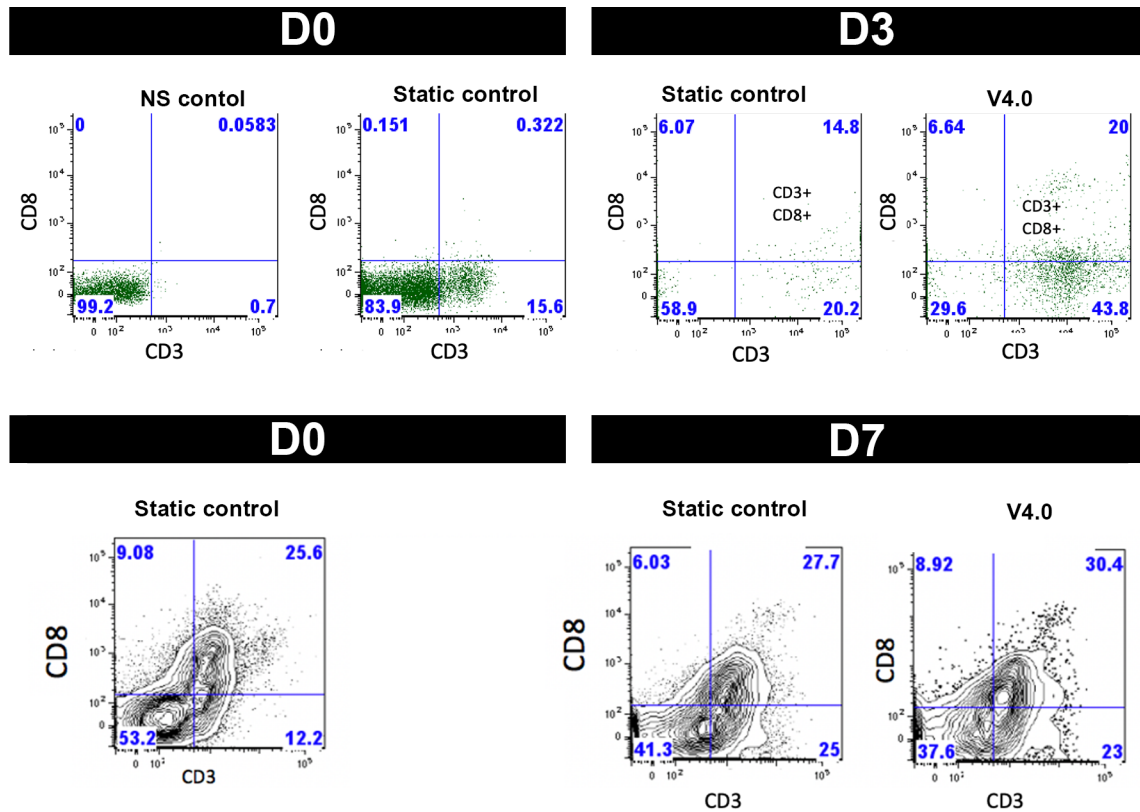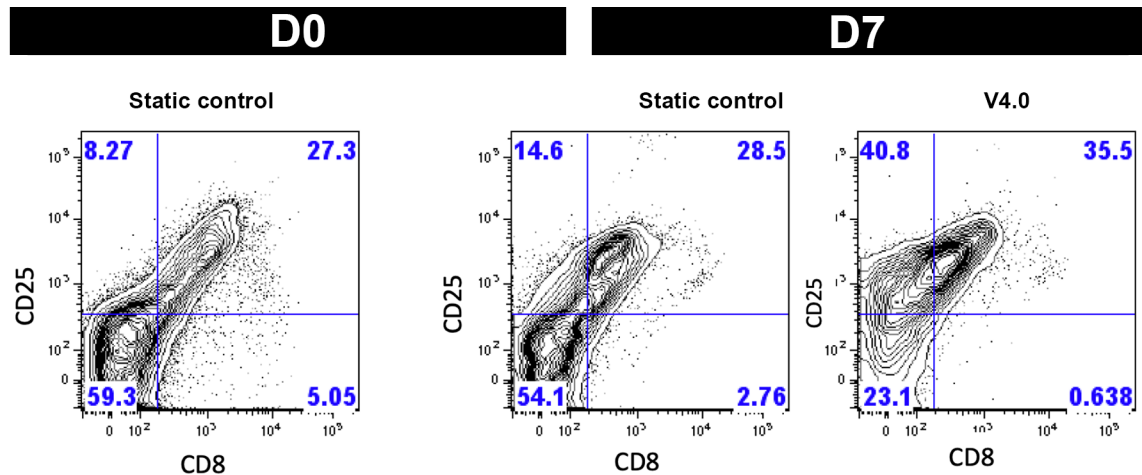
Figure 3.3.12: *CD25+CD8+ T cell populations characterisation.* A set of scatter plots comparing the expression of CD25+ and CD8+ antigens in cells extracted from the skin samples cultured for three and seven days in static and microfluidic cultures. The skin samples were dissociated using a commercial kit produced by Miltenyi Biotec. The cells were then harvested, and stained with APC-H7 Mouse anti-Human CD8 antibody, and PE/Cyanine7 anti-human CD25 antibody, and analysed using flow cytometry. All the samples came from the same patient - HS112, who was a 28 year old female. The skin samples were collected from the abdomen. V4.0 was the version of the microfluidic device used for the experiment, with n = 1 for the biological repeats. NS indicates no-stain. There has been an increase in the expression of CD8+CD25+ cells on both days seven, with the microfluidic device presenting a greater increase.
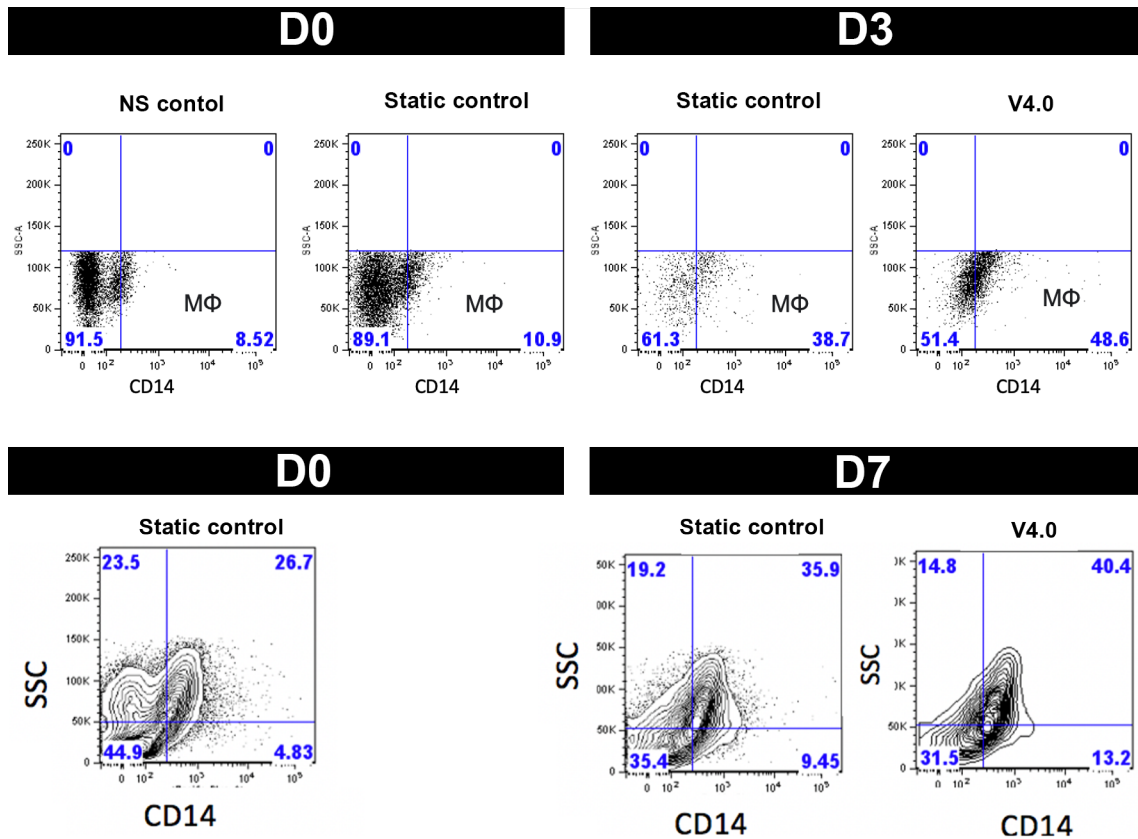
Figure 3.3.13: *Macrophage populations characterisation.* A set of scatter plots comparing the expression of CD14 antigen in cells extracted from the skin samples cultured for three and seven days in static and microfluidic cultures. The skin samples were dissociated using a commercial kit produced by Miltenyi Biotec. The cells were then harvested, and stained with Pacific Blue anti-human CD14 antibody, and analysed using flow cytometry. All the samples came from the same patient - HS112, who was a 28 year old female. The skin samples were collected from the abdomen. V4.0 was the version of the microfluidic device used for the experiment, with n = 1 for the biological repeats. NS indicates no-stain. There has been an increase in the expression of CD14+ cells on both days 3 and 7, with the microfluidic device presenting a greater increase on both days.

three, as per Fig. 3.3.10, where the V4.0 samples demonstrated slightly smaller population size decrease. On the day seven, the population size recovered, and the V4.0 device samples were recorded with larger population rise than the control samples (Fig. 3.3.10). The same behaviour can be observed on day seven with $CD25^+CD8^+$ cell populations (Fig. 3.3.12). The only cell population that clearly did not benefit from the microfluidic culture was that of $CD56^+CD3^+$ Natural Killer T cells. As seen from Fig 3.3.11, the population of Natural Killer T cells largely decreased on day three, with the population sizes being similar for the V4.0 and the static control groups. The decrease was also observable on day seven, however the drop from day zero was not as large this time. Table 3.2 summarises the effects the culture systems had on the population sizes of the different immune cells.

These results show that the V4.0 device helped to maintain higher number of the studied immune cells than the static culture method, with the only exception being the NK T cells. This is important because these cells are important to healthy recruitment of other lymphocytes, antigen presentation, destruction of pathogens capable of slowing down the wound healing process, and down-regulation of the response at the end of healing to allow for allow for anti-inflammatory environment to be established to allow for more efficiently ECM remodelling. It is true that lower levels of NK T cells have been recorded. It is difficult to asses how big of a setback this could cause to the wound healing process, especially that all other studied cells presented with higher levels than in controls. It is likely that the impact would be minor, especially that the Regulatory T cells are similarly involved in the negative regulation of the immune response.

It is most likely that the constant tissue culture flow delivering new nutrients and removing metabolites lies behind the improved immune cell retention. Furthermore, even though the results have shown that the V4.0 device allowed for improved retention of the macrophages, it is impossible to use these results to understand what

states of activation these macrophages occur in. Further investigation with a selection of markers against M1 and M2 subtypes would be informative. The choice of markers could involve CD80 and CD86 for M1 macrophage, and CD206 and CD163 for M2 macrophages (Yunna 2020). Quantifying the ratio of M1 and M2 macrophages would help to understand whether the sample micro-environment is pro or anti inflammatory. The experiments were conducted only once, therefore they have no statistical significance.

Chapter 4

Discussion

In this study, work has been carried out to design and manufacture a microfluidic device capable of prolonged culture of human skin samples, whilst maintaining their state in life-like form. It was hoped that the new microfluidic device would benefit skin viability, and the physiological accuracy of the healing assay.

Here we will discuss the implications of the findings of this study, to assess whether the aims of the project have been accomplished.

4.1 Devices and validation

Four versions of microfluidic device for human skin maintenance were designed, manufactured and tested. Additional two iterations were produced for cell-based work. These included: V1.0 - one inlet - three outlets device, utilising Transwell inserts; V2.0 - one inlet - four outlets device with custom-made sample retainers; V3.0 - one inlet - four outlets device with custom-made sample retainers and PDMS film-containing lid; and V4.0 device - one inlet - one outlet device with the sample retainer and the lid technology inherited from V3.0. Two cell-culture devices were then derived from V4.0 chip: V4.C1 - which utilised a 3D printed holder, and V4.C2 - which made use of on-slide bonding solution.

The V1.0 device was found to be unsuitable for biological experiments with human skin due to liquid lifting up human skin and leaking out through the Transwell inserts. The second (V2.0) and third (V3.0) generation wound-on-a-chip devices however, proved to be compatible with human skin samples.

Both the TUNEL staining, and the Keratin IHC staining results proved that V3.0 device is significantly better at maintaining the human skins samples alive than V2.0. Additionally, the samples collected from the V3.0 showed a larger variability in the reported values. This is likely due to observable differences in the flow rates in the devices. Issues with the flow rate occurred most likely due to the branching structure of the channels, where one inlet supplied a channel that splits symmetrically into four other channels feeding four samples on one device. A small pressure imbalance due to a bubble or manufacturing artefact can lead to unequal flow rates, or it can even completely cut off liquid flow to the tissue sample and the outlet. It is also important to remember that the skin samples rest on membranes, in sample retainer suspended above the fluidic channels. There are several factors that can alter the height of the channel under the tissue. These involve a) the force with which the sample is pressing onto the membrane, which is determined by i) the sample weight, and ii) pressure in the space above the sample; b) the pressure of the liquid in the channel acting onto the membrane. If these are unbalanced, the samples will be exposed to different flow rates, potentially resulting in alterations to tissue's metabolic activity. V3.0 device proved to be more reliable than V2.0 as it does not rely on the pin pushing down onto the skin to prevent it from lifting off.

Additional disadvantage of the use of the pin in the V2.0 device was found to be the mechanical stress it was inflicting on the skin. Strong K6 staining visible in the on-chip sample in Fig. 3.2.3, and the increased epidermal thickness in the same sample category, as observed in Fig. 3.2.4 both suggest that the force originating from the pin, and acting on the skin sample led to cell stress and increased proliferation in

the epidermis. The on-chip samples from V3.0 device presented no increase in the epidermal thickness and K6 staining intensity matching the control, suggesting that the device was not causing cell stress in the maintained skin samples.

The results from V3.0 samples are not statistically different from the static control samples collected on the same day. The means of the apoptotic cell death percentages from the samples are very similar, suggesting that the V3.0 device allowed for maintenance of samples in a state comparable to the one resulting from the static culture. It is believed that the apoptotic cell death rate in the V3.0 samples could be even lower, and it is so high only because of the uneven flow rate through the channels, and random channel shut-offs by air bubbles.

The V4.0 device outperformed all the previously tested versions of the wound-on-a-chip flow cell. It reduced the epidermal and dermal cell death 4-fold, and extended the lifespan of the sample.

It is believed that this cell death reduction could be further improved by increasing the oxygen levels within the medium as it is hypothesised that the flow-rate-dependent dermal cell death, but stable and low epidermal cell death observed in Fig. 3.2.6 suggests that the oxygen availability to the tissue is most likely the viability limiting step significantly reducing the lifespan of the samples. The oxygen metabolism as a rate-limiting step has been favoured over glucose metabolism because the epidermal layer is positioned much further away from the microfluidic channel than the dermis (around 1 mm or more), however it has much lower epidermal cell death than the dermis. Epidermis can obtain its oxygen through passive diffusion either from the air that it's exposed to, or from the supplied medium (dissolved oxygen) that reaches the epidermis through the dermal layer. Dermis, on the other hand, is not directly exposed to the air, and so the flow of medium underneath is the main way of delivering oxygen to the dermal cells. Conversely, nutrient supply (mainly glucose), is solely dependent on the diffusion from the microfluidic channel. It can be concluded

that this diffusion is sufficient to deliver nutrients even to the distant strata of the epidermis because change in flow rate has no effect on the epidermal cell death (Fig. 3.2.6). Increasing the flow rate proportionally increases the amount of nutrients and dissolved oxygen delivered to the cells per time unit. Oxygen is not a limiting factor in the case of the epidermal cell survival in on-chip samples either. This can be explained in terms of epidermis' ability to obtain oxygen from the atmospheric air that it is exposed to.

It is important to point out that the aim is not to achieve hyperoxia in the tissue, but rather, it is believed that the explant oxygen level is hypoxic, and the aim of medium oxygenation is to increase the tissue oxygenation to adequate levels. Since the diffusion rate relies on the concentration gradient, increasing the medium oxygen level would help to improve tissue oxygenation. It is relevant to raise the oxygen level as long as the tissue oxygen level does not fall outside of the physiological level. It is true that the wound environment is hypoxic, but that's limited to the wound and not the healthy part of the tissue. Given the oxygen diffusion limitation, it is highly likely that glucose diffusion is also reduced.

The flow-rate-dependent cell death in the dermis indicates that it is the oxygen availability that is a limiting factor in the skin samples cultured on the V4.0 device. Raising the flow rate from 2.5 µL min^{-1} to 10.0 µL min^{-1} proportionally increases the amount of dissolved oxygen reaching the cells per time unit, which explains the reduction in cell death in samples maintained with the use of higher flow rates. Fig. 3.2.7 shows how this flow-rate depended cell death disappears over time and how the aforementioned "flip" occurs. It can be suggested that the flip occurs because the V4.0 device managed to significantly reduce the epidermal cell death at day 7 time point, however from that moment on, the cell death rate of the epidermal layer from the on-chip samples is greater that the dermal cell death cell rate. Figs. 3.2.8 and 3.2.9 show the samples used for Day-7 time-point.

4.2 Wound healing

When looking at the wound area graph (Fig. 3.3.2), it can be seen that the on-chip samples do present with a smaller wound area than the static controls. There is also higher expression of both keratins on Day 3 in the on-chip samples than in the controls.

Several factors could contribute to reduction in the wound area observed after the culture on V4.0 devices. One of them could be the increase in availability of nutrients as a result of the microfluidic flow under the sample. The small dimensions of the channel mean that greater proportion of the nutrients from the medium can diffuse into the tissue in the time it resides under the tissue. Furthermore, the constant medium flow means that new nutrients are constantly available to the tissue. On the other hand, tissue cultured in a static system needs to rely entirely on diffusion to get the required nutrients.

Furthermore, the smaller wound size amongst the samples maintained on the V4.0 devices can be explained by improved keratinocyte migration, leading to better repithialisation. Such presentation would be expected from improved culture conditions.

The depth of the tissue culture medium below the cultured tissue sample will typically be around 1-2 mm. The time required for a glucose molecule to diffuse 2 mm in tissue culture medium will be around 56 min, based on the glucose diffusion coefficient of 5.9×10^{-10} m^2 s^{-1} (Provin et al., 2008). On the other hand, the time required for the same glucose molecule to diffuse 100 µm in a microfluidic channel is only 8.5 s. The residence time of the medium under the skins sample at the flow rate of 10 µm min^{-1} is 20 s. This means that glucose has sufficient amount of time to diffuse from the bottom of the channel to the skin sample interface within the time it resides underneath it. Conversely, it appears that the samples maintained in the static culture systems suffered from suboptimal nutrient delivery. Another important benefit that

comes with the microfluidic culture is the removal of the metabolites. Removal of the by-products of metabolism is as important as replenishing nutrients needed for normal cell behaviour. The limitations of diffusion speed are equally applicable to the removal of metabolites in the static culture, with the important difference of the fact that they are actually not being removed in the static culture at all, but instead they slowly diffuse away from the sample. This is very different to the physiological removal of metabolites, where in an organism with a circulatory system, the vasculature allows for complete removal of the metabolites out of the organism through the kidneys. This complete removal is necessary to prevent the toxic effects of certain metabolites. Microfluidic culture system is a very strong contestant for a suitable in vitro / ex vivo culture system that replicates the function of the circulatory system in terms of its ability to both provide new nutrients and at the same time remove the metabolic products as they are released into the cell culture medium. It is important to highlight that the flow in the microfluidic devices can have disadvantageous impact on the model. The medium flow can affect the accumulation of molecules such as cytokines. The flow rate, direction, and shear stress can all play a role in determining the distribution of cytokines within the device. A high flow rate can result in a lower accumulation of cytokines in the wound area, while a low flow rate can result in a higher accumulation of cytokines. Cytokines would naturally enter the vascular system at the time of wounding, so this is a physiologically correct behaviour. In order to decide whether the cytokines are removed from the samples at a rate that is excessive, further experiments would have to be conducted in order to determine the depletion rate.

Although impossible to state with utmost certainty without further validation, it is very likely that the observed reduction in the apoptotic cell death and the final wound area are both associated with the improved supply of nutrients, and the active removal of metabolic by-products.

Moreover, both age and sex of the sample donors might influence of the healing assay outcome. Patient age is a significant factor in wound healing. The increase in age is associated with worsened wound healing outcome, and reduced wound healing rate. This is due to decreased blood flow, changes in the immune system, and decreased collagen production. Elderly individuals are also more likely to have comorbidities that can further impede the healing process. Sex is also an important factor in wound healing. Women tend to have a faster wound healing response than men. This is thought to be due to the presence of oestrogen, which has been shown to promote wound healing. Some of these factors might be still active in skin explants, potentially influencing the result.

4.2.1   Immunobiology of wound healing

FACS analysis of the wounded samples maintained on the V4.0 device and in the static culture system revealed that the microfluidic culture on the V4.0 device favoured almost every single immune cell category studied, apart from $CD25^+CD3^+$. This is most likely because the laminar flow of the culture medium improved supply of the nutrients to the sample, together with increasing the oxygen supply. At the same time, the metabolic by-products and carbon dioxide were removed away from the cells more efficiently than it was the case in the static culture.

Chapter 5

Conclusions and further work

The aim of this project was to create a novel tissue on a chip device which would be a more physiologically accurate model suitable for wound healing studies.

This work demonstrated that V4.0 device is a successful platform for maintenance of human skin samples. This was shown by reduced apoptotic cell death in the on-chip samples. The device was also shown to be suitable for wound healing assays. The wound healing assay experiments demonstrated that V4.0 device allows for successful wound closure, resulting in a smaller wound perimeter than in the static culture samples. Furthermore, the immunology experiments showed that the on-chip samples retained a greater number of T cells and macrophages than the control samples, making the V4.0 device a closer representation of the biological wound healing environment. This project is believed to the the first to demonstrate that a human skin wound healing model with improved immunological microenvironment can be achieved using microfluidic principles. Despite being the aforementioned success, no project is without limitations. The global COVID-19 pandemic broke out during the key period of the project, causing severe disruption to the work. Because of the imposed restrictions, only the essential surgeries were able to take place. As a result, human skin sample collection was no longer a possibility, meaning many

planned experiments were not able to go ahead. Lack of metabolomic data is one of the key areas that could be improved. It has been shown that the viability of the skin samples benefit from the microfluidic culture. This is most likely due to increased availability of oxygen and glucose to the metabolically active skin sample, however this has not been studied in details. It is therefore unknown whether the chip design could be improved further to maximise metabolic viability. In-channel oxygen probes could be used in further work to understand to what extent does the sample deplete oxygen levels, and whether external medium oxygenation could be beneficial. Glucose levels could be also analysed in the effluent to get a better picture of the metabolic demand. Information on cellular proliferation would also be beneficial, to improve the understanding of the maintained skin activity.

The next part of this chapter presents information on the next steps in the project. Where some preliminary work has been done on the discussed topics, this will be presented and explained how it needs to be expanded in the future.

5.1 Sample oxygenation

Section 3.2.4 on page 139 suggested that low oxygen levels can be a major limiting factor reducing the dermal viability. A simple device has been designed to increase the oxygen levels in the tissue culture medium (see Fig. 5.1.1 on the next page). The device consists of a plastic box connected to an oxygen cylinder. A vent opening is positioned in one of the walls of the box to allow for excessive oxygen pressure to be released. An oxygen permeable tubing made of silicone (ID of 0.4 mm, and wall thickness of 0.3 mm) was pulled through two openings in the opposite walls of the tubing, however no silicone tubing reached the outside of the box. Silicone tubing was then interfaced with a PTFE tubing (ID 0.3 mm) with very low oxygen permeability. Three sensors were used to monitor oxygen conditions in the system. One needle-

type sensor measured the oxygen levels in the box, and two flow-through sensors were measuring oxygen levels in the water that was passed through the tubing from a syringe pump (one upstream of the box, and one downstream).
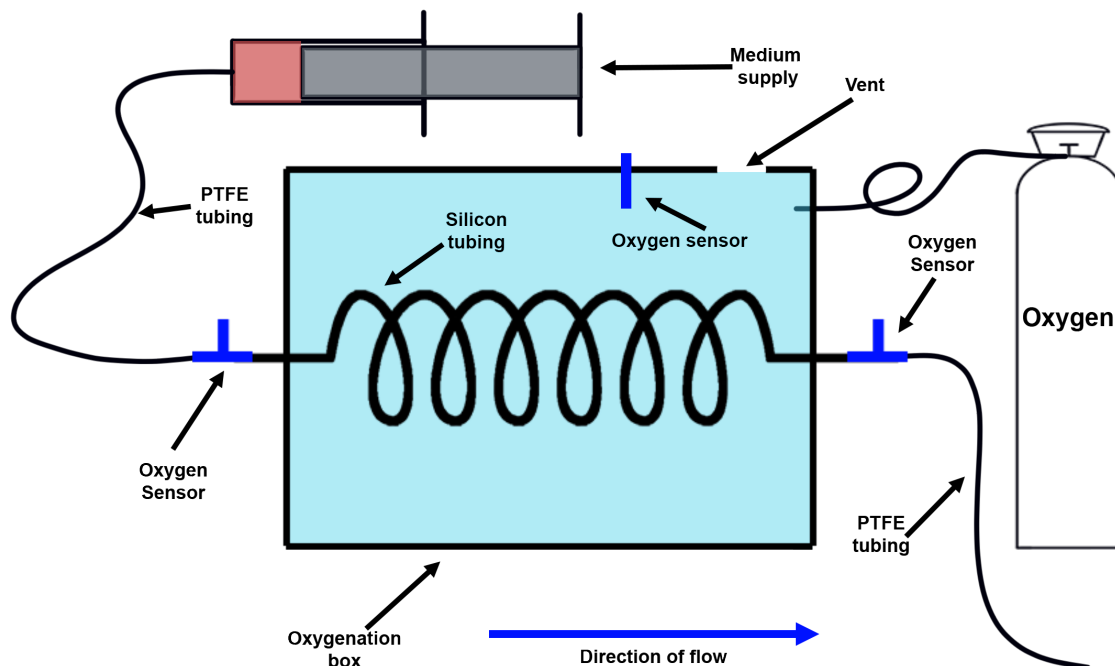
Figure 5.1.1: *Schematic of the oxygenation set-up*

In order to test the effectiveness of the oxygenation device, two lengths of silicone tubing were tested at room temperature (RT) and on ice. The flow rate tested was 2.5 μL min^{-1}. The test was carried out for 3-6 hrs. Figure 5.1.2 presents the findings of the oxygenation tests.

Flick's law (Eq. 5.1 on page 177) can be used to create a simple model describing diffusion of oxygen from the box, through the tubing and into the medium. Flick's law describes the relationship between flux of a gas (F), the diffusion coefficient of a particular gas in a given medium (D), the area of the membrane the diffusion will occur across (A), the difference of the gas of interest between two sides of the
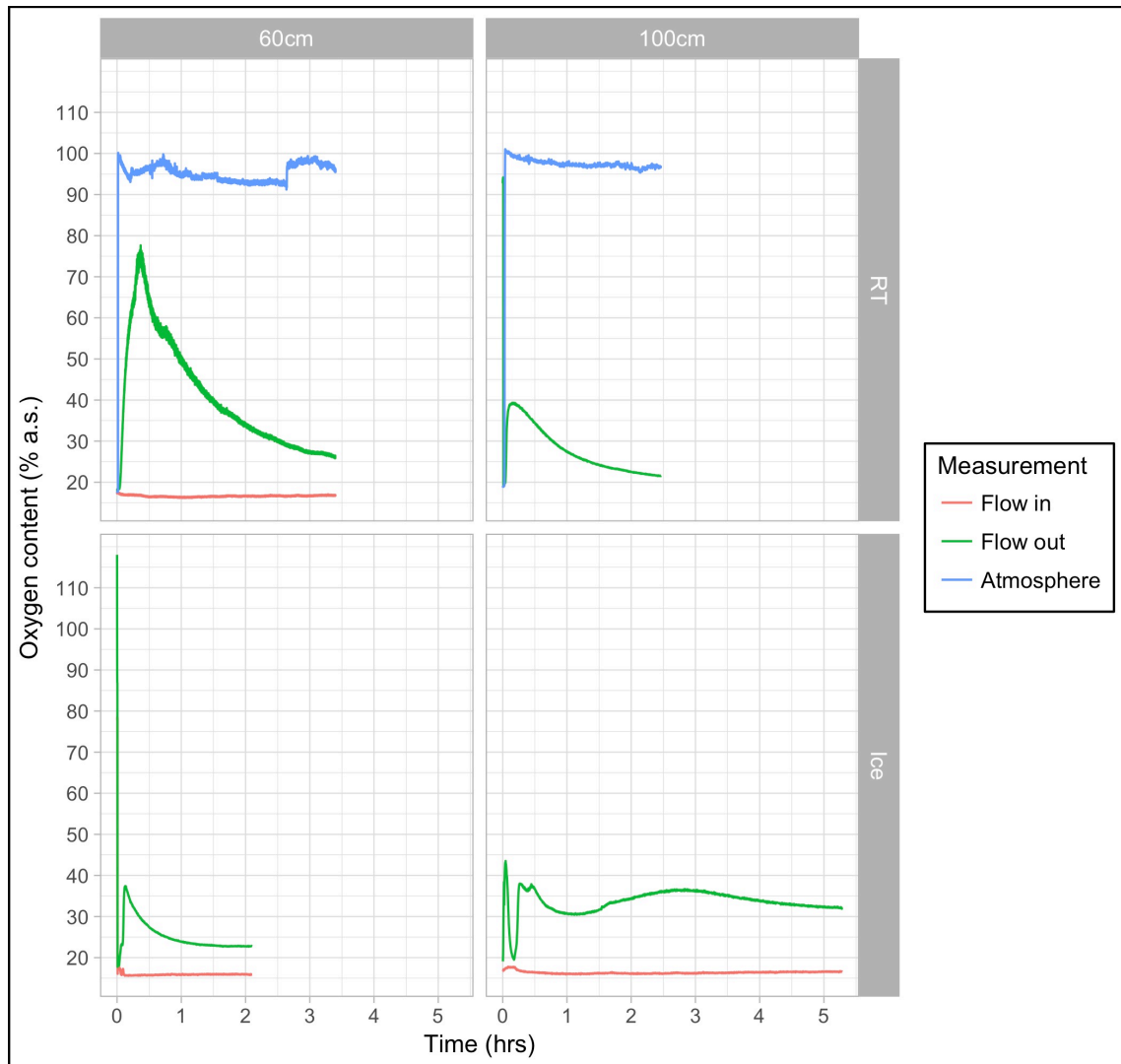
Figure 5.1.2: *Water oxygenation result.* Two tubing lengths (60 cm and 100 cm), and two temperatures (RT - room temperature, and Ice (4°C)) were tested to find the best conditions for sample oxygenation. The "flow in" measurement was recorded with the sensor upstream of the oxygenation box, and the "flow out" measurement was made using the sensor positioned downstream of the box. The "atmosphere" oxygen measurement was recorded using a probe exposed to the oxygen mixture inside of the box.

membrane (ΔC), and the thickness of the membrane (ΔX). The relationship between these factors can be seen in Fig. 5.1.3.

$$F = D \times A \times \frac{\Delta C}{\Delta X} \tag{5.1}$$

$$PV = nRT \tag{5.2}$$
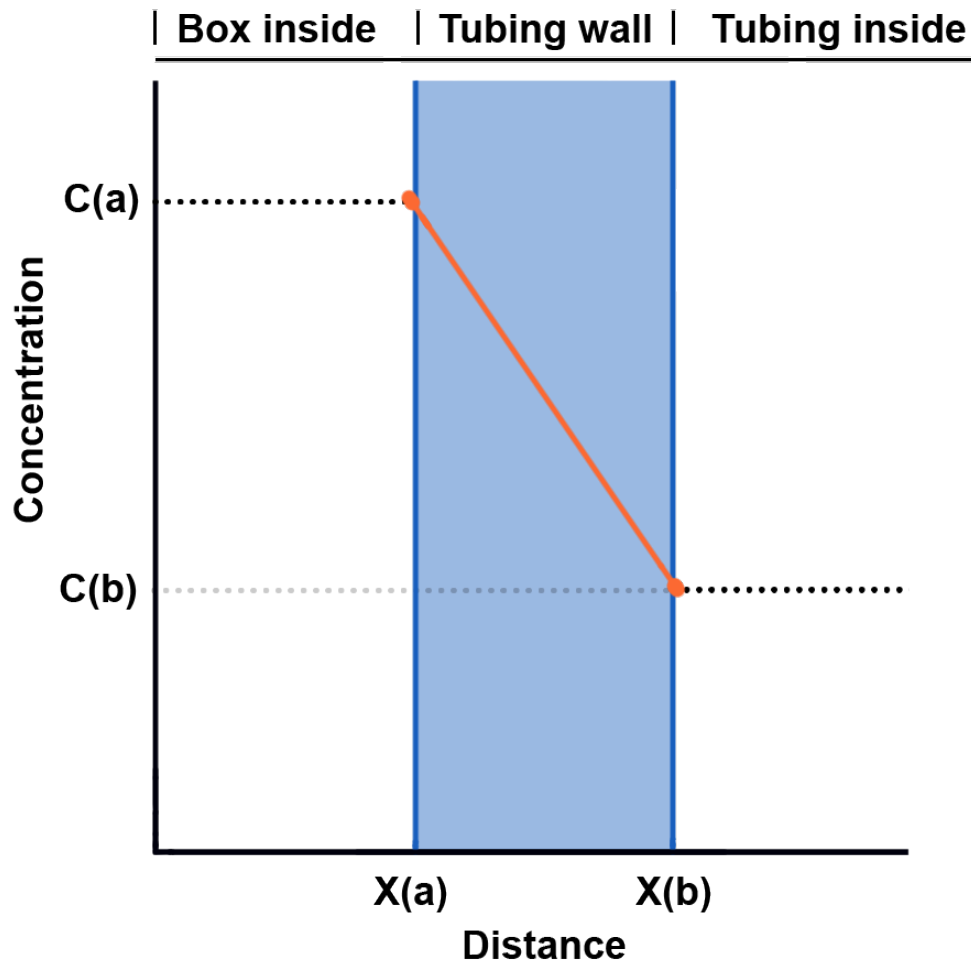
Figure 5.1.3: *Flick's law*

In order to find out ΔC, ideal gas law (Eq. 5.2) has to be employed to calculate the molar concentration of oxygen in the box. We can assume that oxygen pressure

in the box (P) will be 760 mmHg. The volume (V) of the gas can be assumed to be 1 L for the sake of simplicity. We also need to provide the temperature of the system (T = 298 K), and the ideal gas constant (R = 62.364 L mmHg K^{-1}mol^{-1}). According to the ideal gas law, the concentration of oxygen molecules in the oxygenation box will be 0.04088 M. The concentration of oxygen in water that can be assumed to be 8.583 x10^{-5} M. The values of the oxygen flux through 100 cm and 60 cm of silicone membrane (D = 1600 m^{2}s^{-1}) were calculated to be 2.73x10^{-3} mol s^{-1}, and 1.64x10^{-3} mol s^{-1}, which is 40% less than the flux for the 100 cm long piece of tubing. Even though this simplified model doesn't take into account the dynamic nature of the flow, and many other physics, it agrees with the findings presented in Fig. 5.1.2 where it can be observed that the difference in oxygen levels reached by 100 cm long and 60 cm long silicone tubings on ice is 40%. The use of 100 cm long silicone tubing with the system chilled on ice proved to be most successful. The oxygen levels reached just under 45% a.s. in minutes, and then stabilised within the range of 30-40% a.s in less than 30 min. The oxygen concentration remained at that level for the duration of the experiment (5 hrs). The same tubing length (100 cm) used at RT couldn't produce the same oxygen levels. The concentration of the dissolved oxygen in the liquid dropped to around 20% after 2 hrs. No stable oxygen level was achieved in the process. The 60 cm silicone tubing didn't allow for establishment of stable oxygen concentration regardless of the temperature conditions. The concentration would initially raise but then gradually fall during the progress of the experiment. The limitations of this set up were directly associated with the oxygen probes used. The large internal volume of the flow through oxygen probes means that it takes a long period of time for the internal oxygen level to change and reflect the levels in the tubing. As a result, the measurement does not reflect the real time oxygen levels within the capillary.

The oxygen sensors used here were fluorescence-based sensors. This type of sensor uses the principle of fluorescence quenching to detect and measure the concentration

of oxygen. These sensors consist of a light source, a sample chamber, and a detector. The light source emits light at a specific wavelength, which excites a fluorescent dye that is immobilised within the sensor. When oxygen is present, it quenches the fluorescence of the dye, and the detector measures the decrease in fluorescence intensity. From this measurement, the concentration of oxygen can be calculated. PreSense fluorescence-based oxygen sensors have several advantages. They are highly sensitive and can detect very low concentrations of oxygen. They also have a fast response time, which makes them well-suited for dynamic monitoring applications.

Further steps

This work needs to be expanded upon by using smaller diameter flow-through sensors, the device needs to be tested with the human skin samples to analyse the tissue metabolic demand, and the oxygenation device will be used to modulate the sample survival.

The V4.0 device needs to be modified to incorporate a port that will accommodate an O_2 SensorPlug by Presense. One would be placed upstream and one downstream of the tissue culture compartment. This set up will allow for investigation of the metabolic demand of the healing skin sample, and it will help to understand whether the cell death observed in the results presented in section 3.1.4 is a result of lack of hypoxia. The oxygenation chamber would then be used in conjunction with the V4.0 device equipped with the SensorPlugs. As a result, this set up would allow for real time oxygen monitoring with the possibility to modulate the oxygen levels in the tissue culture medium to achieve the desired oxygen levels.

5.1.1 Effluent analysis

Effluent analysis is a potential technique for real-time wound healing analysis without the need to terminate the assay.

A seven day long wound healing assay was carried out to investigate closure of wounded skin samples on the V4.0 microfluidic devices. The static and microfluidic cultures were set up and carried out as described in sections 2.2.11 and 2.2.12 respectively. The explants were wounded in a way outlined in 2.2.10. The effluent was collected daily from the on-chip samples and every two days (and on the day of sample collection) from the control samples. The effluent collected from a device over a period of 24h was 14.4 mL, and the volume collected from the static cultures was 2 mL. LDH assay was carried out on the triplicates of all the samples (biological repeats) in accordance with the manufacturer's guidelines. The LDH levels were measured as an indicator of tissue damage. The manufacturer did not provide the details of the Limit of detection (LOD) for the kit. The LDH activity was expressed in units per 1 mL because the calculation does not make reference to a volume, and it therefore it would be difficult to compare results.

The results of the LDH analysis can be seen in Fig. 5.1.4. It is difficult to assess variations in the LDH level of the on-chip samples as seen in Fig. 5.1.4a because the continuous nature of the culture system means the detected level is ~50 times lower than the one in the control samples. When considering the controls, a drop in the LDH level from day two to day three is evident, after which the detected LDH level raises three-fold on day four and declines over the next three days. The average LDH levels of the wounded and normal skin samples are almost identical on days four and six. The decreasing levels from days four to seven might be correlated to wound healing since many examples of this assay in the literature see an upward slope, especially after a few days of culture.

Closer inspection of the LDH levels of the on-chip samples provides a higher resolution view of the fine changes in the levels of the analyte (see Fig. 5.1.4b). The measured levels from the Day-3 and Day-7 samples exhibit close overlap. It has been observed that there appears to be a strong negative correlation between the LDH level

and the day of the assay. Data from the Day-7 samples were chose for further analysis since it fully covers the entire period of seven days.

(a) LDH assay overview   (b) LDH levels from the on-chip samples
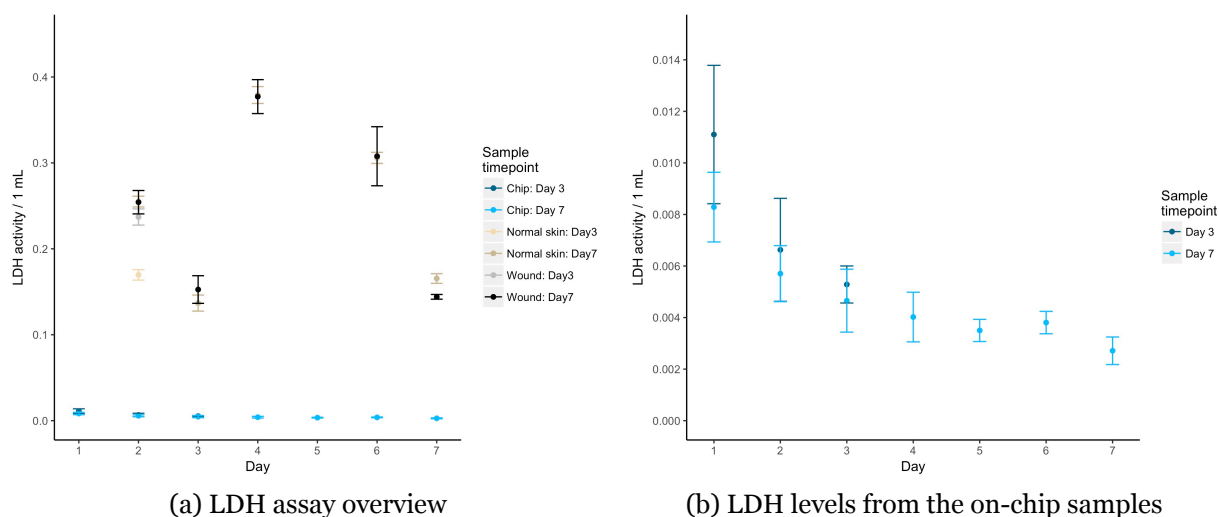
Figure 5.1.4: *LDH assay results*. The samples were cultured in static and microfluidic (V4.0) cultures for the period of up to seven days. The effluent was collected daily from the microfluidic samples, on day three for the unwounded (normal skin) and wounded day three samples, and on days two, three, four, six, and seven for the un-wounded (normal skin) and wounded day seven samples. The day number in the sample name refers to when the sample was removed from the culture. The total effluent produced by the microfluidic devices over the period of 24 h was collected each day (14.4 mL), and the total volume of the conditioned media was collected from the static culture (2 mL). The LOD for the LDH assay is unknown. N = 3 for all the samples (biological replicates). The LDH activity was standardised to units per 1 mL to make the results comparable. (a) Overview of all LDH measurements from both the control samples and the effluent collected from the on-chip samples. The wounded samples in grey and black. (b) LDH levels from the on-chip samples only.

LDH level measurement results were firstly log transformed to achieve normal distribution, and then Pearson's Correlation test was used to assess the strength of the correlation between the LDH level and the assay day. The test returned R value of -0.827 and a p value of 2.2 x10^{-16}, indicating a significant negative relationship.

Such relationship could suggest that the LDH reduction is the result of wound healing, and the healing progression could be assessed off-chip using effluent LDH analysis.

Further, linear models of three polynomial degrees were fitted to the data (see Fig. 5.1.5) and gvlma R package was used to carry out global validation to test the model assumptions. Linear regression analysis suggested that third degree polynomial equation best describes the data (adjusted R^2=0.7411, p <2.2x10^{-16}), which was further confirmed by global validation of model assumptions. The third degree polynomial (cubic) model was the only model meeting all the assumptions.

The coefficients from the model summary were used to derive model equation of $y = -0.01306x^3 + 0.17702x^2 - 0.85537x - 4.09905$. This equation can be used in combination with the histology data to assess whether LDH assay can be successfully used to monitor the progress of wound healing without the need for destructive end-point assays.

Figure 5.1.5: LDH model testing
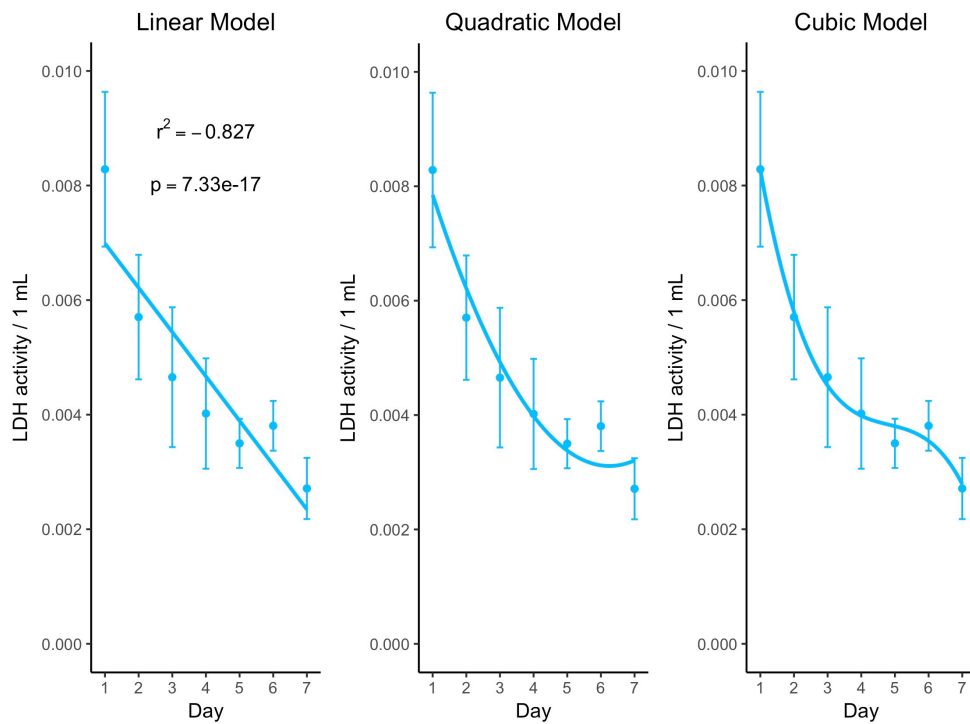
Model	R^2	Adjusted R^2	p-value
Linear	0.6831	0.6779	$<2.2 \times 10^{-16}$
Quadratic	0.7173	0.7079	$<2.2 \times 10^{-16}$
Cubic	0.7536	0.7411	$<2.2 \times 10^{-16}$

Table 5.1: *Summary of alternative models*

Further steps

The effluent analysis could prove to be a powerful technique in real-life monitoring of would healing assays. Although using LDH on its own as the biomarker might not be the best strategy to monitor the wound healing process, combining it with other markers such as MMPs and interleukins could allow for effective monitoring of the healing process.

Final conclusion

To conclude everything that has been said so fat, V4.0 device is a successful platform for maintenance of human skin samples, able to reduce the apoptotic cell death in the cultured samples. Furthermore, this microfluidic flow cell has been shown to be suitable for wound healing assays, where the experiments demonstrated that the device allows for successful wound closure. In addition, the immunological profiling showed that the on-chip samples retained a greater number of T cells and macrophages than the control samples, making the V4.0 device a closer representation of the biological wound healing environment. This project is believed to the the first to demonstrate that a human skin wound healing model with improved immunological microenvironment can be achieved using microfluidic principles. The V4.0 is a good candidate for many research applications that require a physiologically accurate skin or wound biology model. Examples of such applications include therapeutic intervention testing for non healing wounds, where chemical agents or medical devices such as wound

dressings could be applied to the samples on the device, and tested. Pathogen-host interactions could also be studied using V4.0 device, with the improved immune retention making the model more physiological. Permeation assays testing can also be performed by applying a chemical agent topically to the sample, and measuring it, or its metabolite in the effluent. The device could also potentially be used as for personalised medicine applications, where a patient's biopsy could be maintained and tested against potential treatments, so that most suitable therapy can be identified for the patient.

In summary, this thesis has presented data supporting V4.0 as capable platform for maintenance and analysis of wounded and unwounded human skin biopsies, with several potential applications that could contribute to both the field of skin biology, but also potentially to the treatment of the patients suffering from cutaneous wound healing complications.

Bibliography

Abaci, H. E., Gledhill, K., Guo, Z., Christiano, A. M. and Shuler, M. L. (2015a). Pumpless Microfluidic Platform for Drug Testing on Human Skin Equivalents. Lab on a Chip *15*, 882–888.

Abaci, H. E., Gledhill, K., Guo, Z., Christiano, A. M. and Shuler, M. L. (2015b). Pumpless Microfluidic Platform for Drug Testing on Human Skin Equivalents. Lab on a Chip *15*, 882–888.

Abaci, H. E., Guo, Z., Coffman, A., Gillette, B., Lee, W.-h., Sia, S. K. and Christiano, A. M. (2016). Human Skin Constructs with Spatially Controlled Vasculature Using Primary and iPSC-Derived Endothelial Cells. Advanced Healthcare Materials *5*, 1800–1807.

Abdo, J. M., Sopko, N. A. and Milner, S. M. (2020). The Applied Anatomy of Human Skin: A Model for Regeneration. Wound Medicine *28*, 100179.

Alberti, M., Dancik, Y., Sriram, G., Wu, B., Teo, Y. L., Feng, Z., Bigliardi-Qi, M., Wu, R. G., Wang, Z. P. and Bigliardi, P. L. (2017a). Multi-Chamber Microfluidic Platform for High-Precision Skin Permeation Testing. Lab Chip *17*, 1625–1634.

Alberti, M., Dancik, Y., Sriram, G., Wu, B., Teo, Y. L., Feng, Z., Bigliardi-Qi, M., Wu, R. G., Wang, Z. P. and Bigliardi, P. L. (2017b). Multi-Chamber Microfluidic Platform for High-Precision Skin Permeation Testing. Lab on a Chip *17*, 1625–1634.

Allen, C. B., Schneider, B. K. and White, C. W. (2001). Limitations to Oxygen Diffusion and Equilibration in in Vitro Cell Exposure Systems in Hyperoxia and Hypoxia. American Journal of Physiology. Lung Cellular and Molecular Physiology *281*, L1021–1027.

Armstrong, D. G., Wrobel, J. and Robbins, J. M. (2007). Guest Editorial: Are Diabetes-Related Wounds and Amputations Worse than Cancer? International Wound Journal *4*, 286–287.

Ataç, B., Wagner, I., Horland, R., Lauster, R., Marx, U., Tonevitsky, A. G., Azar, R. P. and Lindner, G. (2013a). Skin and Hair On-a-Chip: In Vitro Skin Models versus Ex Vivo Tissue Maintenance with Dynamic Perfusion. Lab on a chip *13*, 3555–61.

Ataç, B., Wagner, I., Horland, R., Lauster, R., Marx, U., Tonevitsky, A. G., Azar, R. P. and Lindner, G. (2013b). Skin and Hair On-a-Chip: In Vitro Skin Models versus Ex Vivo Tissue Maintenance with Dynamic Perfusion. Lab on a chip *13*, 3555–61.

Aulivola, B., Hile, C. N., Hamdan, A. D., Sheahan, M. G., Veraldi, J. R., Skillman, J. J., Campbell, D. R., Scovell, S. D., LoGerfo, F. W. and Pomposelli, F. B. (2004). Major Lower Extremity Amputation: Outcome of a Modern Series. Archives of Surgery (Chicago, Ill.: 1960) *139*, 395–399; discussion 399.

Baggiolini, M. (1998). Chemokines and Leukocyte Traffic. Nature *392*, 565–568.

Barrientos, S., Stojadinovic, O., Golinko, M. S., Brem, H. and Tomic-Canic, M. (2008). Growth Factors and Cytokines in Wound Healing. Wound Repair and Regeneration: Official Publication of the Wound Healing Society [and] the European Tissue Repair Society *16*, 585–601.

Becker, H. and Gärtner, C. (2012). Microfluidics and the Life Sciences. Science Progress *95*, 175–198.

Beidler, S. K., Douillet, C. D., Berndt, D. F., Keagy, B. A., Rich, P. B. and Marston, W. A. (2009). Inflammatory Cytokine Levels in Chronic Venous Insufficiency Ulcer Tissue before and after Compression Therapy. Journal of Vascular Surgery *49*, 1013–1020.

Bergan, J. J., Schmid-Schönbein, G. W., Smith, P. D. C., Nicolaides, A. N., Boisseau, M. R. and Eklof, B. (2006). Chronic Venous Disease. The New England Journal of Medicine *355*, 488–498.

Biglari, S., Le, T. Y. L., Tan, R. P., Wise, S. G., Zambon, A., Codolo, G., Bernard, M. D., Warkiani, M., Schindeler, A., Naficy, S., Valtchev, P., Khademhosseini, A. and Dehghani, F. (2019). Simulating Inflammation in a Wound Microenvironment Using a Dermal Wound-on-a-Chip Model. Advanced Healthcare Materials *8*, 1801307.

Blazić, T. M. and Brajac, I. (2006). Defective Induction of Senescence during Wound Healing Is a Possible Mechanism of Keloid Formation. Medical Hypotheses *66*, 649–652.

Bonifati, C., Mussi, A., D'Auria, L., Carducci, M., Trento, E., Cordiali-Fei, P. and Ameglio, F. (1998). Spontaneous Release of Leukemia Inhibitory Factor and Oncostatin-M Is Increased in Supernatants of Short-Term Organ Cultures from Lesional Psoriatic Skin. Archives of Dermatological Research *290*, 9–13.

Braff, M. H., Nardo, A. D. and Gallo, R. L. (2005). Keratinocytes Store the Antimicrobial Peptide Cathelicidin in Lamellar Bodies. Journal of Investigative Dermatology *124*, 394–400.

Brem, H., Golinko, M. S., Stojadinovic, O., Kodra, A., Diegelmann, R. F., Vukelic, S., Entero, H., Coppock, D. L. and Tomic-Canic, M. (2008). Primary Cultured Fibroblasts Derived from Patients with Chronic Wounds: A Methodology to Produce Hu-

man Cell Lines and Test Putative Growth Factor Therapy Such as GMCSF. Journal of Translational Medicine *6*, 75.

Brem, H. and Tomic-Canic, M. (2007). Cellular and Molecular Basis of Wound Healing in Diabetes. The Journal of Clinical Investigation *117*, 1219–1222.

Bullard, K. M., Longaker, M. T. and Lorenz, H. P. (2003). Fetal Wound Healing: Current Biology. World J Surg *27*, 54–61.

Burden, N., Chapman, K., Sewell, F. and Robinson, V. (2015). Pioneering Better Science through the 3Rs: An Introduction to the National Centre for the Replacement, Refinement, and Reduction of Animals in Research (NC3Rs). Journal of the American Association for Laboratory Animal Science: JAALAS *54*, 198–208.

Calne, R. Y., Alexandre, G. P. and Murray, J. E. (1962). A Study of the Effects of Drugs in Prolonging Survival of Homologous Renal Transplants in Dogs. Annals of the New York Academy of Sciences *99*, 743–761.

Charles, C. A., Tomic-Canic, M., Vincek, V., Nassiri, M., Stojadinovic, O., Eaglstein, W. H. and Kirsner, R. S. (2008). A Gene Signature of Nonhealing Venous Ulcers: Potential Diagnostic Markers. Journal of the American Academy of Dermatology *59*, 758–771.

Chou, W. C., Takeo, M., Rabbani, P., Hu, H., Lee, W., Chung, Y. R., Carucci, J., Overbeek, P. and Ito, M. (2013). Direct Migration of Follicular Melanocyte Stem Cells to the Epidermis after Wounding or UVB Irradiation Is Dependent on Mc1r Signaling. Nature Medicine *19*, 924–929.

Chu, D. H. (2008). Overview of Biology, Development, and Structure of Skin. In Fitzpatrick's Dermatology in General Medicine. McGraw-Hill Medical New York 7th ed edition.

Clark, R. A. (1983). Fibronectin in the Skin. J Invest Dermatol *81*, 475–9.

Clark, R. A., Lanigan, J. M., DellaPelle, P., Manseau, E., Dvorak, H. F. and Colvin, R. B. (1982). Fibronectin and Fibrin Provide a Provisional Matrix for Epidermal Cell Migration during Wound Reepithelialization. J Invest Dermatol *79*, 264–9.

Costin, G.-E. and Hearing, V. J. (2007). Human Skin Pigmentation: Melanocytes Modulate Skin Color in Response to Stress. The FASEB Journal *21*, 976–994.

Coulombe, P. A. (1997). Towards a Molecular Definition of Keratinocyte Activation after Acute Injury to Stratified Epithelia. Biochemical and Biophysical Research Communications *236*, 231–238.

Delavary, B. M., van der Veer, W. M., van Egmond, M., Niessen, F. B. and Beelen, R. H. J. (2011). Macrophages in Skin Injury and Repair. Immunobiology *216*, 753–762.

Denda, M. (2015). Epidermis as the "Third Brain"? Dermatologica Sinica *33*, 70–73.

Diegelmann, R. F. and Evans, M. C. (2004). Wound Healing: An Overview of Acute, Fibrotic and Delayed Healing. Frontiers in Bioscience: A Journal and Virtual Library *9*, 283–289.

Elder, D. E. and Lever, W. F. (1997). Lever's Histopathology of the Skin. 8th ed. / editor-in-chief, david elder; associate editors, rosalie elenitsas, christine jaworsky, bernett johnson, jr. edition, Lippincott-Raven, Philadelphia.

Eming, S. A., Hammerschmidt, M., Krieg, T. and Roers, A. (2009). Interrelation of Immunity and Tissue Repair or Regeneration. Seminars in Cell & Developmental Biology *20*, 517–527.

Eming, S. A., Koch, M., Krieger, A., Brachvogel, B., Kreft, S., Bruckner-Tuderman, L., Krieg, T., Shannon, J. D. and Fox, J. W. (2010). Differential Proteomic Ana-

lysis Distinguishes Tissue Repair Biomarker Signatures in Wound Exudates Obtained from Normal Healing and Chronic Wounds. Journal of Proteome Research *9*, 4758–4766.

Eming, S. A., Krieg, T. and Davidson, J. M. (2007). Inflammation in Wound Repair: Molecular and Cellular Mechanisms. The Journal of Investigative Dermatology *127*, 514–525.

Eming, S. A., Martin, P. and Tomic-Canic, M. (2014). Wound Repair and Regeneration: Mechanisms, Signaling, and Translation. Sci Transl Med *6*, 265sr6.

Ericksen, B., Wu, Z., Lu, W. and Lehrer, R. I. (2005). Antibacterial Activity and Specificity of the Six Human α-Defensins. Antimicrobial Agents and Chemotherapy *49*, 269–275.

Esch, M. B., King, T. L. and Shuler, M. L. (2011). The Role of Body-on-a-Chip Devices in Drug and Toxicity Studies. Annu Rev Biomed Eng *13*, 55–72.

Evans, N. T. S. and Naylor, P. F. D. (1966). Steady States of Oxygen Tension in Human Dermis. Respiration Physiology *2*, 46–60.

Evans, N. T. S. and Naylor, P. F. D. (1967). The Oxygen Tension Gradient across Human Epidermis. Respiration Physiology *3*, 38–42.

Farahat, W. A., Wood, L. B., Zervantonakis, I. K., Schor, A., Ong, S., Neal, D., Kamm, R. D. and Asada, H. H. (2012). Ensemble Analysis of Angiogenic Growth in Three-Dimensional Microfluidic Cell Cultures. PLOS ONE *7*, e37333.

Farrar, M. A. and Schreiber, R. D. (1993). The Molecular Cell Biology of Interferon-Gamma and Its Receptor. Annual Review of Immunology *11*, 571–611.

Gamble, L. J. and Matthews, Q. L. (2010). Current Progress in the Development of a Prophylactic Vaccine for HIV-1. Drug Design, Development and Therapy *5*, 9–26.

Gao, G. F., Rao, Z. and Bell, J. I. (2002). Molecular Coordination of Alphabeta T-cell Receptors and Coreceptors CD8 and CD4 in Their Recognition of Peptide-MHC Ligands. Trends in Immunology *23*, 408–413.

Ghaemmaghami, A. M., Hancock, M. J., Harrington, H., Kaji, H. and Khademhosseini, A. (2012). Biomimetic Tissues on a Chip for Drug Discovery. Drug Discov Today *17*, 173–81.

Godfrey, D. I., Hammond, K. J., Poulton, L. D., Smyth, M. J. and Baxter, A. G. (2000). NKT Cells: Facts, Functions and Fallacies. Immunology Today *21*, 573–583.

Guest, J. F., Ayoub, N., McIlwraith, T., Uchegbu, I., Gerrish, A., Weidlich, D., Vowden, K. and Vowden, P. (2015). Health Economic Burden That Wounds Impose on the National Health Service in the UK. BMJ Open *5*, e009283.

Hackam, D. G. and Redelmeier, D. A. (2006). Translation of Research Evidence from Animals to Humans. JAMA *296*, 1731–1732.

Hall, E. D., Yonkers, P. A., McCall, J. M. and Braughler, J. M. (1988). Effects of the 21-Aminosteroid U74006F on Experimental Head Injury in Mice. Journal of Neurosurgery *68*, 456–461.

Harding, F. A., McArthur, J. G., Gross, J. A., Raulet, D. H. and Allison, J. P. (1992). CD28-mediated Signalling Co-Stimulates Murine T Cells and Prevents Induction of Anergy in T-cell Clones. Nature *356*, 607–609.

Hoffmann, D. C., Willenborg, S., Koch, M., Zwolanek, D., Müller, S., Becker, A.-K. A., Metzger, S., Ehrbar, M., Kurschat, P., Hellmich, M., Hubbell, J. A. and Eming, S. A. (2013). Proteolytic Processing Regulates Placental Growth Factor Activities. The Journal of Biological Chemistry *288*, 17976–17989.

Hübner, J., Raschke, M., Rütschle, I., Gräßle, S., Hasenberg, T., Schirrmann, K., Lorenz, A., Schnurre, S., Lauster, R., Maschmeyer, I., Steger-Hartmann, T. and

Marx, U. (2018). Simultaneous Evaluation of Anti-EGFR-induced Tumour and Adverse Skin Effects in a Microfluidic Human 3D Co-Culture Model. Scientific Reports *8*, 15010.

Huh, D., Hamilton, G. A. and Ingber, D. E. (2011). From 3D Cell Culture to Organs-on-Chips. Trends Cell Biol *21*, 745–54.

Huh, D., Torisawa, Y. S., Hamilton, G. A., Kim, H. J. and Ingber, D. E. (2012). Microengineered Physiological Biomimicry: Organs-on-Chips. Lab Chip *12*, 2156–64.

Jacinto, A., Martinez-Arias, A. and Martin, P. (2001). Mechanisms of Epithelial Fusion and Repair. Nature Cell Biology *3*, E117–E123.

Jackson, S. M., Williams, M. L., Feingold, K. R. and Elias, P. M. (1993). Pathobiology of the Stratum Corneum. West J Med *158*, 279–85.

James, W. D., Elston, D. M., Berger, T. G. and of the skin Andrews, G. C. D. (2011). Andrews' Diseases of the Skin : Clinical Dermatology. 11th ed. edition, Saunders Elsevier, London.

Jones, P. H. (1996). Isolation and Characterization of Human Epidermal Stem Cells. Clin Sci (Lond) *91*, 141–6.

Kanitakis, J. (2002). Anatomy, Histology and Immunohistochemistry of Normal Human Skin. European journal of dermatology : EJD *12*, 390–9; quiz 400–1.

Kety, S. S. (1951). The Theory and Applications of the Exchange of Inert Gas at the Lungs and Tissues. Pharmacological Reviews *3*, 1–41.

Kilkenny, C., Browne, W., Cuthill, I. C., Emerson, M. and Altman, D. G. (2010). Animal Research: Reporting in Vivo Experiments: The ARRIVE Guidelines. British Journal of Pharmacology *160*, 1577–1579.

Kivinen, P. K., Nilsson, G., Naukkarinen, A. and Harvima, I. T. (2003). Mast Cell Survival and Apoptosis in Organ-Cultured Human Skin. Experimental Dermatology *12*, 53–60.

Kolaczkowska, E. and Kubes, P. (2013). Neutrophil Recruitment and Function in Health and Inflammation. Nature Reviews Immunology *13*, 159–175.

Kovarik, M. L., Ornoff, D. M., Melvin, A. T., Dobes, N. C., Wang, Y., Dickinson, A. J., Gach, P. C., Shah, P. K. and Allbritton, N. L. (2013). Micro Total Analysis Systems: Fundamental Advances and Applications in the Laboratory, Clinic, and Field. Analytical Chemistry *85*, 451–472.

Krisp, C., Jacobsen, F., McKay, M. J., Molloy, M. P., Steinstraesser, L. and Wolters, D. A. (2013). Proteome Analysis Reveals Antiangiogenic Environments in Chronic Wounds of Diabetes Mellitus Type 2 Patients. Proteomics *13*, 2670–2681.

Krogh, A. (1919a). The Rate of Diffusion of Gases through Animal Tissues, with Some Remarks on the Coefficient of Invasion. The Journal of Physiology *52*, 391–408.

Krogh, A. (1919b). The Supply of Oxygen to the Tissues and the Regulation of the Capillary Circulation. The Journal of Physiology *52*, 457–474.

Kuniyasu, Y., Takahashi, T., Itoh, M., Shimizu, J., Toda, G. and Sakaguchi, S. (2000). Naturally Anergic and Suppressive CD25(+)CD4(+) T Cells as a Functionally and Phenotypically Distinct Immunoregulatory T Cell Subpopulation. International Immunology *12*, 1145–1155.

Lau, K., Paus, R., Tiede, S., Day, P. and Bayat, A. (2009). Exploring the Role of Stem Cells in Cutaneous Wound Healing. Exp Dermatol *18*, 921–33.

Lauer, G., Sollberg, S., Cole, M., Flamme, I., Stürzebecher, J., Mann, K., Krieg, T. and Eming, S. A. (2000). Expression and Proteolysis of Vascular Endothelial Growth

Factor Is Increased in Chronic Wounds. The Journal of Investigative Dermatology *115*, 12–18.

Lavker, R. M. and Sun, T. T. (1982). Heterogeneity in Epidermal Basal Keratinocytes: Morphological and Functional Correlations. Science *215*, 1239–41.

Lebonvallet, N., Jeanmaire, C., Danoux, L., Sibille, P., Pauly, G. and Misery, L. (2010). The Evolution and Use of Skin Explants: Potential and Limitations for Dermatological Research. European Journal of Dermatology *20*, 671–684.

Lee, S., Jin, S.-P., Kim, Y. K., Sung, G. Y., Chung, J. H. and Sung, J. H. (2017). Construction of 3D Multicellular Microfluidic Chip for an in Vitro Skin Model. Biomedical Microdevices *19*, 22.

Leibovich, S. J. and Ross, R. (1975). The Role of the Macrophage in Wound Repair. A Study with Hydrocortisone and Antimacrophage Serum. Am J Pathol *78*, 71–100.

Lin, J.-Y., Lo, K.-Y. and Sun, Y.-S. (2019). A Microfluidics-Based Wound-Healing Assay for Studying the Effects of Shear Stresses, Wound Widths, and Chemicals on the Wound-Healing Process. Scientific Reports *9*, 20016.

Loots, M. A., Lamme, E. N., Zeegelaar, J., Mekkes, J. R., Bos, J. D. and Middelkoop, E. (1998). Differences in Cellular Infiltrate and Extracellular Matrix of Chronic Diabetic and Venous Ulcers versus Acute Wounds. The Journal of Investigative Dermatology *111*, 850–857.

Lorenz, H. P., Longaker, M. T., Perkocha, L. A., Jennings, R. W., Harrison, M. R. and Adzick, N. S. (1992). Scarless Wound Repair: A Human Fetal Skin Model. Development (Cambridge, England) *114*, 253–259.

Manz, A., Graber, N. and Widmer, H. M. (1990a). Miniaturized Total Chemical Analysis Systems: A Novel Concept for Chemical Sensing. Sensors and Actuators B: Chemical *1*, 244–248.

Manz, A., Miyahara, Y., Miura, J., Watanabe, Y., Miyagi, H. and Sato, K. (1990b). Design of an Open-Tubular Column Liquid Chromatograph Using Silicon Chip Technology. Sensors and Actuators B: Chemical *1*, 249–255.

Marabelle, A., Kohrt, H., Sagiv-Barfi, I., Ajami, B., Axtell, R. C., Zhou, G., Rajapaksa, R., Green, M. R., Torchia, J., Brody, J., Luong, R., Rosenblum, M. D., Steinman, L., Levitsky, H. I., Tse, V. and Levy, R. (2013). Depleting Tumor-Specific Tregs at a Single Site Eradicates Disseminated Tumors. The Journal of Clinical Investigation *123*, 2447–2463.

Martin, P. (1997). Wound Healing–Aiming for Perfect Skin Regeneration. Science *276*, 75–81.

Martin, P. and Leibovich, S. J. (2005). Inflammatory Cells during Wound Repair: The Good, the Bad and the Ugly. Trends in Cell Biology *15*, 599–607.

Martinez, A. W., Phillips, S. T., Butte, M. J. and Whitesides, G. M. (2007). Patterned Paper as a Platform for Inexpensive, Low-Volume, Portable Bioassays. Angewandte Chemie (International Ed. in English) *46*, 1318–1320.

Martinez, A. W., Phillips, S. T., Wiley, B. J., Gupta, M. and Whitesides, G. M. (2008). FLASH: A Rapid Method for Prototyping Paper-Based Microfluidic Devices. Lab on a Chip *8*, 2146–2150.

Marx, U., Walles, H., Hoffmann, S., Lindner, G., Horland, R., Sonntag, F., Klotzbach, U., Sakharov, D., Tonevitsky, A. and Lauster, R. (2012). 'Human-on-a-chip'developments: A Translational Cutting-Edge Alternative to Systemic Safety Assessment and Efficiency Evaluation of Substances in Laboratory Animals and Man? Alternatives to Laboratory Animals-ATLA *40*, 235.

Maschmeyer, I., Hasenberg, T., Jaenicke, A., Lindner, M., Lorenz, A. K., Zech, J., Garbe, L. A., Sonntag, F., Hayden, P., Ayehunie, S., Lauster, R., Marx, U. and

Materne, E. M. (2015a). Chip-Based Human Liver-Intestine and Liver-Skin Co-Cultures–A First Step toward Systemic Repeated Dose Substance Testing in Vitro. Eur J Pharm Biopharm *95*, 77–87.

Maschmeyer, I., Hasenberg, T., Jaenicke, A., Lindner, M., Lorenz, A. K., Zech, J., Garbe, L.-A., Sonntag, F., Hayden, P., Ayehunie, S., Lauster, R., Marx, U. and Materne, E.-M. (2015b). Chip-Based Human Liver–Intestine and Liver–Skin Co-Cultures – A First Step toward Systemic Repeated Dose Substance Testing in Vitro. European Journal of Pharmaceutics and Biopharmaceutics *95*, 77–87.

Maschmeyer, I., Lorenz, A. K., Schimek, K., Hasenberg, T., Ramme, A. P., Hubner, J., Lindner, M., Drewell, C., Bauer, S., Thomas, A., Sambo, N. S., Sonntag, F., Lauster, R. and Marx, U. (2015c). A Four-Organ-Chip for Interconnected Long-Term Co-Culture of Human Intestine, Liver, Skin and Kidney Equivalents. Lab Chip *15*, 2688–99.

Maschmeyer, I., Lorenz, A. K., Schimek, K., Hasenberg, T., Ramme, A. P., Hübner, J., Lindner, M., Drewell, C., Bauer, S., Thomas, A., Sambo, N. S., Sonntag, F., Lauster, R. and Marx, U. (2015d). A Four-Organ-Chip for Interconnected Long-Term Co-Culture of Human Intestine, Liver, Skin and Kidney Equivalents. Lab on a Chip *15*, 2688–2699.

Matoltsy, A. G. (1976). Keratinization. Journal of Investigative Dermatology *67*, 20–25.

McLimans, W. F., Blumenson, L. E. and Tunnah, K. V. (1968). Kinetics of Gas Diffusion in Mammalian Cell Culture Systems. II. Theory. Biotechnology and Bioengineering *10*, 741–763.

Mehling, M. and Tay, S. (2014). Microfluidic Cell Culture. Current Opinion in Biotechnology *25*, 95–102.

Meyvantsson, I. and Beebe, D. J. (2008). Cell Culture Models in Microfluidic Systems. Annu Rev Anal Chem (Palo Alto Calif) *1*, 423–49.

Miller, S. J., Burke, E. M., Rader, M. D., Coulombe, P. A. and Lavker, R. M. (1998). Re-Epithelialization of Porcine Skin by the Sweat Apparatus. J Invest Dermatol *110*, 13–9.

Moll, R., Divo, M. and Langbein, L. (2008). The Human Keratins: Biology and Pathology. Histochemistry and Cell Biology *129*, 705.

Mori, N., Morimoto, Y. and Takeuchi, S. (2017a). Skin Integrated with Perfusable Vascular Channels on a Chip. Biomaterials *116*, 48–56.

Mori, N., Morimoto, Y. and Takeuchi, S. (2017b). Skin Integrated with Perfusable Vascular Channels on a Chip. Biomaterials *116*, 48–56.

Murphy, G. (1997). Histology of the Skin. In Lever's Histopathology of the Skin pp. 5–45. Wolters Kluwer Philadelphia eighth edition edition.

Murray, P. J. and Wynn, T. A. (2011). Protective and Pathogenic Functions of Macrophage Subsets. Nature Reviews. Immunology *11*, 723–737.

Nagasaka, T., Cabanac, M., Hirata, K. and Nunomura, T. (1987). Control of Local Heat Gain by Vasomotor Response of the Hand. Journal of Applied Physiology *63*, 1335–1338.

Nemes, Z. and Steinert, P. M. (1999). Bricks and Mortar of the Epidermal Barrier. Experimental & Molecular Medicine *31*, 5–19.

Newby, D., Marks, L. and Lyall, F. (2005). Dissolved Oxygen Concentration in Culture Medium: Assumptions and Pitfalls. Placenta *26*, 353–357.

Nickoloff, B. J., Lingen, M. W., Chang, B.-D., Shen, M., Swift, M., Curry, J., Bacon, P., Bodner, B. and Roninson, I. B. (2004). Tumor Suppressor Maspin Is Up-Regulated during Keratinocyte Senescence, Exerting a Paracrine Antiangiogenic Activity. Cancer Research *64*, 2956–2961.

Nobes, C. D. and Hall, A. (1995). Rho, Rac, and Cdc42 GTPases Regulate the Assembly of Multimolecular Focal Complexes Associated with Actin Stress Fibers, Lamellipodia, and Filopodia. Cell *81*, 53–62.

Nobes, C. D. and Hall, A. (1999). Rho GTPases Control Polarity, Protrusion, and Adhesion during Cell Movement. J Cell Biol *144*, 1235–44.

Nolan, C. J., Damm, P. and Prentki, M. (2011). Type 2 Diabetes across Generations: From Pathophysiology to Prevention and Management. Lancet (London, England) *378*, 169–181.

Olsson, M., Järbrink, K., Divakar, U., Bajpai, R., Upton, Z., Schmidtchen, A. and Car, J. (2019). The Humanistic and Economic Burden of Chronic Wounds: A Systematic Review. Wound Repair and Regeneration *27*, 114–125.

Palacio-Castañeda, V., Velthuijs, N., Le Gac, S. and Verdurmen, W. P. R. (2022). Oxygen Control: The Often Overlooked but Essential Piece to Create Better *in Vitro* Systems. Lab on a Chip *22*, 1068–1092.

Pappas, A. (2009). Epidermal Surface Lipids. Dermato-endocrinology *1*, 72–76.

Pastar, I., Khan, A. A., Stojadinovic, O., Lebrun, E. A., Medina, M. C., Brem, H., Kirsner, R. S., Jimenez, J. J., Leslie, C. and Tomic-Canic, M. (2012). Induction of Specific microRNAs Inhibits Cutaneous Wound Healing. The Journal of Biological Chemistry *287*, 29324–29335.

Pastar, I., Nusbaum, A. G., Gil, J., Patel, S. B., Chen, J., Valdes, J., Stojadinovic, O., Plano, L. R., Tomic-Canic, M. and Davis, S. C. (2013). Interactions of Methicillin

Resistant Staphylococcus Aureus USA300 and Pseudomonas Aeruginosa in Polymicrobial Wound Infection. PloS One *8*, e56846.

Pastar, I., Stojadinovic, O., Krzyzanowska, A., Barrientos, S., Stuelten, C., Zimmerman, K., Blumenberg, M., Brem, H. and Tomic-Canic, M. (2010). Attenuation of the Transforming Growth Factor Beta-Signaling Pathway in Chronic Venous Ulcers. Molecular Medicine (Cambridge, Mass.) *16*, 92–101.

Patel, G. K., Wilson, C. H., Harding, K. G., Finlay, A. Y. and Bowden, P. E. (2006). Numerous Keratinocyte Subtypes Involved in Wound Re-Epithelialization. Journal of Investigative Dermatology *126*, 497–502.

Perel, P., Roberts, I., Sena, E., Wheble, P., Briscoe, C., Sandercock, P., Macleod, M., Mignini, L. E., Jayaram, P. and Khan, K. S. (2007). Comparison of Treatment Effects between Animal Experiments and Clinical Trials: Systematic Review. BMJ : British Medical Journal *334*, 197.

Pillai, S., Bikle, D. D. and Elias, P. M. (1988). Vitamin D and Epidermal Differentiation: Evidence for a Role of Endogenously Produced Vitamin D Metabolites in Keratinocyte Differentiation. Skin Pharmacology and Physiology *1*, 149–160.

Piotrowska, A., Wierzbicka, J. and Żmijewski, M. A. (2016). Vitamin D in the Skin Physiology and Pathology. Acta Biochimica Polonica *63*, 17–29.

Pittman, R. N. (2011). Regulation of Tissue Oxygenation. Colloquium Series on Integrated Systems Physiology: From Molecule to Function *3*, 1–100.

Place, T. L., Domann, F. E. and Case, A. J. (2017). Limitations of Oxygen Delivery to Cells in Culture: An Underappreciated Problem in Basic and Translational Research. Free Radical Biology and Medicine *113*, 311–322.

Poole, D. C., Copp, S. W., Hirai, D. M. and Musch, T. I. (2011). Dynamics of Muscle Microcirculatory and Blood–Myocyte O2 Flux during Contractions. Acta Physiologica *202*, 293–310.

Provin, C., Takano, K., Sakai, Y., Fujii, T. and Shirakashi, R. (2008). A Method for the Design of 3D Scaffolds for High-Density Cell Attachment and Determination of Optimum Perfusion Culture Conditions. Journal of Biomechanics *41*, 1436–1449.

Ramadan, Q. and Ting, F. C. W. (2016). In Vitro Micro-Physiological Immune-Competent Model of the Human Skin. Lab on a Chip *16*, 1899–1908.

Ravi, M., Paramesh, V., Kaviya, S., Anuradha, E. and Solomon, F. P. (2014). 3D Cell Culture Systems: Advantages and Applications. Journal of Cellular Physiology *230*, 16–26.

Redd, M. J., Cooper, L., Wood, W., Stramer, B. and Martin, P. (2004). Wound Healing and Inflammation: Embryos Reveal the Way to Perfect Repair. Philos Trans R Soc Lond B Biol Sci *359*, 777–84.

Reinke, J. M. and Sorg, H. (2012). Wound Repair and Regeneration. Eur Surg Res *49*, 35–43.

Reish, R. G. and Eriksson, E. (2008). Scars: A Review of Emerging and Currently Available Therapies. Plastic and reconstructive surgery *122*, 1068–1078.

Reyes, D. R., Iossifidis, D., Auroux, P.-A. and Manz, A. (2002). Micro Total Analysis Systems. 1. Introduction, Theory, and Technology. Analytical Chemistry *74*, 2623–2636.

Reynolds, O. (1883). An Experimental Investigation of the Circumstances Which Determine Whether the Motion of Water Shall Be Direct or Sinuous, and of the Law of Resistance in Parallel Channels. Philosophical Transactions of the Royal Society of London *174*, 935–982.

Rich, K. (2001). Transcutaneous Oxygen Measurements: Implications for Nursing. Journal of Vascular Nursing *19*, 55–60.

Rigual-González, Y., Gómez, L., Núñez, J., Vergara, M., Díaz-Barrera, A., Berrios, J. and Altamirano, C. (2016). Application of a New Model Based on Oxygen Balance to Determine the Oxygen Uptake Rate in Mammalian Cell Chemostat Cultures. Chemical Engineering Science *152*, 586–590.

Rodier, F. and Campisi, J. (2011). Four Faces of Cellular Senescence. The Journal of Cell Biology *192*, 547–556.

Roh, C. and Lyle, S. (2006). Cutaneous Stem Cells and Wound Healing. Pediatr Res *59*, 100R–3R.

Romanovsky, A. A. (2014). Skin Temperature: Its Role in Thermoregulation. Acta Physiologica *210*, 498–507.

Sallusto, F. and Baggiolini, M. (2008). Chemokines and Leukocyte Traffic. Nature Immunology *9*, 949–952.

Sargen, M. R., Hoffstad, O. and Margolis, D. J. (2013). Geographic Variation in Medicare Spending and Mortality for Diabetic Patients with Foot Ulcers and Amputations. Journal of Diabetes and Its Complications *27*, 128–133.

Schimek, K., Hsu, H. H., Boehme, M., Kornet, J. J., Marx, U., Lauster, R., Portner, R. and Lindner, G. (2018). Bioengineering of a Full-Thickness Skin Equivalent in a 96-Well Insert Format for Substance Permeation Studies and Organ-on-a-Chip Applications. Bioengineering (Basel) *5*.

Sen, C. K., Gordillo, G. M., Roy, S., Kirsner, R., Lambert, L., Hunt, T. K., Gottrup, F., Gurtner, G. C. and Longaker, M. T. (2009). Human Skin Wounds: A Major and

Snowballing Threat to Public Health and the Economy. Wound Repair and Regeneration: Official Publication of the Wound Healing Society [and] the European Tissue Repair Society *17*, 763–771.

Shabestani Monfared, G., Ertl, P. and Rothbauer, M. (2021). Microfluidic and Lab-on-a-Chip Systems for Cutaneous Wound Healing Studies. Pharmaceutics *13*, 793.

Sharma, S., Venzac, B., Burgers, T., Schlatt, S. and Le Gac, S. (2022). Testis-on-Chip Platform to Study Ex Vivo Primate Spermatogenesis and Endocrine Dynamics. Organs-on-a-Chip *4*, 100023.

Shpichka, A., Butnaru, D., Bezrukov, E. A., Sukhanov, R. B., Atala, A., Burdukovskii, V., Zhang, Y. and Timashev, P. (2019). Skin Tissue Regeneration for Burn Injury. Stem Cell Research & Therapy *10*, 94.

Shuler, M. L. (2012). Modeling Life. Ann Biomed Eng *40*, 1399–407.

Shuler, M. L., Ghanem, A., Quick, D., Wong, M. C. and Miller, P. (1996). A Self-Regulating Cell Culture Analog Device to Mimic Animal and Human Toxicological Responses. Biotechnol Bioeng *52*, 45–60.

Sindrilaru, A., Peters, T., Wieschalka, S., Baican, C., Baican, A., Peter, H., Hainzl, A., Schatz, S., Qi, Y., Schlecht, A., Weiss, J. M., Wlaschek, M., Sunderkötter, C. and Scharffetter-Kochanek, K. (2011). An Unrestrained Proinflammatory M1 Macrophage Population Induced by Iron Impairs Wound Healing in Humans and Mice. The Journal of Clinical Investigation *121*, 985–997.

Smigiel, K. S. and Parks, W. C. (2018). Macrophages, Wound Healing, and Fibrosis: Recent Insights. Current Rheumatology Reports *20*, 17.

Sonntag, F., Schilling, N., Mader, K., Gruchow, M., Klotzbach, U., Lindner, G., Horland, R., Wagner, I., Lauster, R., Howitz, S., Hoffmann, S. and Marx, U. (2010).

Design and Prototyping of a Chip-Based Multi-Micro-Organoid Culture System for Substance Testing, Predictive to Human (Substance) Exposure. J Biotechnol *148*, 70–5.

Sticker, D., Lechner, S., Jungreuthmayer, C., Zanghellini, J. and Ertl, P. (2017). Microfluidic Migration and Wound Healing Assay Based on Mechanically Induced Injuries of Defined and Highly Reproducible Areas. Analytical Chemistry *89*, 2326–2333.

Stojadinovic, O., Pastar, I., Vukelic, S., Mahoney, M. G., Brennan, D., Krzyzanowska, A., Golinko, M., Brem, H. and Tomic-Canic, M. (2008). Deregulation of Keratinocyte Differentiation and Activation: A Hallmark of Venous Ulcers. Journal of Cellular and Molecular Medicine *12*, 2675–2690.

Sung, J. H. and Shuler, M. L. (2012). Microtechnology for Mimicking in Vivo Tissue Environment. Ann Biomed Eng *40*, 1289–300.

Sunkara, V., Park, D.-K., Hwang, H., Chantiwas, R., Soper, S. A. and Cho, Y.-K. (2011). Simple Room Temperature Bonding of Thermoplastics and Poly(Dimethylsiloxane). Lab on a Chip *11*, 962–965.

Tang, L. and Lee, N. Y. (2010). A Facile Route for Irreversible Bonding of Plastic-PDMS Hybrid Microdevices at Room Temperature. Lab on a Chip *10*, 1274–1280.

Tarnuzzer, R. W. and Schultz, G. S. (1996). Biochemical Analysis of Acute and Chronic Wound Environments. Wound Repair and Regeneration: Official Publication of the Wound Healing Society [and] the European Tissue Repair Society *4*, 321–325.

Temenoff, J. S. and Mikos, A. G. (2008). Biomaterials: The Intersection of Biology and Materials Science. Pearson Prentice Hall Bioengineering, Pearson/Prentice Hall, Upper Saddle River, N.J.

Terry, S., Jerman, J. and Angell, J. (1979). A Gas Chromatographic Air Analyzer Fabricated on a Silicon Wafer. IEEE Transactions on Electron Devices *26*, 1880–1886.

Toepke, M. W. and Beebe, D. J. (2006). PDMS Absorption of Small Molecules and Consequences in Microfluidic Applications. Lab on a Chip *6*, 1484–1486.

Trowell, O. A. (1959). The Culture of Mature Organs in a Synthetic Medium. Experimental Cell Research *16*, 118–147.

van der Meer, A. D. and van den Berg, A. (2012). Organs-on-Chips: Breaking the in Vitro Impasse. Integr Biol (Camb) *4*, 461–70.

Vlachopoulou, M.-E., Tserepi, A., Pavli, P., Argitis, P., Sanopoulou, M. and Misiakos, K. (2008). A Low Temperature Surface Modification Assisted Method for Bonding Plastic Substrates. Journal of Micromechanics and Microengineering *19*, 015007.

Wagner, I., Materne, E.-M., Brincker, S., Süßbier, U., Frädrich, C., Busek, M., Sonntag, F., Sakharov, D. A., Trushkin, E. V., Tonevitsky, A. G., Lauster, R. and Marx, U. (2013a). A Dynamic Multi-Organ-Chip for Long-Term Cultivation and Substance Testing Proven by 3D Human Liver and Skin Tissue Co-Culture. Lab on a Chip *13*, 3538–3538.

Wagner, I., Materne, E.-M., Brincker, S., Süßbier, U., Frädrich, C., Busek, M., Sonntag, F., Sakharov, D. A., Trushkin, E. V., Tonevitsky, A. G., Lauster, R. and Marx, U. (2013b). A Dynamic Multi-Organ-Chip for Long-Term Cultivation and Substance Testing Proven by 3D Human Liver and Skin Tissue Co-Culture. Lab on a Chip *13*, 3538–3538.

Wahlsten, A., Rütsche, D., Nanni, M., Giampietro, C., Biedermann, T., Reichmann, E. and Mazza, E. (2021). Mechanical Stimulation Induces Rapid Fibroblast Prolifera-

tion and Accelerates the Early Maturation of Human Skin Substitutes. Biomaterials *273*, 120779.

Wilgus, T. A., Roy, S. and McDaniel, J. C. (2013). Neutrophils and Wound Repair: Positive Actions and Negative Reactions. Advances in Wound Care *2*, 379–388.

Willenborg, S. and Eming, S. A. (2014). Macrophages - Sensors and Effectors Coordinating Skin Damage and Repair. Journal der Deutschen Dermatologischen Gesellschaft = Journal of the German Society of Dermatology: JDDG *12*, 214–221, 214–223.

Winter, G. D. (1978). Oxygen and Epidermal Wound Healing. In Oxygen Transport to Tissue — III, (Silver, I. A., Erecińska, M. and Bicher, H. I., eds), Advances in Experimental Medicine and Biology pp. 673–678. Springer US New York, NY.

Wittenberg, B. A. and Wittenberg, J. B. (1989). Transport of Oxygen in Muscle. Annual Review of Physiology *51*, 857–878.

Wlodarczyk, K. L., Hand, D. P. and Maroto-Valer, M. M. (2019). Maskless, Rapid Manufacturing of Glass Microfluidic Devices Using a Picosecond Pulsed Laser. Scientific Reports *9*, 20215.

Wolff, K. and in general medicine Fitzpatrick, T. B. D. (2008). Fitzpatrick's Dermatology in General Medicine. 7th ed. / editors, klaus wolff ... [et al.]. edition, McGraw-Hill, New York ; London.

Wufuer, M., Lee, G., Hur, W., Jeon, B., Kim, B. J., Choi, T. H. and Lee, S. (2016a). Skin-on-a-Chip Model Simulating Inflammation, Edema and Drug-Based Treatment. Scientific Reports *6*, 37471–37471.

Wufuer, M., Lee, G., Hur, W., Jeon, B., Kim, B. J., Choi, T. H. and Lee, S. (2016b). Skin-on-a-Chip Model Simulating Inflammation, Edema and Drug-Based Treatment. Scientific Reports *6*, 37471–37471.

Yager, D. R., Zhang, L. Y., Liang, H. X., Diegelmann, R. F. and Cohen, I. K. (1996). Wound Fluids from Human Pressure Ulcers Contain Elevated Matrix Metalloproteinase Levels and Activity Compared to Surgical Wound Fluids. The Journal of Investigative Dermatology *107*, 743–748.

Yu, L. and Shi, Z. Z. (2015). Microfluidic Paper-Based Analytical Devices Fabricated by Low-Cost Photolithography and Embossing of Parafilm®. Lab on a Chip *15*, 1642–1645.

Zhao, Q., Wang, S., Xie, Y., Zheng, W., Wang, Z., Xiao, L., Zhang, W. and Jiang, X. (2012). A Rapid Screening Method for Wound Dressing by Cell-on-a-Chip Device. Advanced Healthcare Materials *1*, 560–566.

Zhou, L., Zhang, X., Paus, R. and Lu, Z. (2018). The Renaissance of Human Skin Organ Culture: A Critical Reappraisal. Differentiation *104*, 22–35.